NASA CR- 145221

SCHOOL OF ENGINEERING
OLD DOMINION UNIVERSITY
NORFOLK, VIRGINIA

RADIATION INDUCED PRECURSOR FLOW FIELD AHEAD OF A JOVIAN ENTRY BODY

(NASA-CR-145221) RADIATION INDUCED PRECURSOR FLOW FIELD AHEAD OF A JOVIAN ENTRY BODY Final Report (Old Dominion Univ. Research Foundation) 94 p HC A05/MF A01 CSCL 22C G3/13

N77-27158

Unclas
40508

By

S.N. Tiwari

and

K.Y. Szema

Final Report

Prepared for the
National Aeronautics and Space Administration
Langley Research Center
Hampton, Virginia 23665

Under
Master Contract Agreement NAS1-11707
Task Authorization No. 92

April 1977

SCHOOL OF ENGINEERING
OLD DOMINION UNIVERSITY
NORFOLK, VIRGINIA

RADIATION INDUCED PRECURSOR FLOW FIELD AHEAD OF A JOVIAN ENTRY BODY

By

S.N. Tiwari

and

K.Y. Szema

Final Report

Prepared for the
National Aeronautics and Space Administration
Langley Research Center
Hampton, Virginia 23665

Under
Master Contract Agreement NAS1-11707
Task Authorization No. 92

Submitted by the
Old Dominion University Research Foundation
Norfolk, Virginia 23508

April 1977

FOREWORD

This report constitutes a part of the work completed during the year 1975-1976 on a research project entitled "Radiation-Induced Precursor Flow Field Ahead of an Entry Body in the Outer Planetary Atmospheres." The work was supported by the NASA-Langley Research Center through Contract NAS1-11707-92. The contract was monitored by Mr. Randolph A. Graves, Jr. of SSD-Aerothermodynamics Branch.

TABLE OF CONTENTS

LIST OF FIGURES

(cont'd.)

LIST OF FIGURES - CONCLUDED

LIST OF TABLES

RADIATION INDUCED PRECURSOR FLOW FIELD AHEAD OF A JOVIAN ENTRY BODY

by

S. N. Tiwari* and K. Y. Szema**

SUMMARY

The change in flow properties ahead of the bow shock of a Jovian entry body, resulting from absorption of radiation from the shock layer, is investigated. Ultraviolet radiation is absorbed by the free stream gases, causing dissociation, ionization, and an increase in enthalpy of flow ahead of the shock wave. As a result of increased fluid enthalpy, the entire flow field in the precursor region is perturbed. The variation in flow properties is determined by employing the small perturbation technique of classical aerodynamics as well as the thin layer approximation for the preheating zone. By employing physically realistic models for radiative transfer, solutions are obtained for velocity, pressure, density, temperature, and enthalpy variations. The results indicate that the precursor flow effects, in general, are greater at higher altitudes. Just ahead of the shock, however, the effects are larger at lower altitudes. Pre-heating of the gas significantly increases the static pressure and temperature ahead of the shock for velocities exceeding 36 km/sec. The agreement between the small perturbation and thin layer approximation results are found to be excellent.

---

*Professor, Old Dominion University
**Research Assistant, Old Dominion University

LIST OF SYMBOLS

A_ν	radiative strength of source, ergs [Eq. (3.13)]
a_ν	quantity defined in [Eq. (2.24a)], in cm-sec/erg
$B_\nu(T)$	Planck black-body radiation function [Eq. (4.3)], erg/cm^2
b_ν	quantity defined in Eq. (2.24b)
C_α	mass fraction of species α
D	dissociation energy, erg/mole
F_j	perturbation potential function [Eqs. (3.16), (3.17)]
G_j	quantity defined in Eq. (3.19)
H	specific enthalpy, ergs/gm
H_j	quantity defined in Eqs. (3), (20)
H_T	total enthalpy per unit mass, ergs/gm
H_{T_1}	total perturbation enthalphy [Eq. (2.12)]
H_ν	specific irradiance of radiation of frequency ν, erg/cm^2
H_o	enthalpy of mixture [Eq. (5.5)], erg/gm
$H_{o\alpha}$	enthalpy of species α, cal/mole
H_1	specific perturbation enthalpy [Eq. (2.7d)]
h	Planck's constant = 6.6256×10^{27} erg-sec
I	ionization energy, erg/mole
K_H	net rate of production of species H, gm/cm^3-sec
$K_{H_2^+}$	net rate of production of species H_2+, gm/cm^3-sec
K_α	net rate of production of species α, gm/cm^3-sec
M_∞	free stream Mach number
m_1	net weight of a H_2 molecule, gm/molecule
N_{H_2}	number density of H_2
P	pressure, dyne/cm^2
P_ν	quantity defined in Eq. (2.23b)

P_1	pressure perturbation
P_∞	free stream pressure, dyne/cm^2
Q_R	divergence of net radiant heat flux, erg/cm^3-sec
$q_\nu(0)$	specific radiative flux density at shock wave, erg/cm^2
R	universal gas constant = 8.3143×10^7 erg/mole-°K
R_c	radius of the radiating gas cap, cm
R_s	radius of the bow shock wave, cm
r	cylindrical radial coordinate, cm
s	spherical radial coordinate, cm
T	temperature, °K
T_s	temperature at the shock front, °K
T_∞	free-stream temperature, °K
T_1	first-order temperature perturbation, °K
T_2	second-order temperature perturbation, °K
$\bar{V}$	velocity vector, cm/sec
$\bar{V}_1$	first-order velocity perturbation, cm/sec
$\bar{V}_2$	second-order velocity perturbation, cm/sec
V	velocity component normal to the shock surface, cm/sec
V_∞	free-stream velocity, cm/sec
V_{1r}	velocity perturbation component at the r-direction in cylindrical coordinate, cm/sec
V_{1x}	velocity perturbation component at the x-direction, cm/sec
V_{1y}	velocity perturbation component at the y-direction, cm/sec
V_{1z}	velocity perturbation component at the z-direction, cm/sec
W_α	molecular weight, gm/mole
Y_D	photodissociation yield
Y_I	photoionization yield

Z	altitude of entry, km (Table 5.1)
z	longitudinal coordinate, cm
β	quantity defined in Eq. (4.5)
Γ	quantity defined in Eq. (2.23a)
γ	specific heat ratio
ϵ	effective emissivity
ζ	optical depth defined in Eq. (3.3)
η	quantity defined in Eq. (3.14)
κ_ν	inverse of photon mean free path, 1/cm
Λ	quantity defined in Eq. (3.14)
μ	quantity defined in Eq. (3.14)
ρ	density, g/cm^3
ρ_1	first-order density perturbation
σ	Stefan-Boltzmann constant = 5.6697×10^{-5} $erg/cm^2\text{-}sec\text{-}°K^4$
$\sigma_D(\nu)$	photodissociation absorption cross section, cm^2
$\sigma_I(\nu)$	photoionization absorption cross section, cm^2
Φ	potential function defined in Eq. (2.27)
ϕ	potential function defined in Eq. (2.13)
ψ	quantity defined in Eq. (4.5)

1. INTRODUCTION

The word "precursor" gets its name from a Latin word "praecursor" (prae = before + currere = run) which means "forerunner." In the present context, precursor region flow (or flow in the precursor zone) means flow field ahead of a shock layer which is influenced by the conditions of the shock layer. It is well understood now that at high speed entry conditions (entry speeds in excess of parabolic speed), radiation plays a very important role in the analyses of flow phenomena around the body and that the radiative energy transferred to the body usually overtakes the aerodynamic heat transfer [1-10].* Radiative energy transfer from the shock layer of a blunt body into the free stream reduces the total enthalpy of the shock layer while increasing the enthalpy of the free stream gases. Because of this increase in enthalpy the entire flow field ahead of the shock layer and around the body is influenced significantly. The precursor flow region is considered to be the region ahead of a shock wave in which the flow field parameters have been changed from free stream conditions due to absorption of radiation from the incandescent shock layer. Most of the radiative energy transferred from the shock layer into the cold region ahead of the shock is lost to infinity unless it is equal to or greater than the energy required for dissociation of the cold gas. When the photon energy is greater than the dissociation energy, it is strongly absorbed by the cold gas in the ultraviolet continuum range. The absorbed energy dissociates and ionizes the gas and this results in change of flow properties in the precursor region. In particular, the temperature and pressure of the gas is increased while velocity is decreased. The change in flow properties of the precursor region, in turn, influences the flow characteristics within the shock layer itself. The problem, therefore, becomes a coupled one and iterative methods are required for its solution.

*Numbers in brackets indicate references.

Only a limited number of analyses on radiation-induced precursor flow are available in the literature. Works available until 1968 are discussed, in detail, by Smith [11,12]. By employing the linearized theory of aerodynamics, Smith [11,12] investigated the flow in the precursor region of a reentry body in the earth's atmosphere. The cases of plane, spherical, and cylindrical point sources were considered and solutions were obtained for a range of altitudes and free stream conditions. It was found that for velocities exceeding 18 km/sec, precursor flow effects are greatest at altitudes between 30 and 46 km. It was further concluded that preheating of air may cause an order of magnitude increase in the static pressure and temperature ahead of the shock wave for velocities exceeding 15 km/sec. Lasher and Wilson [13,14] investigated the level of precursor absorption and its resultant effect on surface radiation heating for earth's entry conditions. They concluded that, for velocities less than 18 km/sec, precursor heating effects are relatively unimportant in determining the radiative flux reaching the surface. At velocities greater than 18 km/sec, the amount of energy loss from the shock layer and resultant precursor heating correction was found to be significantly large. Liu [15,16] also investigated the influence of upstream absorption by cold air on the stagnation region shock layer radiation. The thin layer approximation was applied to both the shock layer and the preheating zone (the precursor region). The problem was formulated for the inviscid flow over smooth blunt bodies but the detailed calculations were carried out only for the stagnation region. The general results were compared with results of two approximate formulations. The first approximate formulation neglects the upstream influence and the second one essentially uses the iterative procedure described by Lasher and Wilson [13,14]. The results are compared for different values of a radiation/convection parameter. A few other works, related to the effects of upstream absorption by air

on the shock layer radiation, are discussed by Liu [15,16]. Some works on precursor ionization for air as well as hydrogen-helium atmosphere are presented in [17-21].

The purpose of this study is to investigate the changes in flow properties in the preheating zone of a Jovian entry body resulting from absorption of the radiation from the shock layer. As a first approach, the perturbation technique adapted by Smith [11,12] for the earth's atmosphere is used here for the hydrogen-helium atmosphere. By introducing appropriate thermodynamic and spectral information on hydrogen-helium atmosphere, proper modifications are made in the governing equations and results are obtained for Jupiter's entry conditions. Basic formulation of the problem is presented in Sec. 2 and solutions for special cases are obtained in Sec. 3. Perturbation equations are specialized for the photoabsorption model in Sec. 4, sources of data and solution procedures are discussed in Sec. 5, and results of flow perturbations are presented in Sec. 6. Finally, in Sec. 7, an alternate approach of thin precursor region approximation is adopted for analysis of the entire problem and the results are compared with the results of small perturbation theory.

2. BASIC FORMULATION

The physical model and coordinate system for a Jovian entry body is shown in Fig. 2.1. The flow field ahead of the body can be divided primarily into two regions, the precursor region and the shock layer. In this study, attention is directed to the precursor region where flow is assumed to be steady and inviscid. The flow properties are considered to be uniform at large distances from the body. For this region, conservation equations can be written as [22-24]

Mass Continuity: $$\nabla \cdot (\rho \bar{V}) = 0 \tag{2.1}$$

Momentum: $$\rho(\bar{V} \cdot \nabla \bar{V}) = -\nabla p \tag{2.2}$$

Energy: $$\rho(\bar{V} \cdot \nabla H_T) = Q_R \tag{2.3}$$

Species Continuity: $$\rho(\bar{V} \cdot \nabla C_\alpha) = K_\alpha \tag{2.4}$$

State: $$p = \rho RT \sum_\alpha (C_\alpha / W_\alpha) \tag{2.5}$$

where the total enthalpy per unit mass is given by

$$H_T = H + V^2/2 \tag{2.6}$$

In the above equations, $Q_R = \nabla \cdot q_R$ is the net rate of radiant energy absorbed per unit volume per unit time, K_α represents the net rate of production of species α per unit volume per unit time, and W_α is the molecular weight of species α.

As a result of increased fluid enthalpy, the entire flow field in the precursor region is perturbed. By following the small perturbation technique of classical aerodynamics, the flow properties can be expressed in perturbation series as [11,12,22,23]

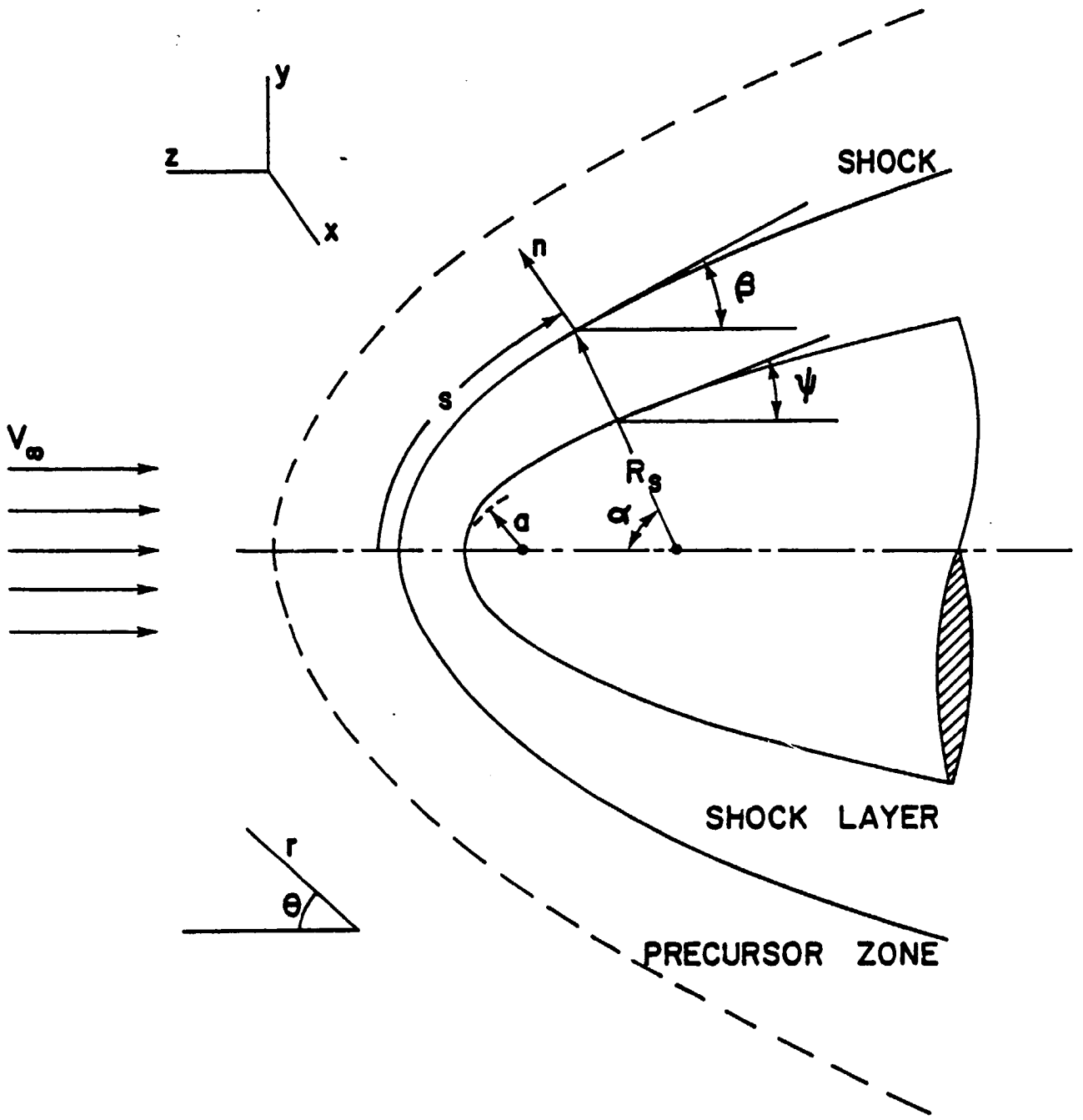

Figure 2.1. Physical model and coordinate system for a Jovian entry body.

$$\rho = \rho_\infty(1 + \rho_1 + \rho_2 + \ldots) \tag{2.7a}$$

$$p = p_\infty(1 + p_1 + p_2 + \ldots) \tag{2.7b}$$

$$\bar{V} = V_\infty(\bar{k} + \bar{V}_1 + \bar{V}_2 + \ldots) \tag{2.7c}$$

$$H = H_\infty + V_\infty^2(H_1 + H_2 + \ldots) \tag{2.7d}$$

$$T = T_\infty + T_1 + T_2 + \ldots \tag{2.7e}$$

$$C_\alpha = C_{\alpha_\infty} + C_{\alpha_1} + C_{\alpha_2} + \ldots \tag{2.7f}$$

In these equations, all the perturbation variables (except temperature) are expressed in nondimensional form. The unit vector $\bar{k}$ represents the direction of unperturbed free-stream velocity.

If Q_R and K_α can be considered as first-order perturbation terms, then substitution of Eqs. (2.7) into Eqs. (2.1)-(2.6) results in the first-order perturbation equations as

Continuity: $$\nabla \cdot \bar{V}_1 + \partial\rho_1/\partial z = 0 \tag{2.8}$$

Momentum: $$\partial\bar{V}_1/\partial z = -(1/\gamma M_\infty^2)\nabla p \tag{2.9}$$

Energy: $$\partial H_{T_1}/\partial z = Q_R/(\rho_\infty V_\infty^3) \tag{2.10}$$

Species: $$\partial C_{\alpha_1}/\partial z = K_\alpha/(\rho_\infty V_\infty) \tag{2.11}$$

$$H_{T_1} = H_1 + V_{1z} \tag{2.12}$$

The boundary conditions are that perturbation quantities vanish at $z \to \infty$ and that no singularities exist except at the origin.

It can be shown that the flow under consideration is irrotational [11,22]. Thus, there exists a potential ϕ such that

$$\bar{V}_1 = \nabla\phi \tag{2.13}$$

For z-direction, integration of Eq. (2.9) results in

$$p_1 = -(\gamma M_\infty^2)\ \partial\phi/\partial z = -(\gamma M_\infty^2)V_{1z} \tag{2.14}$$

Equation (2.8) now can be expressed as

$$\nabla^2\phi + \partial\rho_1/\partial z = 0 \tag{2.15}$$

In order to evaluate $\partial\rho_1/\partial z$ and to relate H_1 to other variables, it is necessary to consider the gas model and radiation.

For the Jupiter's atmosphere, the gas model is taken to be: $C_{H_2} = 89\%$ and $C_{H_e} = 11\%$ by mole fraction (or $C_{H_2} = 80.82\%$ and $C_{H_2} = 19.18\%$ by mass fraction). The radiation effect on the gas ahead of the shock produces H_2^+, H, and electrons e^- by photodissociation and photoionization, and also increases the enthalpy. Any other species which may be produced are neglected. The contribution of radiation to the gas pressure is neglected. It is further assumed that the internal degrees of freedom of various species (i.e., vibrational and electronic modes) are not excited. For this gas model, the equation of state (for the first order perturbation) can be expressed as

$$p_1 = (400/180.17)\left[\left(C_H + C_{H_2^+}\right)/2\right] + (T_1/T_\infty) + \rho_1 \tag{2.16}$$

By following the procedure described by Smith [11,12], the first-order perturbation relation for enthalpy is found to be

$$H_1 = (1/V_\infty^2)\left\{1.527\ RT_1 + \left[(5/4)RT_\infty + I/2\right]C_{H_2^+} + \left[(3/4)RT_\infty + D\right]C_H\right\} \tag{2.17}$$

where I and D represent the ionization and dissociation energy respectively. It should be pointed out here that D in the above equation actually represents half the energy required for dissociation.

As pointed out earlier, the upstream gas absorbs the energy radiated from the shock layer in the ultraviolet continuum range. The radiation from the perturbed gas due to recombination (i.e., emission) is neglected. The amount of radiative energy absorbed by the perturbed gas per unit volume and time, Q_R , is given by

$$Q_R = N_{H_2} \int_o^\infty H_\nu \, \sigma(\nu) d\nu \tag{2.18}$$

where N_{H_2} is the number density of H_2, H_ν is specific irradiance and $\sigma(\nu)$ is the photon absorption cross section of H_2 at frequency ν.

In determining the rate of production of species in the precursor region, only photodissociation and photoionization are considered. Recombination is assumed to be a second-order effect and, therefore, is neglected in the present linearized treatment. The net rate of production of species, therefore, is given by [11,24]

$$K_H = m_1 N_{H_2} \int_o^\infty (H_\nu/h\nu) \, \sigma_D(\nu) d\nu \tag{2.19a}$$

$$K_{H_2^+} = m_1 N_{H_2} \int_o^\infty (H_\nu/h\nu) \, \sigma_I(\nu) d\nu \tag{2.19b}$$

where m_1 represents the weight of a H_2 molecule (in grams per molecule), and $\sigma_D(\nu)$ and $\sigma_I(\nu)$ are the absorption cross section for photodissociation and photoionization, respectively.

Since the problem treated here is linear, it is permissible to obtain a solution for arbitrary frequency, and then integrate this solution over the spectrum to obtain the solution for the problem. Thus, in the development that

follows, flow-field perturbations will be considered for a unit frequency interval. Equations (2.10) and (2.11) now can be written as

$$\partial H_{-1}/\partial z = N_{H_2}\, \sigma(\nu)/(\rho_\infty V_\infty^3)\, H_\nu \tag{2.20}$$

$$\partial C_H/\partial z = \left[m_1 N_{H_2} Y_D\, \sigma(\nu)/(\rho_\infty V_\infty h\nu)\right] H_\nu \tag{2.21a}$$

$$\partial C_{H_2^+}/\partial z = \left[m_1 N_{H_2} Y_I\, \sigma(\nu)/(\rho_\infty V_\infty h\nu)\right] H_\nu \tag{2.21b}$$

where Y_D and Y_I represent photodissociation and photoionization yields, respectively.

In order to express the governing equations in terms of perturbation potential, p_1 is first eliminated by combining Eqs. (2.14) and (2.16). The resulting equation is then differentiated with respect to z and use is made of Eqs. (2.21). Next Eqs. (2.12,2.13,2.17,and 2.20) are combined to give

$$\partial \rho_1/\partial z = -\Gamma\, \partial^2\phi/\partial z^2 - P_\nu H_\nu \tag{2.22}$$

where

$$\Gamma = 0.727\, \gamma M_\infty^2 \tag{2.23a}$$

$$P_\nu = a_\nu + b_\nu/h\nu \tag{2.23b}$$

$$a_\nu = N_{H_2}\, \sigma(\nu)/(\rho_\infty V_\infty H_\infty) \tag{2.24a}$$

$$b_\nu = -(a_\nu m_1/2)\left[(I - 0.89\, RT_\infty)Y_I + (2D - 1.89\, RT_\infty)Y_D\right] \tag{2.24b}$$

Upon combining Eqs. (2.15) and (2.22), the governing equation for the flow is obtained as

$$\nabla^2_{x,y}\phi - \Gamma\, \partial^2\phi/\partial z^2 = P_\nu H_\nu \tag{2.25}$$

For axisymmetric case, this is expressed as

$$r^{-1}\ \partial/\partial r\ (r\partial\phi/\partial r) - \Gamma\ \partial^2\phi/\partial z^2 = P_\nu\ H_\nu \tag{2.26}$$

Equations (2.25) and (2.26) are seen to be the classical potential equations for compressible flow with a forcing term proportional to radiation added. It should be pointed out that the form of Eq. (2.25) and (2.26) will be retained for any linearized gas model, although the expression for P_ν will depend on the gas model used. The potential for the flow induced by a radiant source with a spectral distribution is obtained by integrating the contributions of each frequency as

$$\Phi = \int_0^\infty \phi\ d\nu \tag{2.27}$$

3. SOLUTIONS FOR SPECIAL CASES

As discussed by Smith [11,12], solutions of the governing equations, presented in the previous section, can be obtained in special cases depending on the model used for the distribution of spatial radiation. If the radius of the radiating gas cap, R_c, is large compared to the photon mean free path, then the problem can be treated like radiation from a plane source. On the other hand, when the radius of the radiating gas cap is small, then the problem can be treated like a spherical point source for radiation from the gas cap and a cylindrical point source for radiation from the wake. Note that, in general, R_c may not be the same as the radius of the bow shock, R_s.

3.1 Radiation from a Plane Source

For radiation from a plane source, it is essential to integrate the H_ν contribution over the plane, as attenuated by passage through the absorbing medium. The relation for H_ν, in this case, is given by [24]

$$H_\nu = 2q_\nu(0)\, E_2(-\kappa_\nu z) \tag{3.1}$$

where $q_\nu(0)$ is the spectral radiative flux density at the shock wave, κ_ν is the spectral absorption coefficient, and $E_n(t)$ is the exponential integral of order n. The expression for κ_ν (which may also be interpreted as inverse of the photon mean free path) is given by

$$\kappa_\nu = N_{H_2}\, \sigma(\nu) \tag{3.2}$$

In this form κ_ν represents the absorption coefficient of H_2 molecules. If the number density N_{H_2} (and hence κ_ν) can be taken to be independent of z (which is a good approximation for small ionization and dissociation), then the optical depth is defined by

$$\zeta = \kappa_\nu z \tag{3.3}$$

For the plane radiating source (where $\nabla^2_{x,y}\,\phi = 0$), therefore, a combination of Eqs. (2.25,3.1-3.3) results in

$$-\partial^2\phi/\partial\zeta^2 = [2\,P_\nu\,q_\nu(0)/(\Gamma\,\kappa_\nu^2)]E_2(-\zeta) \tag{3.4}$$

Integration of this yields the result

$$\phi = -[2\,P_\nu\,q_\nu(0)/(\Gamma\kappa_\nu^2)]E_4(-\zeta) \tag{3.5}$$

where the boundary condition of $(\partial\phi/\partial\zeta) \to 0$ as $\zeta \to -\infty$ has been used.

From Eq. (2.13), the velocity perturbations, ahead of the shock front, now can be written as

$$v_{1x} = v_{1y} = 0 \tag{3.6}$$

$$v_{1z} = -[2\,P_\nu\,q_\nu(0)/(\Gamma\kappa_\nu)]E_3(-\zeta) \tag{3.7}$$

From Eq. (2.14), the expression for pressure perturbation is found to be

$$p_1 = [2\,\gamma\,P_\nu\,q_\nu(0)/\kappa_\nu]\,(M_\infty^2/\Gamma)E_3(-\zeta) \tag{3.8a}$$

For high speed entry, $M_\infty^2 >> 1$ and $(M_\infty^2/\Gamma) \simeq 1$. Thus, Eq. (3.8a) can be approximated by

$$p_1 = [2\,\gamma\,P_\nu\,q_\nu(0)/\kappa_\nu]E_3(-\zeta) \tag{3.8b}$$

The expression for density perturbation is obtained by combining Eqs. (2.15) and (3.4) and integrating the resulting expression such that

$$\rho_1 = [2\,P_\nu\,q_\nu(0)/(\Gamma\kappa_\nu)]E_3(-\zeta) \tag{3.9}$$

By combining Eqs. (2.20,3.1-3.3), one obtains

$$\partial H_{T_1}/\partial\zeta = [2\,q_\nu(0)/(\rho_\infty\,V_\infty^3)]E_3(-\zeta)$$

Integration of this over the plane of the shock wave gives the result for the total enthalpy as

$$H_{T_1} = [2\, q_\nu(0)/(\rho_\infty V_\infty^3)]E_3(-\zeta) \tag{3.10}$$

By employing Eqs. (2.12,3.7, and 3.10), the expression for the static enthalpy is found to be

$$H_1 = 2q_\nu(0)\left\{[1/(\rho_\infty V_\infty^3)] + P_\nu/(\Gamma\kappa_\nu)\right\}E_3(-\zeta) \tag{3.11}$$

The concentrations of H and H_2^+ are given by integration of Eqs. (2.21) as

$$C_H = [2\, W_{H_2}\, m_1/(\rho_\infty V_\infty h\nu)]Y_D(\nu)\; q_\nu(0)E_3(-\zeta) \tag{3.12a}$$

$$C_{H_2^+} = [2\, W_{H_2}\, m_1/(\rho_\infty V_\infty h\nu)]Y_I(\nu)\; q_\nu(0)E_3(-\zeta) \tag{3.12b}$$

By employing Eqs. (3.8,3.9, and 3.12), Eq. (2.16) is solved for the temperature variation. For this case now all the flow properties at any point upstream of the shock can be determined.

3.2 Radiation from Spherical and Cylindrical Point Sources

The physical model for radiation from spherical and cylindrical point sources is shown in Fig. 3.1. A spherical point source is a source which radiates equally in all directions. A cylindrical point source is a source which radiates as a cylinder of infinitesimal radius and length. For both cases, the incident radiation at any field point s is given by [11,12]

$$H_\nu = (A_\nu/s^2)\, \exp(-\kappa_\nu s)(\sin\theta)^j \tag{3.13}$$

In this equation, A_ν represents the radiative strength of the source, s is the distance from the source, and θ is the angle between the free stream velocity vector and a line from the field point to the center of the source.

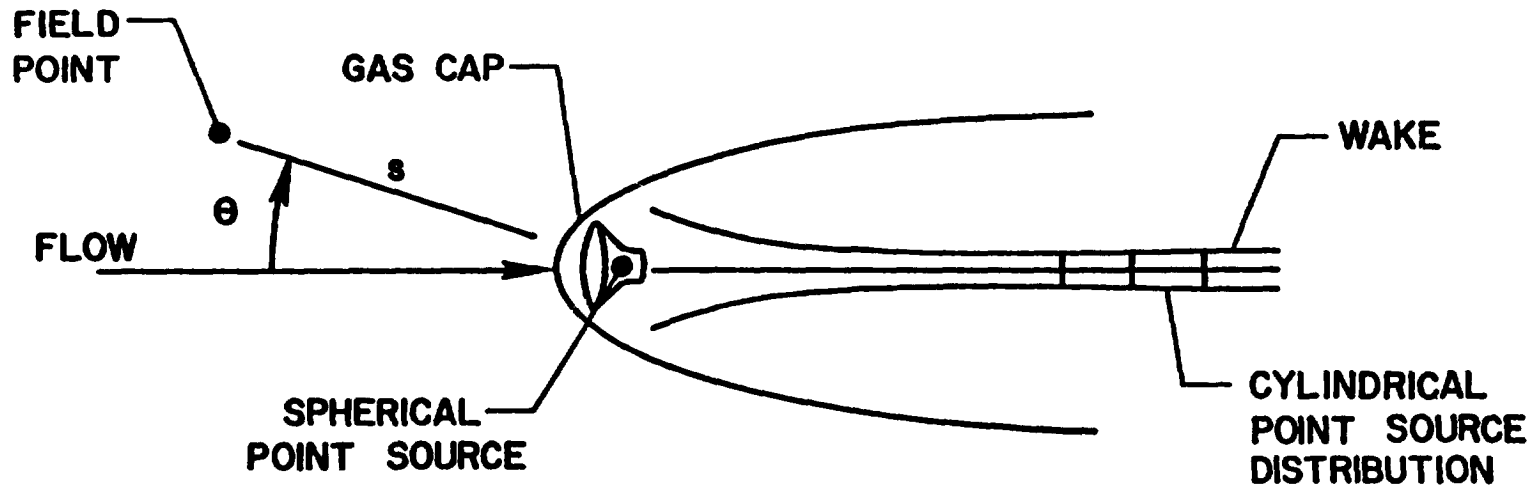

Figure 3.1. Approximation of radiating flow by point sources.

The superscript $j = 0$ for a spherical point source and 1 for a cylindrical point source.

Equation (3.13) can be substituted in Eqs. (2.25) and (2.26) to obtain the corresponding equations for the perturbation potential. Within the confines of the assumptions made in obtaining Eq. (3.13), however, both problems (spherical as well as cylindrical point source) can be considered to be axisymmetric. The governing equation for the perturbation potential, therefore, can be written as

$$\eta^{-1}\,\partial/\partial\eta\,(\eta\partial\phi'/\partial\eta) - \Gamma\,\partial^2\phi'/\partial\zeta^2 = \Lambda\,\mu^{-2}\,e^{-\mu}\,(\sin\theta)^j \tag{3.14}$$

where

$$\mu = \kappa_\nu s, \quad \eta = \kappa_\nu r, \quad \phi' = \kappa_\nu \phi, \quad \Lambda = \Lambda(\nu) = \kappa_\nu\, P_\nu\, A_\nu$$

A procedure for general solution of this equation is suggested by Smith [11]. For entry flows, however, $M_\infty^2 >> 1$ and Eq. (3.14) can be solved by expanding ϕ' in a series in $(1/\Gamma)$ in the vicinity of the body. Thus, one can express ϕ' as

$$\phi' = -(\kappa_\nu/\Gamma)\left[F_j(\zeta,\eta) + (1/\Gamma)F_j^{(1)}(\zeta,\eta) + (1/\Gamma)^2\,F_j^{(2)}(\zeta,\eta) + \ldots\right] \tag{3.15}$$

where F_j's are functions for perturbation potential. Substitution of this relation into Eq. (3.14) gives

$$\partial^2 F_j/\partial\zeta^2 = \mu^{-2}\,\exp(-\mu)(\sin\theta)^j \tag{3.16}$$

and

$$\partial^2 F_j^{(n)}/\partial\zeta^2 = -\eta^{-1}\,\partial/\partial\eta(\eta\,\partial F_j^{(n-1)}/\partial\eta) \tag{3.17}$$

The problem, therefore, is reduced to quadratures in the vicinity of the body. In the present analysis only the term in $(1/\Gamma)$ will be retained. By integrating Eq. (3.16) twice the expression for F_j is obtained as

$$F_j(\zeta,\eta) = \int_{-\infty}^{\infty} \mu_o^{-2}\,\exp(-\mu_o)(\eta/\mu_o)^j\,(\zeta - \zeta_o)d\zeta_o \tag{3.18}$$

where $\mu_o^2 = \eta^2 + \zeta_o^2$. For convenience, let us denote

$$G_j(\zeta,\eta) = \partial F_j/\partial\zeta = \int_{-\infty}^{\zeta} \mu^{-2} \exp(-\mu_o)(\eta/\mu_o)^j \, d\zeta_o \tag{3.19}$$

$$H_j(\zeta,\eta) = \partial F_j/\partial\eta = \int_{-\infty}^{\zeta} \mu_o^{-3} \exp(-\mu_o)\Big\{(\eta/\mu)^j \, [\eta + (\eta/\mu_o)(2 + j)] - j\Big\}(\zeta - \zeta_o)d\zeta_o \tag{3.20}$$

With these definitions of F_j , G_j , and H_j , the perturbation quantities can be expressed as

$$\phi' = -(\Lambda/\Gamma)F_j(\zeta,\eta) \tag{3.21}$$

$$v_{1r} = (\Lambda/\Gamma)H_j(\zeta,\eta) \tag{3.22}$$

$$v_{1z} = -(\Lambda/\Gamma)G_j(\zeta,\eta) \tag{3.23}$$

$$p_1 = \gamma\Lambda G_j(\zeta,\eta) \tag{3.24}$$

$$\rho_1 = (\Lambda/\Gamma)G_j(\zeta,\eta) \tag{3.25}$$

$$H_{T_1} = (\kappa_\nu A_\nu/\rho_\infty V_\infty^3)G_j(\zeta,\eta) \tag{3.26}$$

$$C_H = (m_1 A_\nu \kappa_\nu^2/\rho_\infty V_\infty h\nu)Y_D(\nu) \, G_j(\zeta,\eta) \tag{3.27a}$$

$$C_{H_2^+} = (m_1 A_\nu \kappa_\nu^2/\rho_\infty V_\infty h\nu)Y_i(\nu) \, G_j(\zeta,\eta) \tag{3.27b}$$

Note that for the case of spherically radiating point source $j = 1$ in the above equations. Also, these equations are obtained for arbitrary frequency. The expression for total potential, for this case, can be obtained by combining Eqs. (2.27) and (3.15) as

$$\phi = -(1/\Gamma)\int_o^\infty [\Lambda(\nu)/\kappa_\nu]F_j(\zeta,\eta)d\nu \tag{3.28}$$

Furthermore, it should be noted that the above solutions are valid in the region where $[\mu^{-2} \exp(-\mu) (\sin \theta)^j]$ does not vanish. This is the case of spherically symmetric flow ahead of the entry body and is of primary concern in the present study. Other cases involving cylindrical point source are discussed in [11,12].

3.3 Solutions for the Transition Range ($\lambda R_c = O(1)$)

As mentioned earlier, for $\kappa_\nu R_c \ll 1$, the axisymmetric solutions for the spherically and cylindrically radiating point source are valid and for $\kappa_\nu R_c \gg 1$, the one-dimensional equations apply. The solutions for the spherically radiating point source approach one-dimensional solutions as $\kappa_\nu R_c \to \infty$. Thus, spherically radiating point source solutions are valid for the precursor flow ahead of a blunt body with $\kappa_\nu R_c \gg 1$ and $\kappa_\nu R_c \ll 1$. Since the $\kappa_\nu R_c = O(1)$ range lies between these two limits, the spherically radiating point source analysis could be applied (to a good approximation) also in the transitional range.

4. PERTURBATION EQUATIONS FOR PHOTOABSORPTION MODEL

In order to obtain specific results for the perturbed quantities, it is essential to have a realistic model for the spectral absorption coefficient of the absorbing gas. The photoabsorption model employed in this study is discussed in this section and the governing perturbation equations are expressed in special form for this model.

4.1 Photoabsorption Model

Photoionization absorption coefficient is a continuous non-zero function of photon energy (because of bound-free transition) for all values of photon energy that exceed the ionization potential of the atom. Similar remarks apply to the photodissociation and radiative recombination. A critical review of ultraviolet photoabsorption cross sections for molecules of astrophysical and aeronomic interest, available in the literature up to 1971, is given by Hudson [25]. Specific information on photoionization and absorption coefficient of molecular hydrogen is available in [25-31].

Photoionization and absorption cross sections of H_2, as obtained from references [25-31], are plotted in Fig. 4.1. From this figure it is evident that the ionization continuum starts at about 804 Å and continues towards lower wave lengths. Between the wave lengths of 600 Å and 804 Å, the absorption cross section for ionization continuum are included in the total absorption (i.e., absorption due to ionization as well as dissociation). For wavelengths below 600 Å, however, the ionization continuum absorption is equal to the total absorption. The total absorption cross section for continuum range below 804 Å can be closely approximated by the two rectangles (I and II) shown in the figure with broken lines. The ratio of ionization cross section

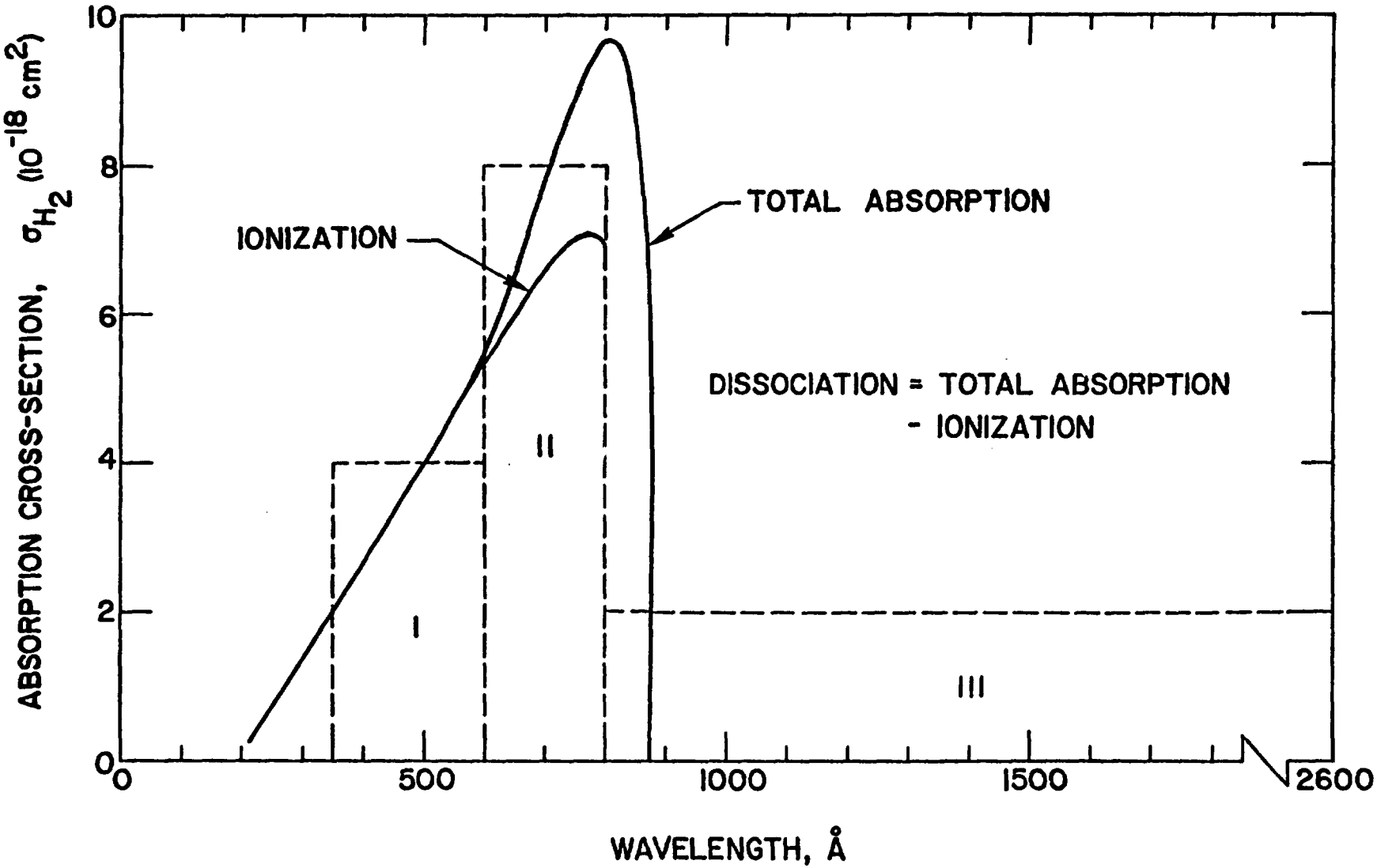

Figure 4.1. Absorption cross section of H_2 in ultraviolet region.

to the total absorption cross-section (i.e., the value of Y_I) is taken to be unity for rectangle I and 0.875 for rectangle II. For wavelength greater than 804 Å (where $h\nu$ is below ionization energy), the value of Y_I is taken to be zero. Little information is available in the literature on the absorption cross-section for dissociation of H_2 molecules. There is strong evidence, however, that photodissociation starts at about 2600 Å and continues towards lower wavelengths to about 750 Å [26-28]. There are also a few diffuse bands in this spectral range [26,28]. Thus, it becomes difficult to evaluate the absorption cross section in this spectral range. For this study, the absorption cross section in the spectral range between 804 Å and 2600 Å was approximated by the rectangle III. The specific values of $\sigma(\nu)$ for the three rectangles are found to be $\sigma_I(\nu) = 4.1$ E-18, $\sigma_{II}(\nu) = 8.2$ E-18, and $\sigma_{III}(\nu) = 2.1$ E-18. The value of Y_D is taken to be zero for rectangle I and 0.125 for rectangle II.

4.2 Precursor Equations for the Photoabsorption Model

In accordance with the photoabsorption model assumed in the previous subsection, quantities $\sigma(\nu)$, λ, Y_I and Y_D are taken to be constant within a given frequency range. Thus, these quantities are assumed to have constant (but different) values for rectangles I, II, and III in Fig. 4.1. It is further assumed that the gas cap radiates as a gray body and the effective emissivity of the gas cap is given by

$$\varepsilon = q(0)/(\sigma T_s^4) \tag{4.1}$$

where $q(0)$ is the radiative flux density from the shock layer and T_s is the shock temperature.

The spectral radiative flux at the shock front is given by the relation

$$q_\nu(0) = \varepsilon \pi B_\nu(T_s) \tag{4.2}$$

In this equation, $B_\nu(T_s)$ represents the Planck function which is given by

$$B_\nu(T) = (2h/c^2)(kT/h)^3\left\{v^3/[\exp(v) - 1]\right\} \tag{4.3}$$

where $v = h\nu/kT$.

It now remains to obtain the relation for A_ν in Eq. (3.13). By noting that at the shock front $H_\nu = q_\nu(0)$ and $s = R_c$, a rearrangement of Eq. (3.13) gives

$$A_\nu = q_\nu(0)\ R_c^2\ \exp(\kappa_\nu R_c) \tag{4.4}$$

With the above information, final relations for the total perturbation quantities now can be obtained. For spherically radiating case, the perturbation quantities can be expressed by an equation of the form [11,12]

$$\psi = \beta\int_o^\infty \Lambda(\nu)\ G_j(\zeta,\eta)d\nu \tag{4.5}$$

where ψ represents V_{1z} , p_1 , or ρ_1 , and β represents the factor ahead of the integral. The radial component of the velocity perturbation takes this same form but G_j is replaced by H_j . By employing the definition of $\Lambda(\nu)$, and combining Eqs. (2.24) and (4.5) results in

$$\psi = \beta R_c^2\int_o^\infty \kappa_\nu[a_\nu + (b_\nu/h\nu)]\ \exp(\kappa_\nu R_c)\ q_\nu(0)\ G_j\ d\nu \tag{4.6}$$

Since a_ν , b_ν , and κ_ν are assumed to be constant over sections of the wavelength range, Eq. (4.6) can be expressed as

$$\psi = \beta R_c^2 \sum_{i=1}^{n} \kappa_i\ \exp(\kappa_i\ R_c)\ G_j(\kappa_i z,\ \kappa_i r)\ \times$$

$$\left\{a_i\int_{\nu_{1i}}^{\nu_{2i}} q_\nu(0)d\nu + (b_i/h)\int_{\nu_{1i}}^{\nu_{2i}} [q_\nu(0)/\nu]d\nu\right\} \tag{4.7}$$

The two integrals in the above equation are evaluated by using Eqs. (4.2) and

(4.3). The first one can be written as

$$\int_{\nu_{1i}}^{\nu_{2i}} q_\nu(0)d\nu = \varepsilon\,\pi(2h/c^2)(kT_s/h)^4 \int_{v_{1i}}^{v_{2i}} [v^3/(e^v - 1)]dv \tag{4.8}$$

By employing the definition of σ and denoting

$$N_p(v) = \int_v^\infty [v^p/(e^v - 1)]dv \tag{4.9}$$

Eq. (4.8) can be expressed as

$$\int_{\nu_{1i}}^{\nu_{2i}} q_\nu(0)d\nu = (15/\pi^4)\,\varepsilon\,\sigma\,T_s^4\,[N_3(v_{1i}) - N_3(v_{2i})] \tag{4.10}$$

Similarly, the second integral in Eq. (4.7) can be expressed as

$$\int_{\nu_{1i}}^{\nu_{2i}} [q_\nu(0)/\nu]d\nu = (15/\pi^4)\,\varepsilon\,\sigma\,T_s^4\,(h/kT_s)\,[N_2(v_{1i}) - N_2(v_{2i})] \tag{4.11}$$

Substitution of Eqs. (4.10 and (4.11) into Eq. (4.7) gives the final relation for ψ from which the perturbation quantities can be determined. The quantities H_{T_1}, C_H, $C_{H_2}+$ have the form of Eq. (4.7) with the κ_i which appears ahead of the $\exp(\kappa_i R_c)$ squared.

In order to write specific relations for the perturbation quantities, it would be convenient to define

$$\beta_1 = (15/\pi^4)\,[q(0)/\Gamma] \tag{4.12a}$$

$$\beta_2 = (15/\pi^4)\,\gamma\,q(0) \tag{4.12b}$$

$$\beta_3 = (15/\pi^4)\,[q(0)/(\rho_\infty\,V_\infty^3)] \tag{4.12c}$$

$$\beta_4 = (15/\pi^4)\,[q(0)\,m_1/(\rho_\infty\,V_\infty)] \tag{4.12d}$$

$$I(v_i^p) = \int_{v_{1i}}^{v_{2i}} \left\{ v^p/[\exp(v) - 1] \right\} dv \tag{4.13}$$

$$B(a_i,b_i) = a_i\,I(v_i^3) + (b_i/kT_s)\,I(v_i^2) \tag{4.14}$$

For the spherically radiating case, the perturbation quantities now can be expressed as

$$V_{1z} = -\beta_1 R_c^2 \sum_{i=1}^{n} \kappa_i \exp(\kappa_i R_c) G_j(\zeta,\eta) B(a_i,b_i) \tag{4.15}$$

$$V_{1r} = \beta_1 R_c^2 \sum_{i=1}^{n} \kappa_i \exp(\kappa_i R_c) H_j(\zeta,\eta) B(a_i,b_i) \tag{4.16}$$

$$p_1 = -(\beta_2/\beta_1)V_{1z} \tag{4.17}$$

$$\rho_1 = -V_{1z} \tag{4.18}$$

$$H_1 = \beta_3 R_c^2 \sum_{i=1}^{n} \kappa_i^2 \exp(\kappa_i R_c) G_j(\zeta,\eta) I(v_i^3) \tag{4.19}$$

$$C_H = \beta_4 R_c^2 \sum_{i=1}^{n} Y_{D_i} \kappa_i^2 \exp(\kappa_i R_c) G_j(\zeta,\eta) I(v_i^2) \tag{4.20}$$

$$C_{H_2^+} = \beta_4 R_c^2 \sum_{i=1}^{n} Y_{I_i} \kappa_i^2 \exp(\kappa_i R_c) G_j(\zeta,\eta) I(v_i^2) \tag{4.21}$$

$$T_1 = T_\infty [p_1 - \rho_1 - (200/180.17)(C_{H_2^+} + C_H)] \tag{4.22}$$

For the plane radiating source, the perturbation quantities can be written as

$$V_{1z} = -2\beta_1 \sum_{i=1}^{n} \kappa_i^{-1} E_3(-\zeta_i) B(a_i,b_i) \tag{4.23}$$

$$H_1 = 2\beta_3 \sum_{i=1}^{n} E_3(-\zeta_i) \tag{4.24}$$

$$C_H = 2\beta_4 \sum_{i=1}^{n} Y_{D_i} E_3(-\zeta_i) (kT_s)^{-1} I(v_i^2) \tag{4.25}$$

$$C_{H_2^+} = 2\beta_4 \sum_{i=1}^{n} Y_{I_i} E_3(-\zeta_i) (kT_s)^{-1} I(v_i^2) \tag{4.26}$$

The expressions for p_1 , ρ_1 and T_1 in this case are the same as for the spherically radiating source but care should be taken in using the right relations for V_{1z} , $C_{H_2^+}$ and C_H .

Depending on the order of optical thickness, either spherical or plane radiating source relations are employed in actual calculations of the perturbation quantities.

5. DATA SOURCE AND SOLUTION PROCEDURE

Jupiter's atmospheric conditions, as obtained from reference [32], are shown in Fig. 5.1 for different altitudes. The temperature of the atmosphere (i.e., T_∞) is taken to be constant at 145°K and the enthalpy is given by $H_\infty = 1.527\ R\ T_\infty$. The entry velocity range considered are between 28-45 km/sec. The value of $R_c = 25$ cm was assumed for this study. The number density of H_2 can be computed by using the relation

$$N_{H_2} = (7.2431172 \times 10^{22})\ (P_\infty/T_\infty) X_{H_2} \tag{5.1}$$

where x_{H_2} is the mole fraction of H_2 and P_∞ has units of N/m^2 .

Free stream and shock conditions used in this study are listed in Table 5.1. Shock temperature and q(0)-values were calculated by employing the computational procedure developed by Sutton [4] and Moss [9]. Since viscous effects are pronounced primarily in the vicinity of the body, only inviscid shock layer formulations were considered in calculating T_s and q(0). Further details on shock layer solutions and effects of shock precursor heating on radiative flux to the body are given in a separate report [33].

Before evaluating actual values of the perturbation quantities, it was considered necessary to investigate the range of different intervening parameters of the governing equations. The values of the inverse mean free path (i.e., $\kappa_\nu = \sigma(\nu)\ N_{H_2}$) and the product $\kappa_\nu\ R_c$ were calculated for the Jovian entry conditions and these are shown in Fig. 5.2 for the three different values of the photoabsorption cross section of Fig. 4.1. From this figure it is evident that the product $(\kappa_\nu\ R_c) >> 1$ in most cases of interest for the Jovian entry. Thus, one could employ only the plane radiating source formulations for determining the perturbation quantities in the precursor region.

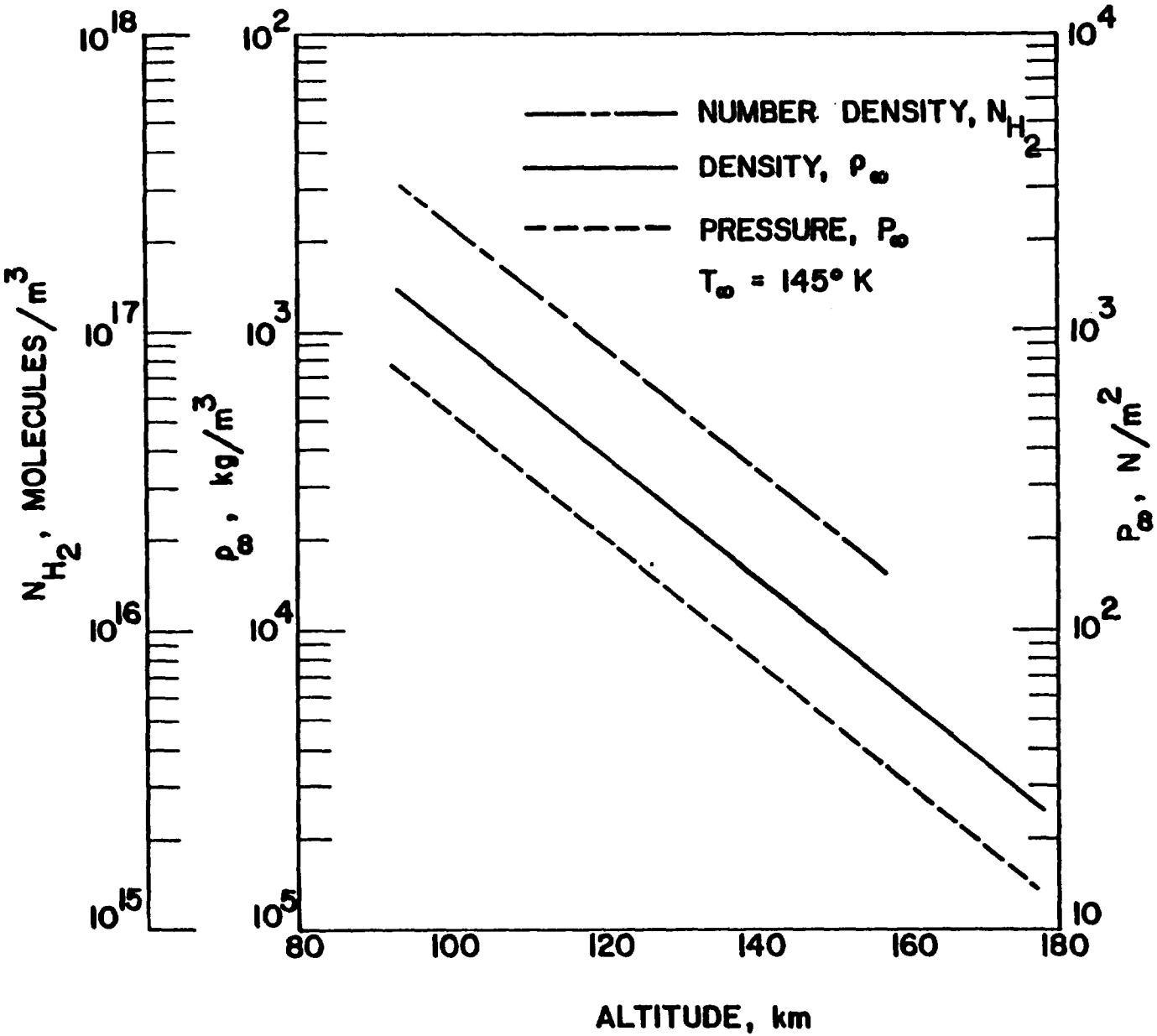

Figure 5.1. Atmospheric conditions for Jupiter's entry.

Table 5.1 Free-stream and shock conditions for Jovian entry.

Free stream	V_∞, km/sec	T_s, °K	$\dot{q}(0)$, erg/cm^2
Z = 95, km ρ_∞ = 1.29 E-3, kg/m^3 P_∞ = 673, N/m^2	38	16,610	1.35 E12
	35	15,400	7.75 E11
	32	14,080	3.52 E11
	30	13,550	2.01 E11
Z = 103 ρ_∞ = 8.56 E-4 P_∞ = 448	40	16,890	1.16 E11
	35	15,040	4.70 E11
	33	14,250	3.28 E11
	30	12,810	1.142 E11
Z = 116 ρ_∞ = 4.65 E-4 P_∞ = 244	45	18,227	1.09 E12
	39.09	15,886	4.76 E11
	35	14,480	2.18 E11
	30	12,480	4.87 E10
Z = 131 ρ_∞ = 2.32 E-4 P_∞ = 122	43.21	16,390	3.86 E11
	38	15,210	1.61 E11
	35	13,880	8.72 E10
	30	12,030	1.90 E10
Z = 150 ρ_∞ = 9.29 E-5 P_∞ = 49	42	15,050	9.60 E10
	40	14,520	6.96 E10
	35	13,140	2.57 E10
	30	11,600	6.20 E9

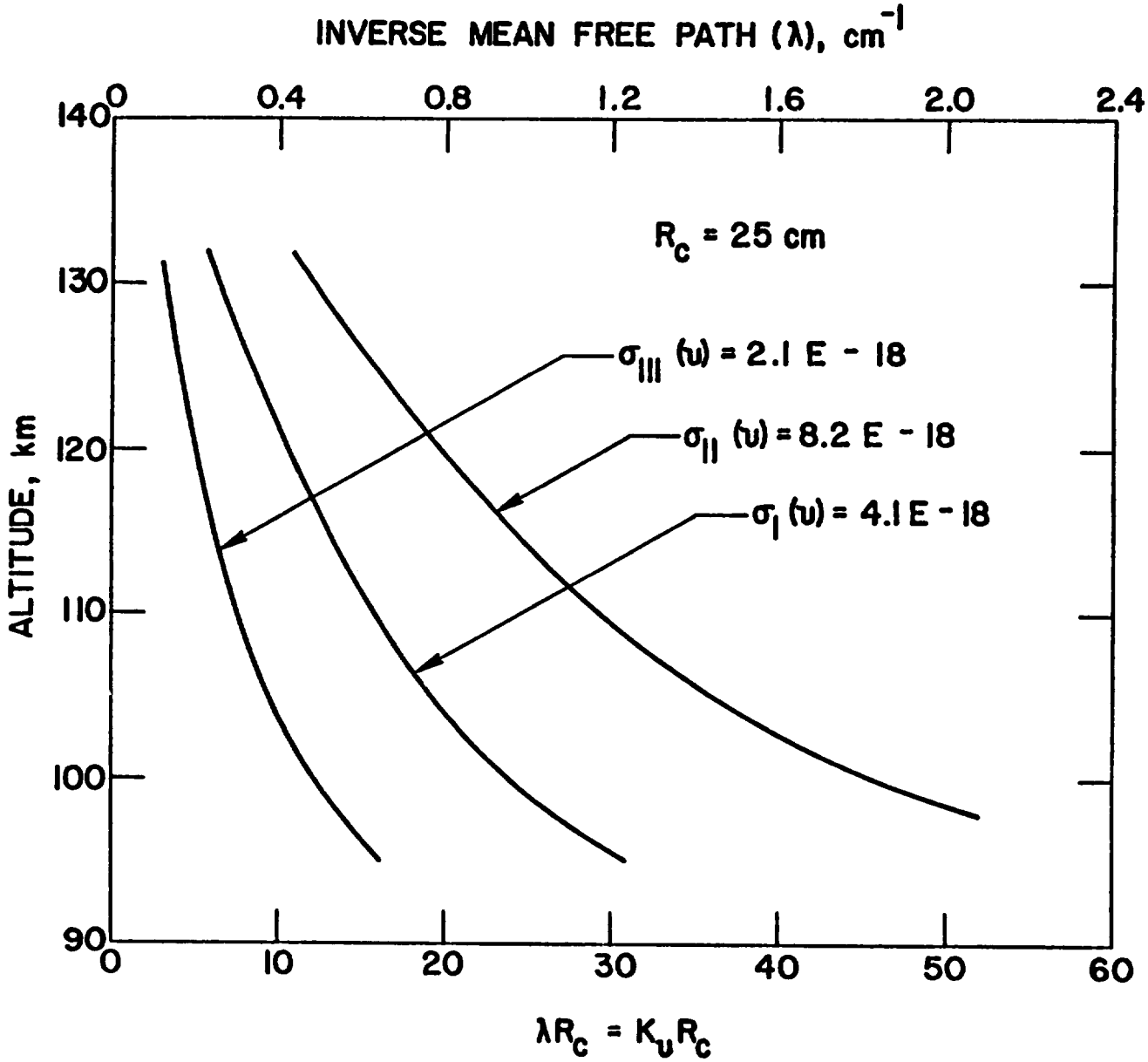

Figure 5.2. Inverse mean free path and ($2R_c$) as a function of altitude for the three regions of photoabsorption model.

Values of the intermediate functions a_ν and b_ν (defined by Eq. (2.24)) were calculated for the photoabsorption model at different altitudes. Since T_∞ is taken to be constant, the values of functions $(a_\nu V_\infty)$ and $(b_\nu V_\infty)$ were found to be constant for all altitudes. Another intermediate function, $\Lambda(\nu)$, is defined in Eqs. (3.14) and (4.5). For $\kappa_\nu R_c >> 1$, the expression for $\Lambda(\nu)$ can be written as

$$\Lambda(\nu_i) = (15/\pi^4)\, q(0)/\kappa_{\nu i}\, E_3(0)\, B(a_i, b_i) \tag{5.2}$$

The values of $\Lambda(\nu_i)$ were calculated for the three spectral range of the photoabsorption model and the results are illustrated in Fig. 5.3. For any altitude, the value of this function increases with increasing entry velocity.

The set of Eqs.(4.15)-(4.22) for spherically radiating source and Eqs. (4.23)-(4.26) for plane radiating source can be solved numerically to obtain the perturbation quantities. As mentioned earlier, for Jovian entry conditions, it is necessary to solve only the set of equations belonging to the plane radiating source case.

For multicomponent systems, it is physically realistic (and a general practice) to define the total enthalpy of the gas entering the shock layer by the relation

$$H_T = H_o + V^2/2 \tag{5.3}$$

In this equation, V represents the local fluid velocity, and H_o is referred to as the absolute enthalpy and is equal to the sum of sensible enthalpy and chemical energy at 0°K [34,35]. In terms of the perturbation velocity, the local fluid velocity is given by

$$V = V_\infty (1 + V_{1z}) \tag{5.4}$$

For a multicomponent system, the expression for H_o is given by

$$H_o = \sum_\alpha C_\alpha H_{o_\alpha} \tag{5.5}$$

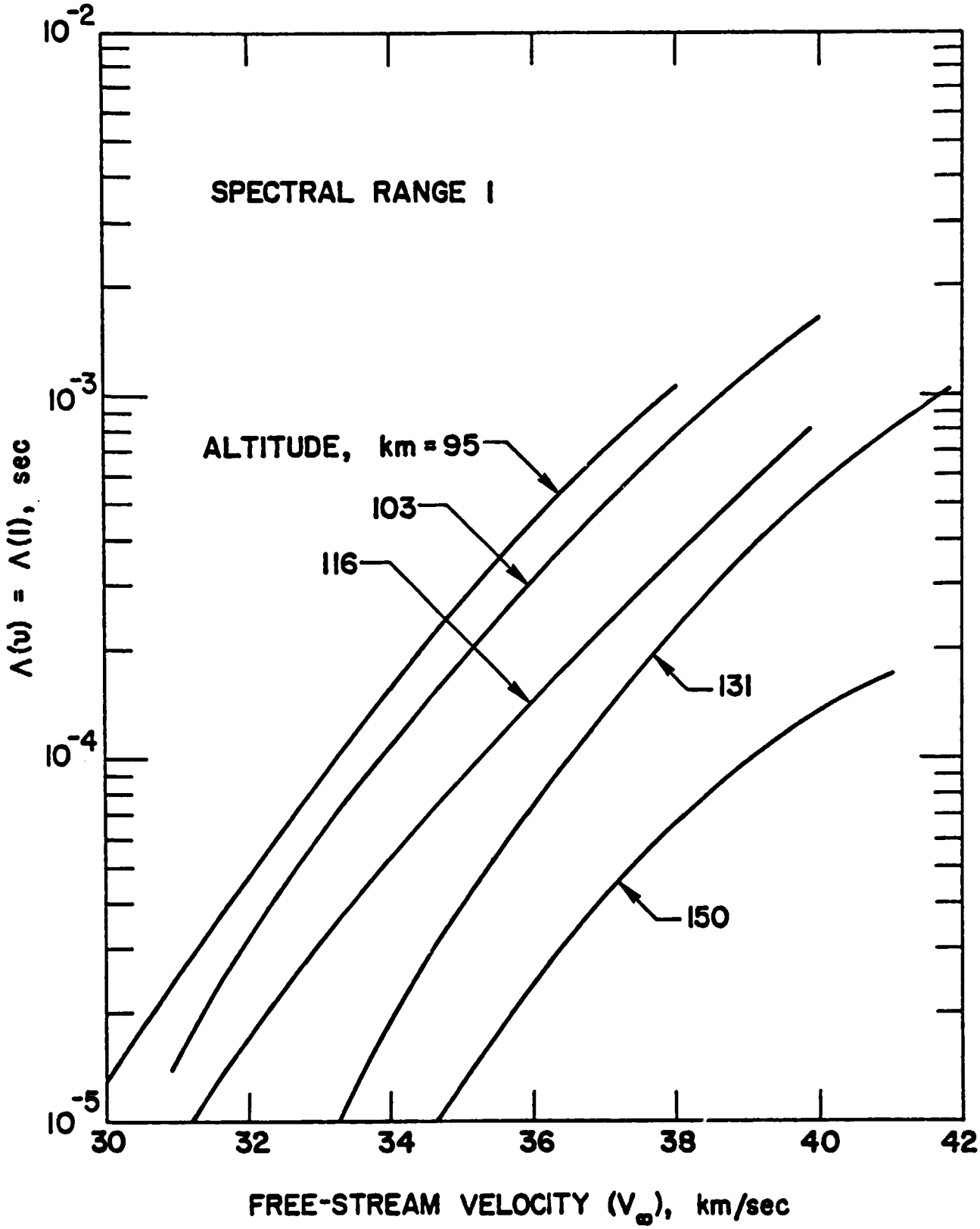

Figure 5.3a. $\Lambda(v)$ as a function of free-stream velocity for spectral range I.

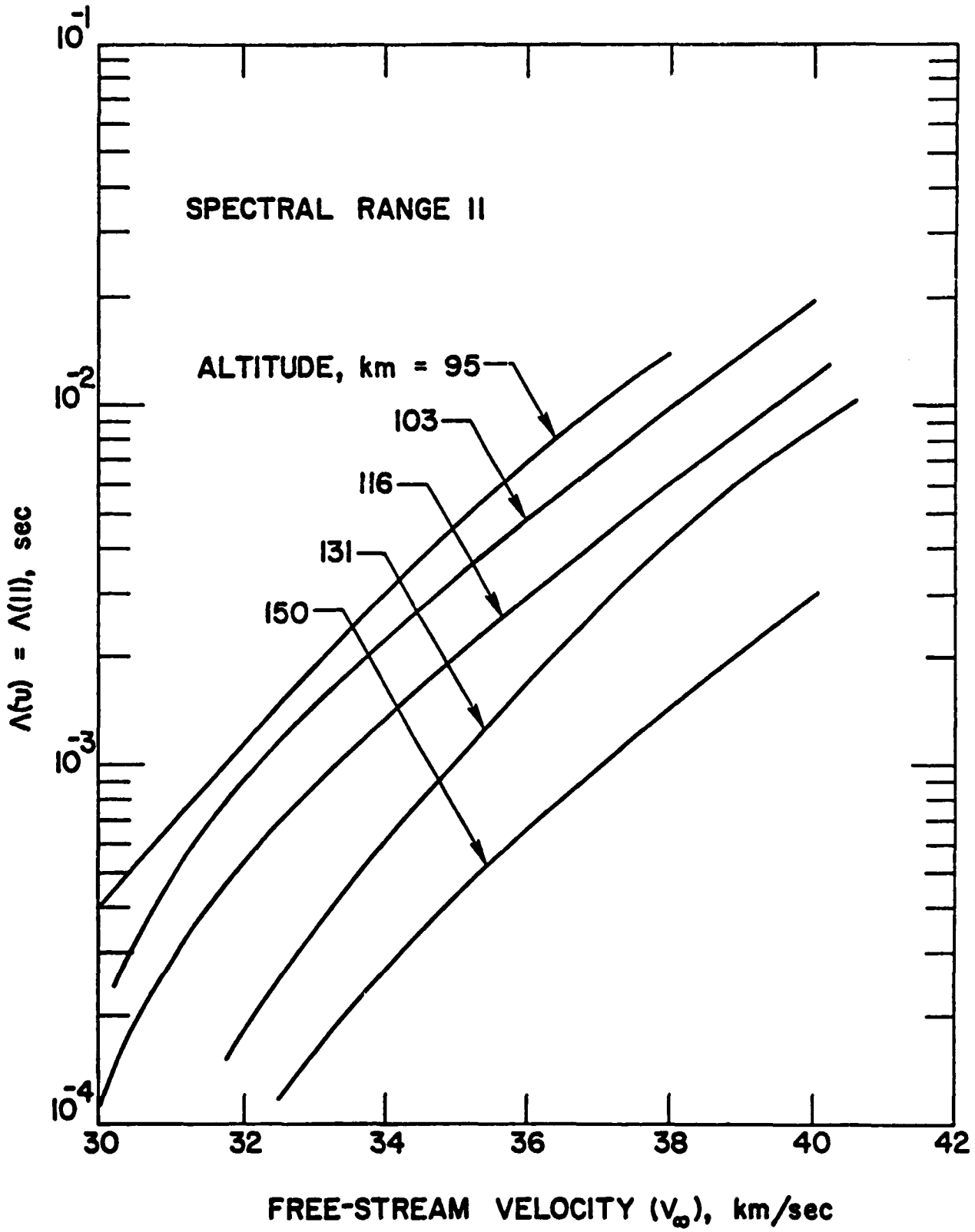

Figure 5.3b. $\Lambda(\nu)$ as a function of free-stream velocity for spectral range II.

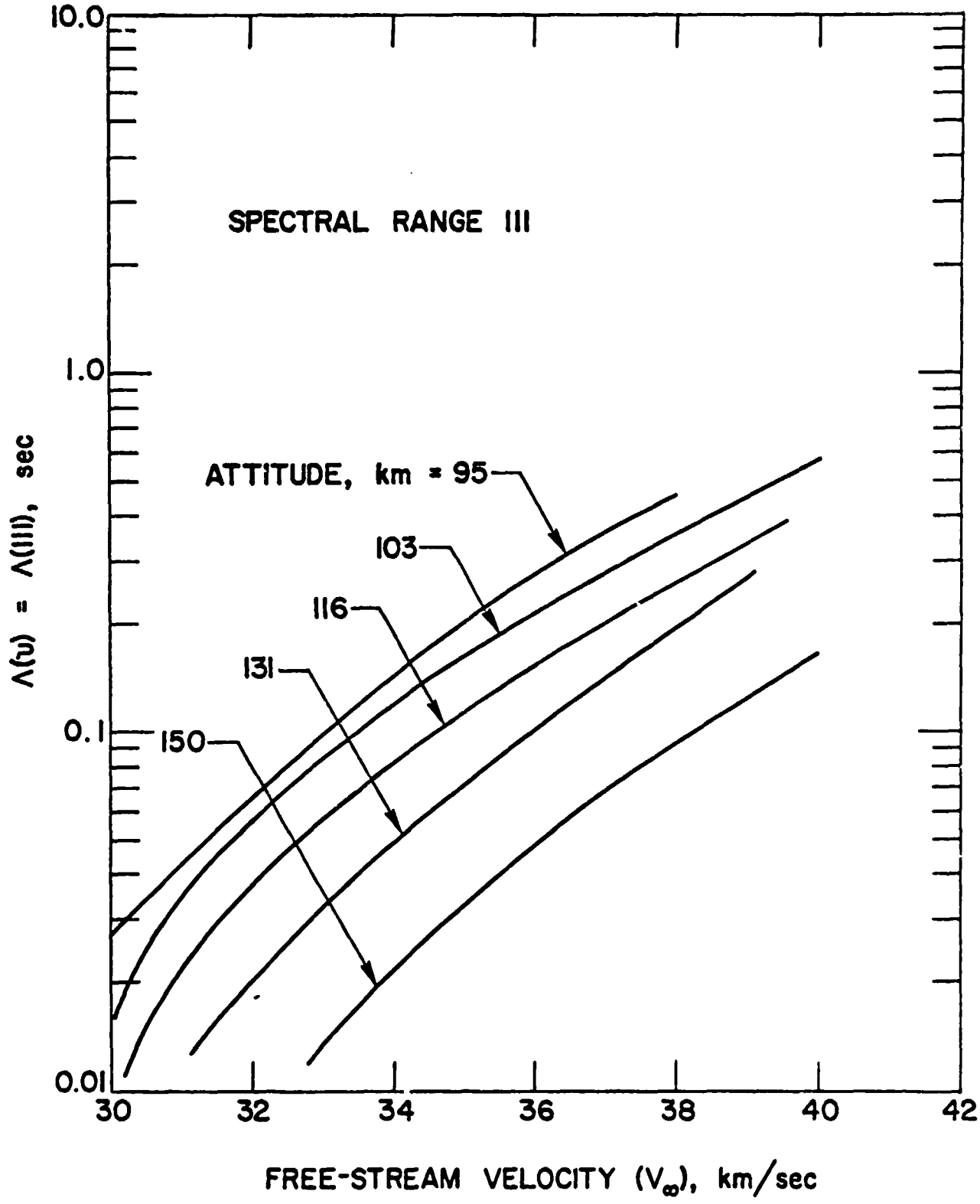

Figure 5.3c. $\Lambda(\nu)$ as a function of free-stream velocity for spectral range III.

where c_α is the mass fraction of species α. For any species α, the relation for H_{o_α} is given by [34,35]

$$H_{o_\alpha} = RT[a_1 + (a_2/2)T + (a_3/3)T^2 + (a_4/4)T^3 + (a_5/5)T^4 + a_6/T] \tag{5.6}$$

where R is the universal gas constant (= 1.98726 cal/mole - °K) and T is the local fluid temperature in °K. For different species, values of constants $a_1, a_2, \ldots a_6$ are given in [35], and for species under present investigation they are listed in Table 5.2.

It should be noted that values of H_T can be calculated by considering or neglecting the precursor effects. When precursor effects are considered, then H_T is defined by

$$H_T = (H_T)_{PE} = (H_o)_{PE} + V^2/2 \tag{5.7}$$

For the case with no precursor effects, H_T is given by

$$H_T = (H_T)_{NPE} = (H_o)_{NPE} + V_\infty^2/2 \tag{5.8}$$

It should be emphasized here that, for the case with no precursor effects, the temperature in Eq. (5.6) is the free-stream temperature T_∞.

The per cent difference in the total enthalpy with and without the precursor effects can be expressed by

$$\% = PD = \left\{[(H_T)_{PE} - (H_T)_{NPE}]/(H_T)_{NPE}\right\} \times 100 \tag{5.9}$$

It should be noted that an appropriate value of H_T is needed to determine the conditions inside the bow shock by employing the Rankine-Hugoniot relations.

Table 5.2. Temperature coefficients for thermodynamic functions for hydrogen species.

Substance	Temperature Interval, °K	Coefficients					
		a_1	a_2	a_3	a_4	a_5	a_6
H_2	1000 < T < 5000	3.0436897	6.1187110E-4	-7.3993551E-9	-2.0331907E-11	2.459379E-15	-8.5491002E2
	300 < T < 1000	2.8460849	4.1932116E-3	-9.6119332E-6	9.5122662E-9	-3.309342E-12	-9.6725372E2
H_2^+	1000 < T < 5000	3.3287156	2.5050678E-4	1.4224521E-7	-4.4590247E-11	3.733756E-15	1.7997470E5
	300 < T < 1000	2.817375	3.657610E-3	-7.9655480E-6	8.2614000E-9	-3.090228E-12	1.8002739E5
H	1000 < T < 5000	2.500	0	0	0	0	2.5470497E4
	300 < T < 1000	2.500	0	0	0	0	2.5470497E4

6. PERTURBATION RESULTS

The flow perturbation quantities V_{1z} , p_1 , C_H , $C_{H_2^+}$, T_1 , and H_{T_1} were calculated numerically and the results are illustrated in Figs. 6.1 - 6.12. In Figs. 6.1 - 6.6, perturbation quantities are shown as a function of distance from the shock for different altitudes and a constant entry velocity of 35 km/sec. The first set of curves (Figs. 6.1a - 6.6a) are plotted against the nondimensional distance z/R_c , while the second set (Figs. 6.1b-6.6b) are plotted as a function of the physical distance z from the shock. In Figs. 6.7 - 6.12, the perturbation quantities (just ahead of the bow shock) are illustrated as a function of the free-stream velocities. Since $\rho_1 = -V_{1z}$, separate results were not illustrated for the density perturbation. From these figures it is evident that the magnitude of perturbation quantities, in general, depend on the distance from the shock, altitude of entry, and entry speeds.

Figures 6.1 - 6.6 show that at a fixed entry velocity, the perturbation effects are greater for lower altitudes and at locations just ahead of the shock. This, however, would be expected because the number densities of participating species are greater at lower altitudes and at these altitudes most radiative energy from the shock gets absorbed in the immediate vicinity of the shock front. At higher altitudes, perturbation effects are significant to a larger distance from the shock front. This is because, at these altitudes, the number densities of participating species are small and radiation effects are felt farther into the free-stream.

Specific results presented in Figs. 6.1b - 6.6b indicate that use of the small perturbation theory is justified in determining the velocity, density, mass fraction and total enthalpy variations. These variations are small because at high entry speeds, the gas has not had enough time for expanding.

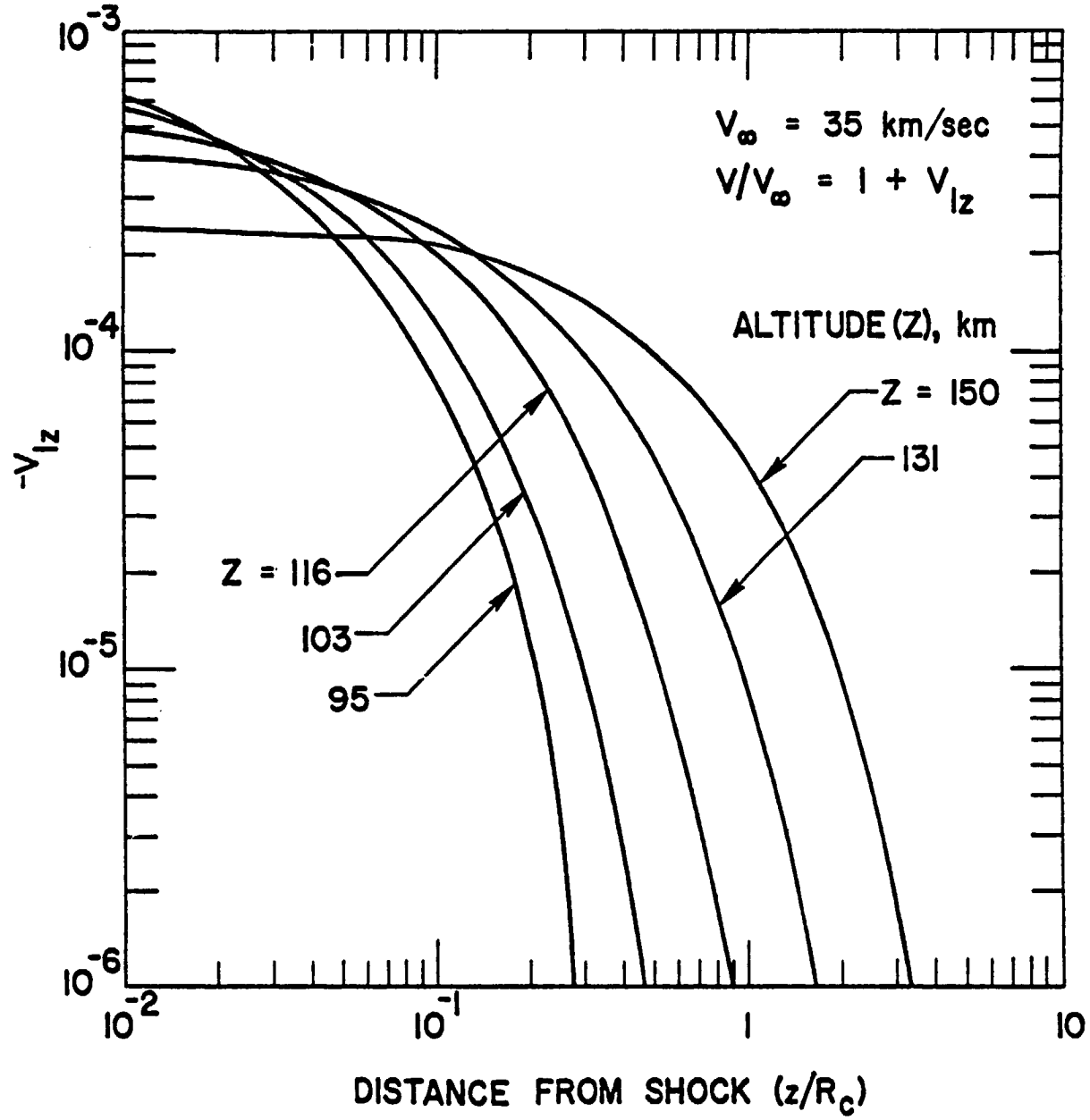

Figure 6.1a. Velocity perturbation as a function of distance from the shock at different altitudes and a constant free-stream velocity.

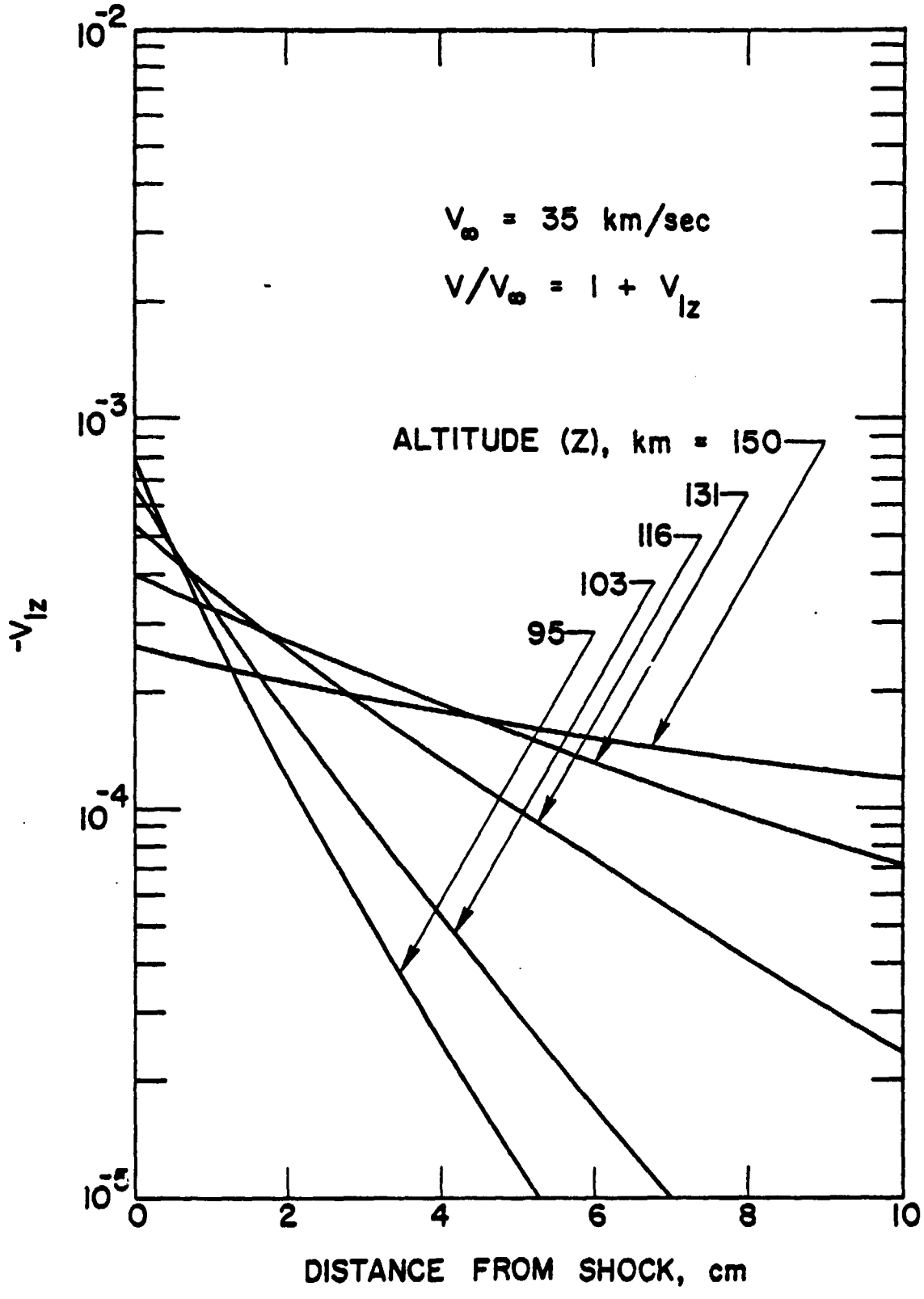

Figure 6.1b. Velocity perturbation as a function of distance from the shock at different altitudes and a constant free-stream velocity.

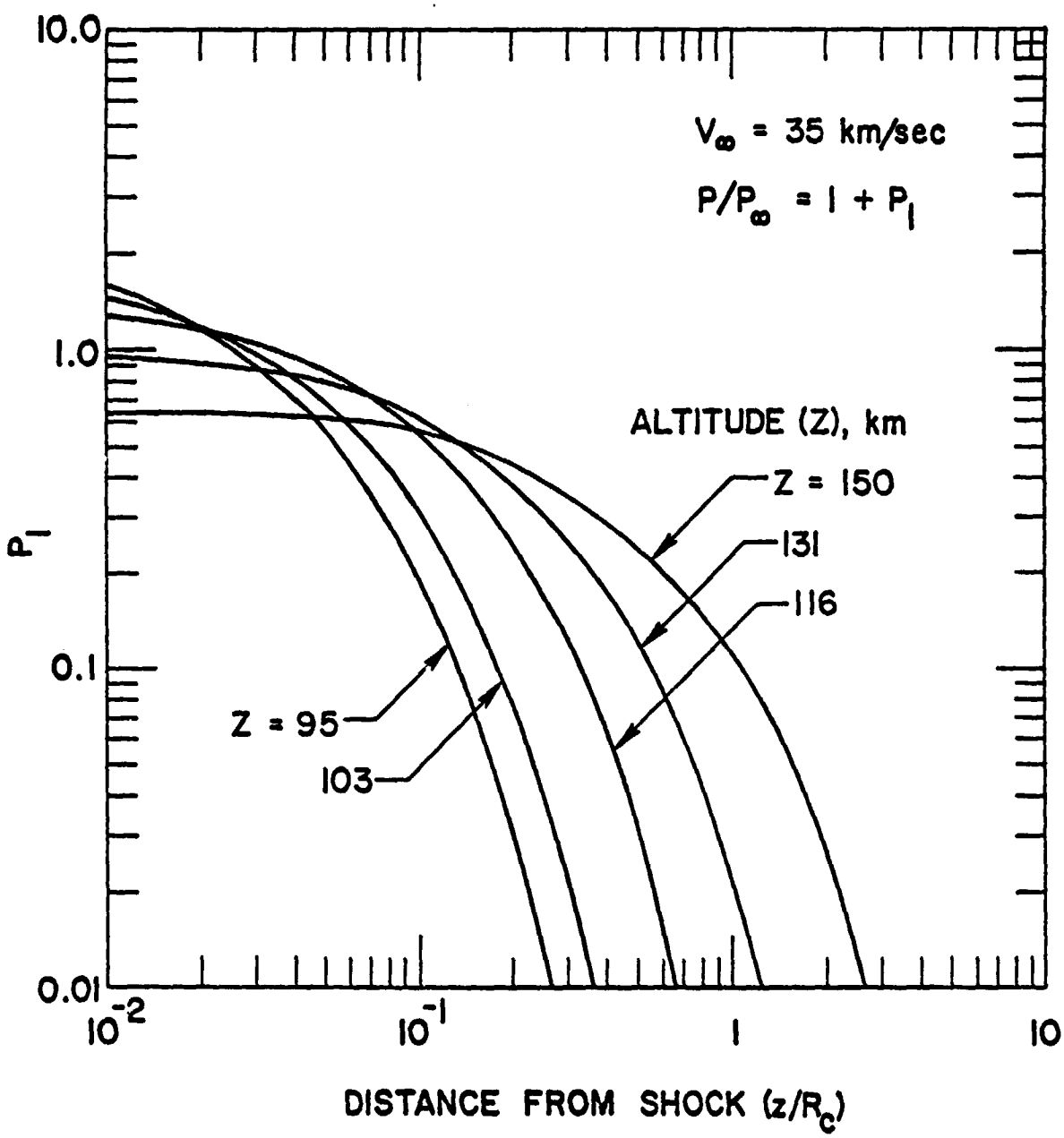

Figure 6.2a. Pressure perturbation as a function of distance from the shock at different altitudes and a constant free-stream velocity.

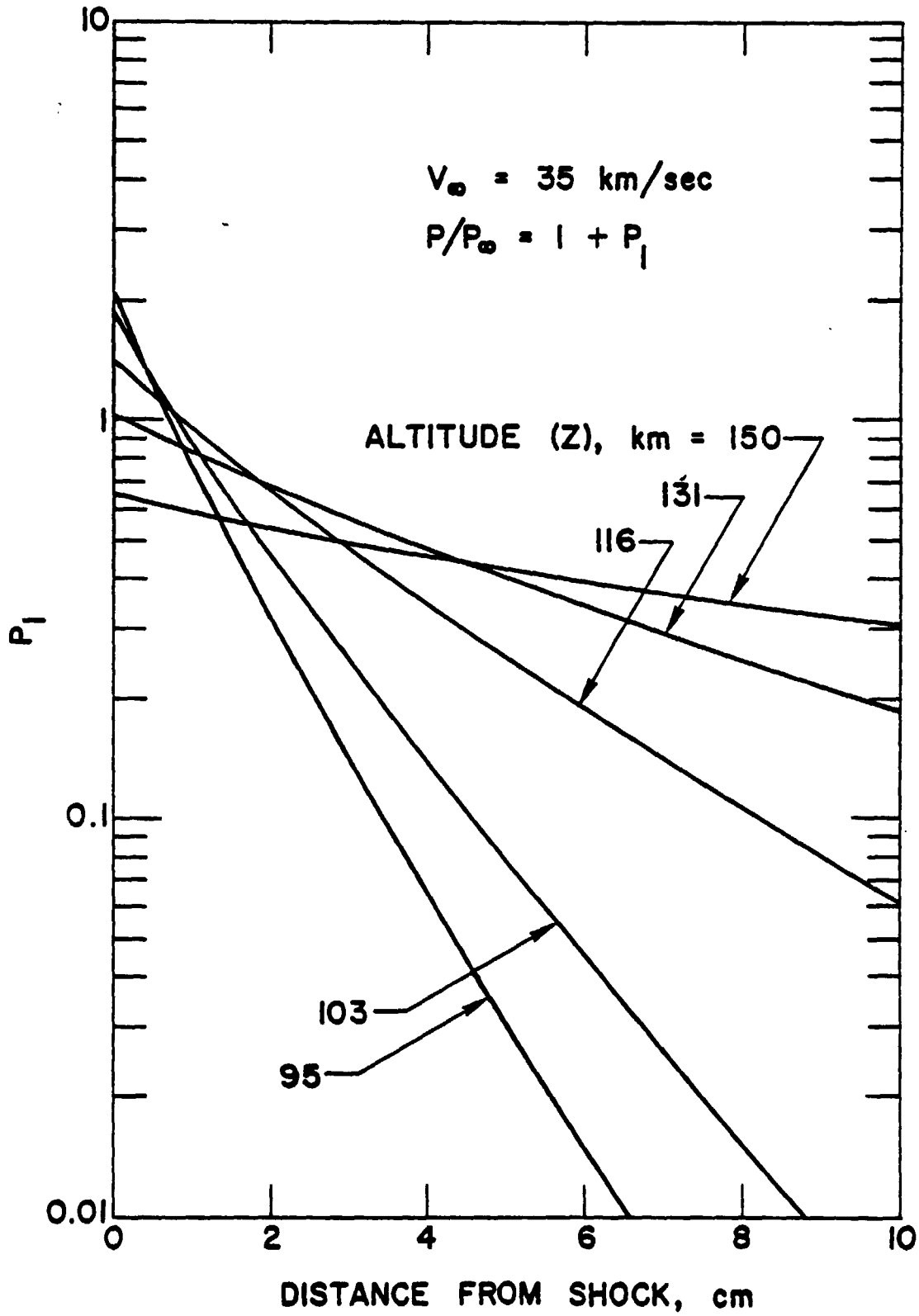

Figure 6.2b. Pressure perturbation as a function of distance from the shock at different altitudes and a constant free-stream velocity.

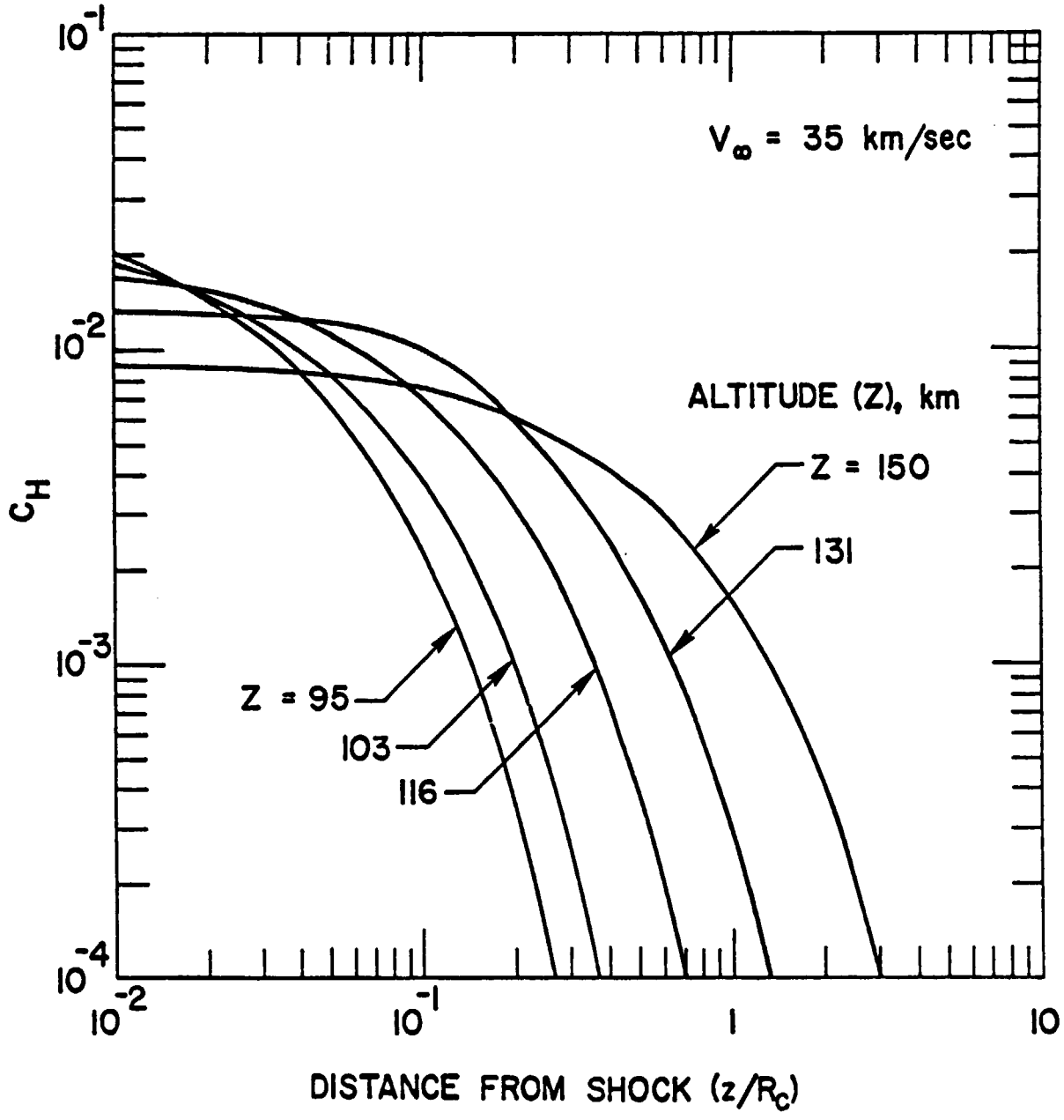

Figure 6.3a. Mass fraction of H as a function of distance from the shock at different altitudes and a constant free-stream velocity.

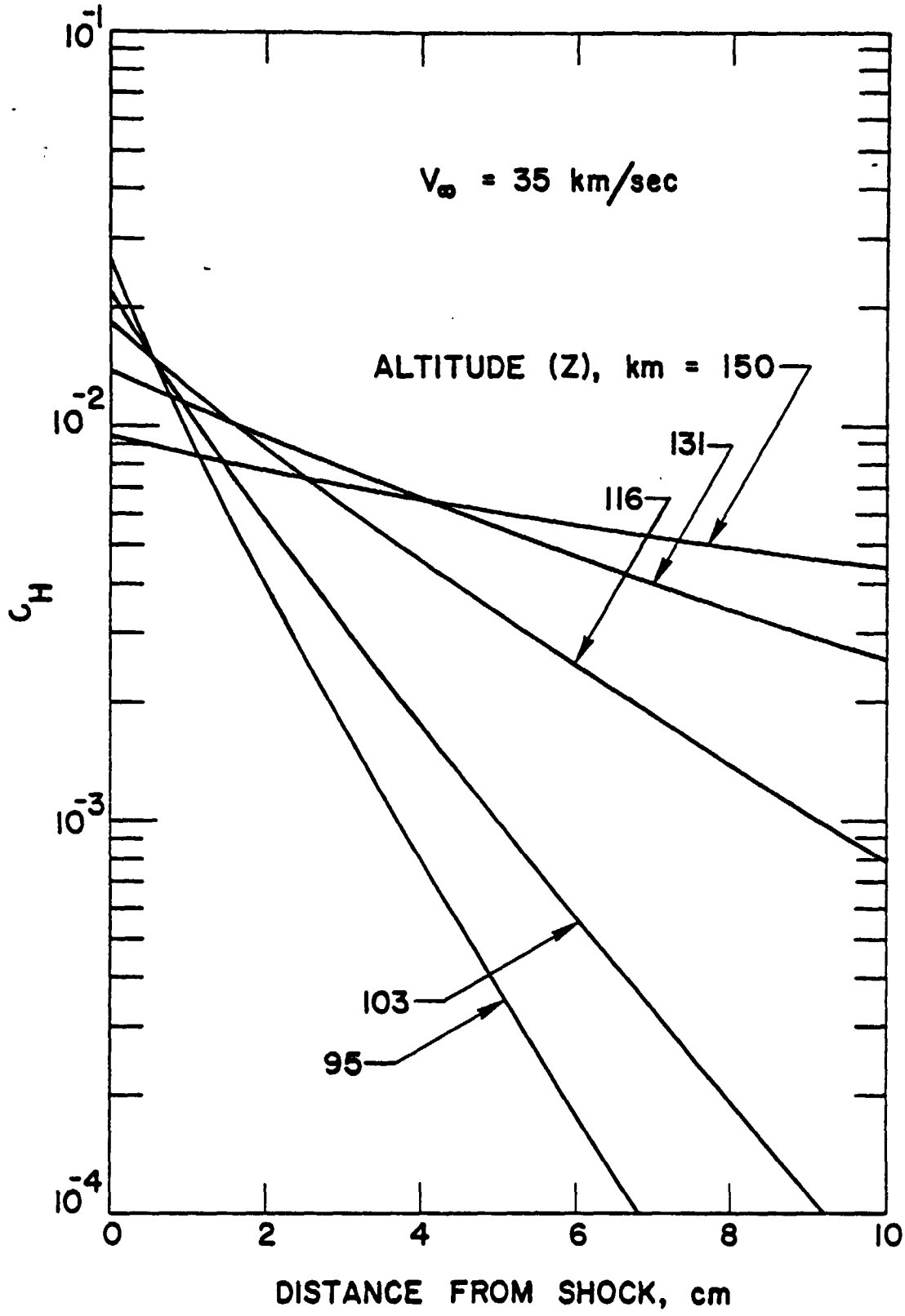

Figure 6.3b. Mass fraction of H as a function of distance from the shock at different altitudes and a constant free-stream velocity.

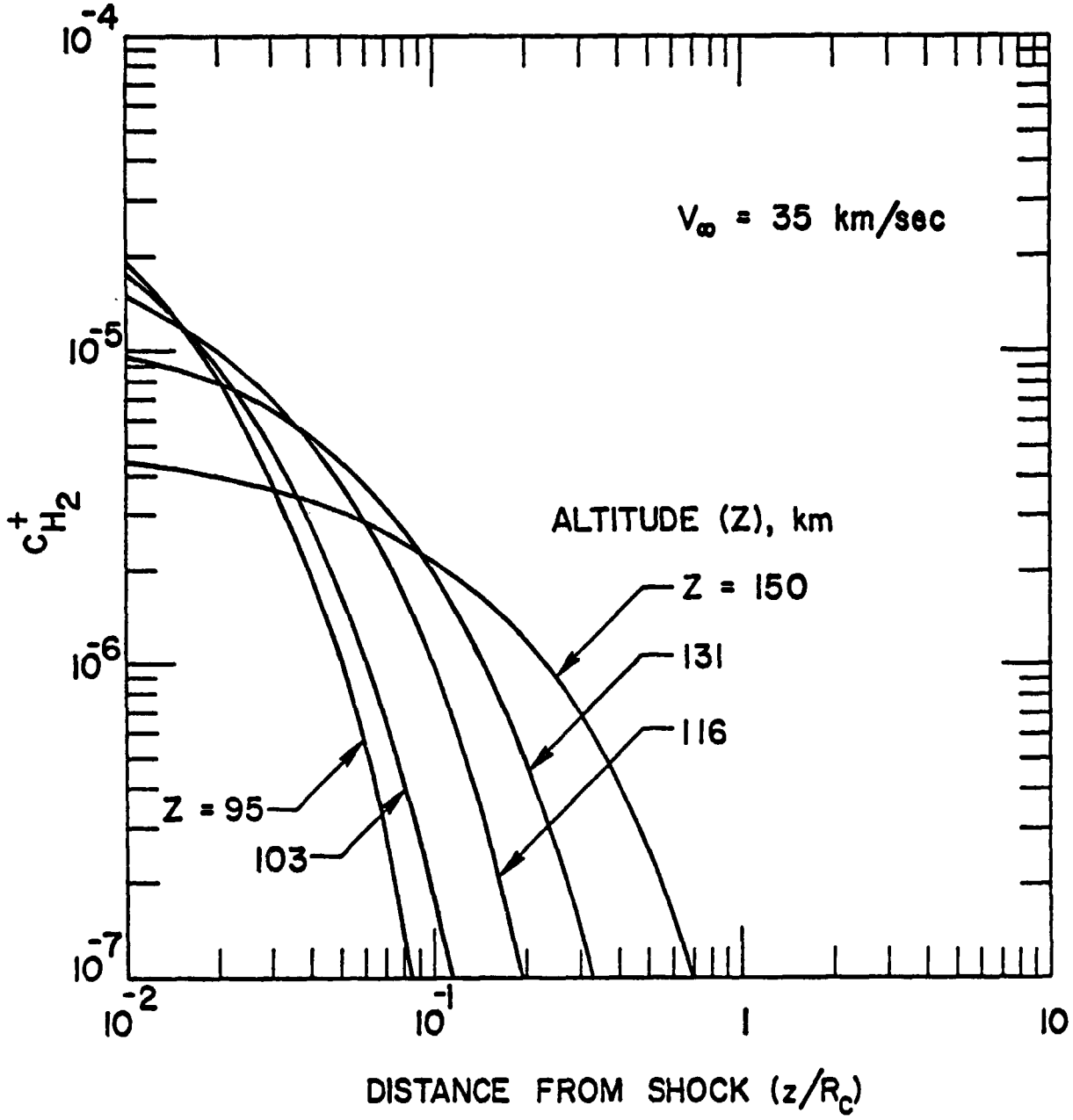

Figure 6.4a. Mass fraction of H_2^+ as a function of distance from the shock at different altitudes and a constant free-stream velocity.

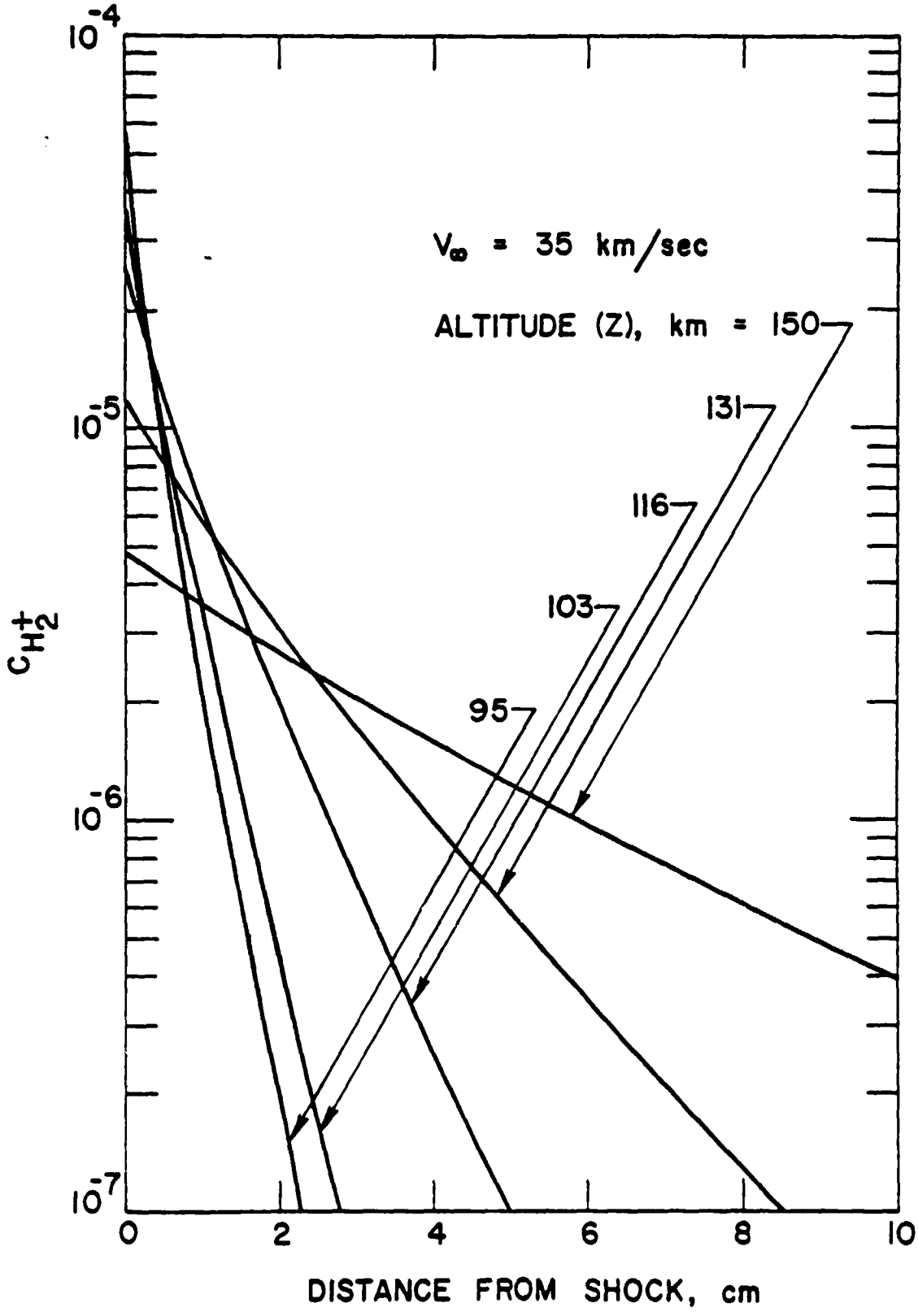

Figure 6.4b. Mass fraction of H_2^+ as a function of distance from the shock at different altitudes and a constant free-stream velocity.

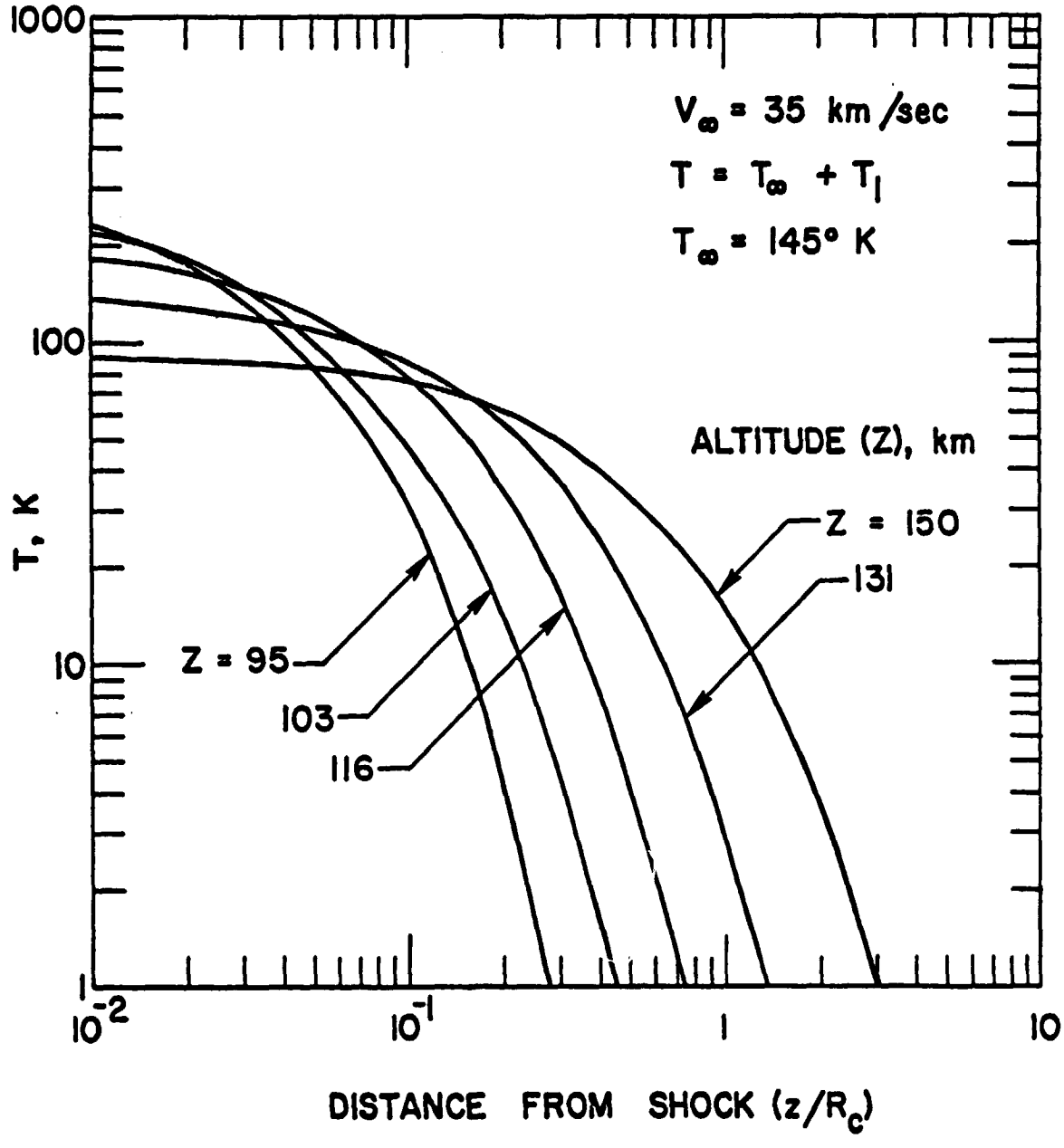

Figure 6.5a. Temperature perturbation as a function of distance from the shock at different altitudes and a constant free-stream velocity.

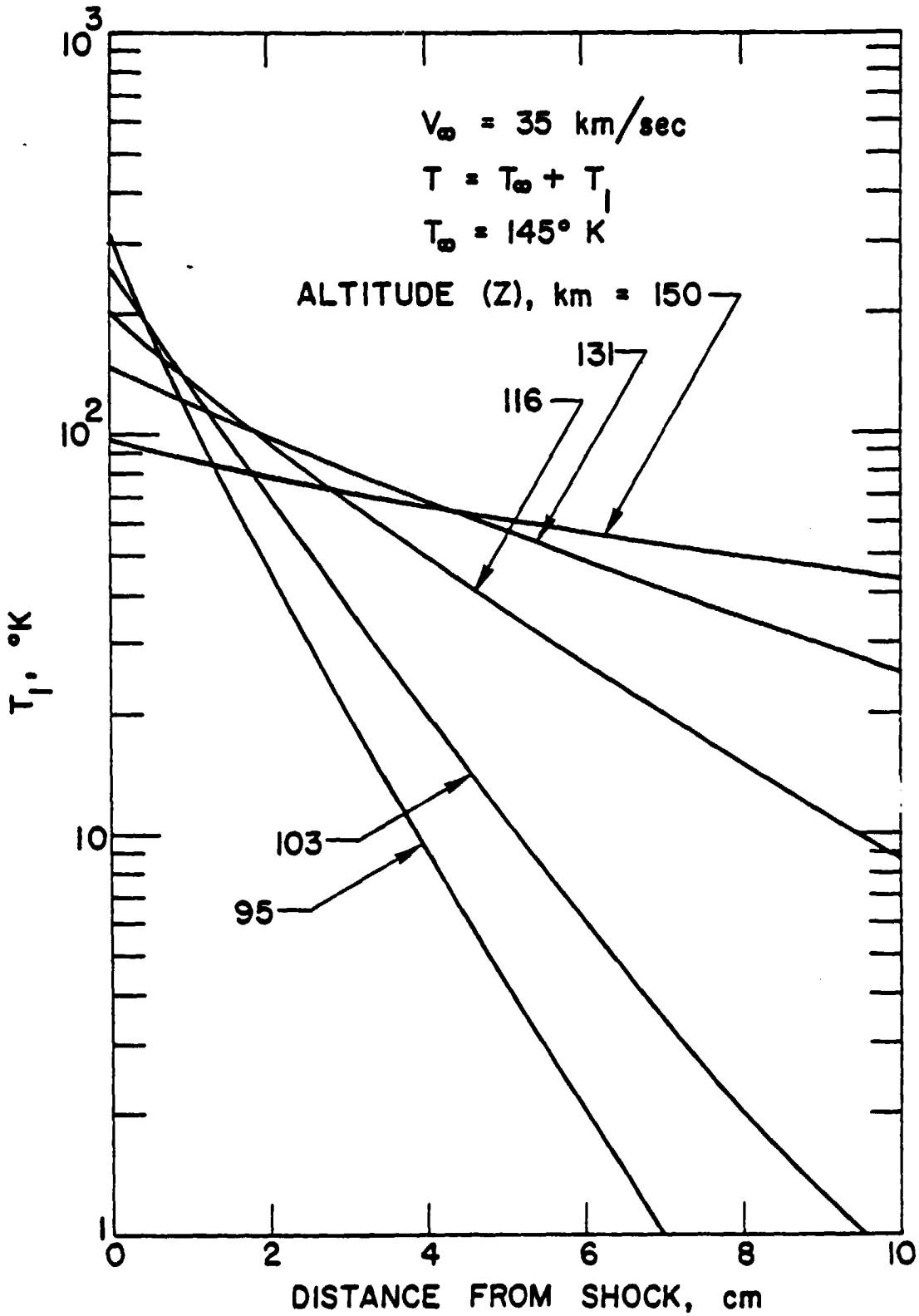

Figure 6.5b. Temperature perturbation as a function of distance from the shock at different altitudes and a constant free-stream velocity.

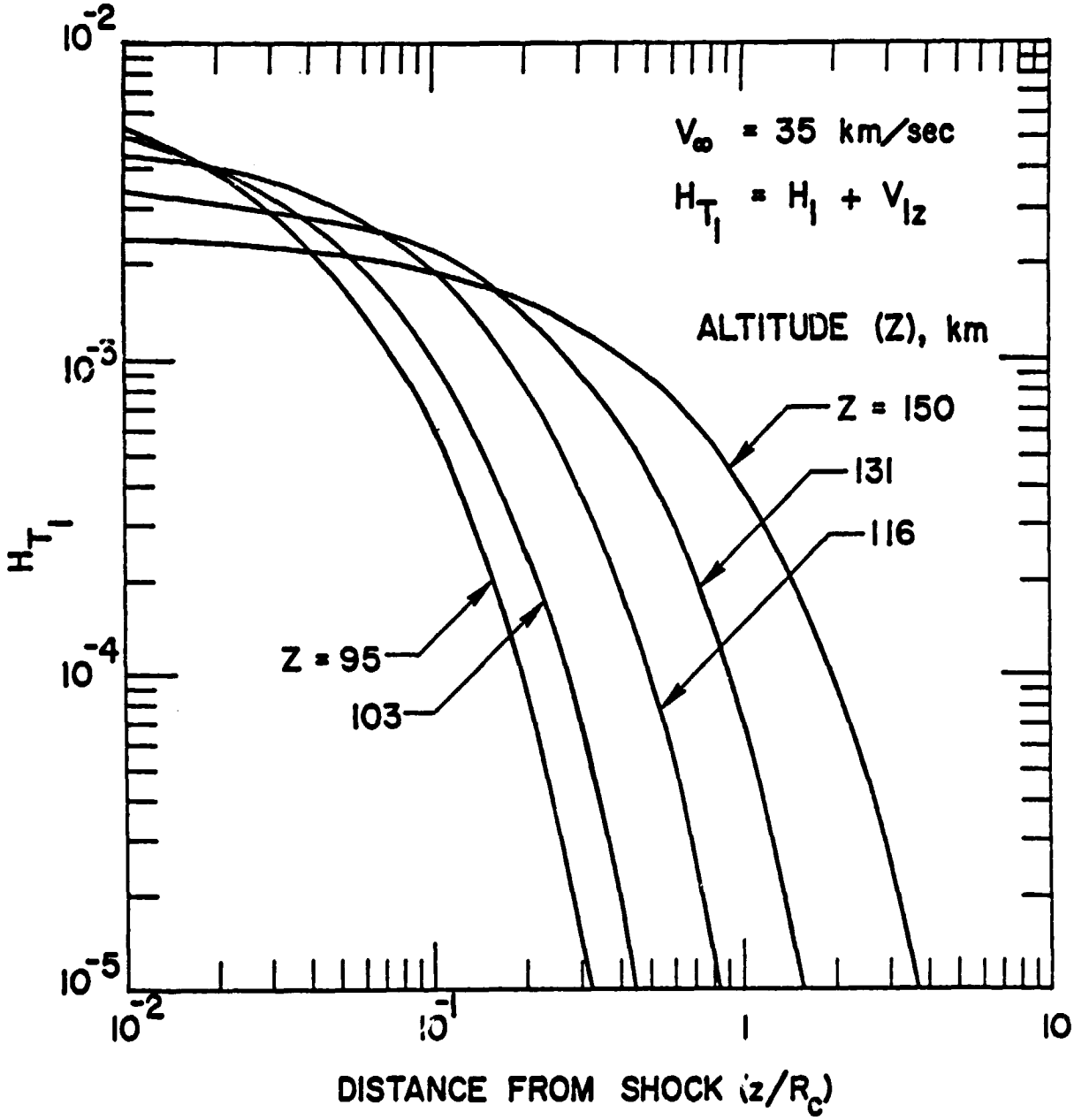

Figure 6.6a. Specific total enthalpy perturbation as a function of distance from the shock at different altitudes an a constant free-stream velocity.

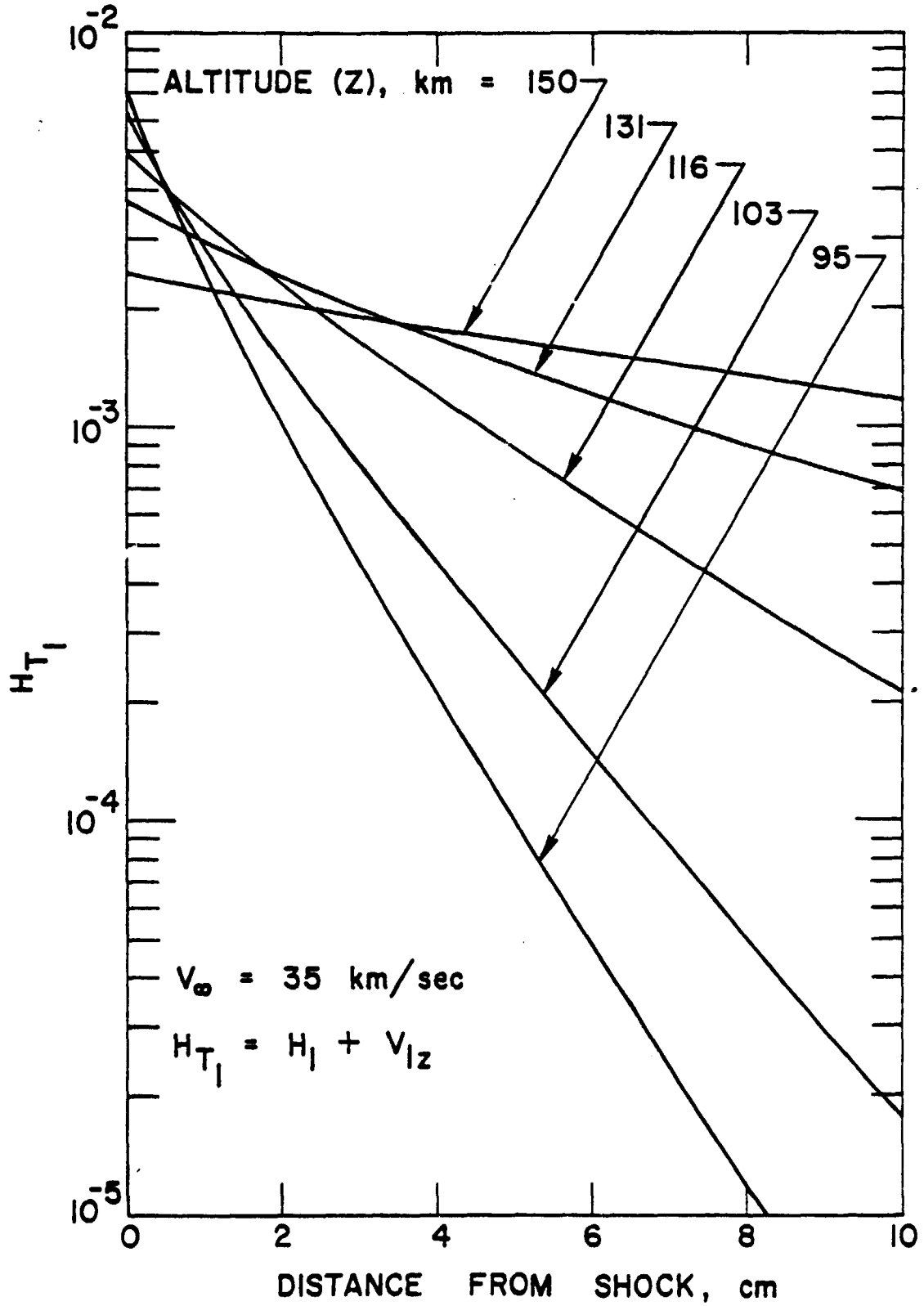

Figure 6.6b. Specific total enthalpy perturbation as a function of distance from the shock at different altitudes and a constant free-stream velocity.

For example, just ahead of the shock, the value of (V/V_∞) is 0.9992 for $Z = 95$ km and is equal to 0.99975 for $Z = 150$ km. Similarly, $H_{T_1} = 6.8 \times 10^{-3}$ for $Z = 95$ km and $H_{T_1} = 2.4 \times 10^{-3}$ for $Z = 150$ km (i.e., 0.68% increase in total enthalpy at 95 km and 0.24% increase at 150 km). The static pressure and temperature variations, however, cannot be considered small This is because for $Z = 95$ km, $p_1 = 2$ and $T_1 = 300°K$, and for $Z = 150$ km, $p_1 = 0.64$ and $T_1 = 94°K$. For these variations, therefore, one could question the validity of the small perturbation theory.

For different altitudes of entry, perturbation results (just ahead of the shock) are illustrated in Figs. 6.7 - 6.12 as a function of entry velocities. The results are shown only for the range of entry velocities for which free-stream and shock conditions are available (see Table 5.1). These results again indicate that the perturbation effects are greater for lower altitudes. As would be expected, for any specific altitude, the effects are larger for higher entry velocities. This is a direct consequence of greater radiative energy transfer from the shock to the free-stream at high entry speeds. For the most part, variations in the velocity, mass fractions, and total enthalpy again are seen to be small. For example, for an entry body at an altitude of 95 km, the total enthalpy of the gas (H_{T_1}) entering the shock wave is increased from about 0.68% at $V = 35$ km/sec to 1% at $V = 38$ km/sec. For $Z = 150$ km, however, H_{T_1} increases from 0.24% at 35 km/sec to 0.66% at 42 km/sec. The variations in the static pressure and temperature, in some cases, are seen to be several times greater than the ambient values. These large variations, however, occur for conditions where dissociation is high and the validity of the entire theory is questionable [11,12]. This point is discussed further in the next section.

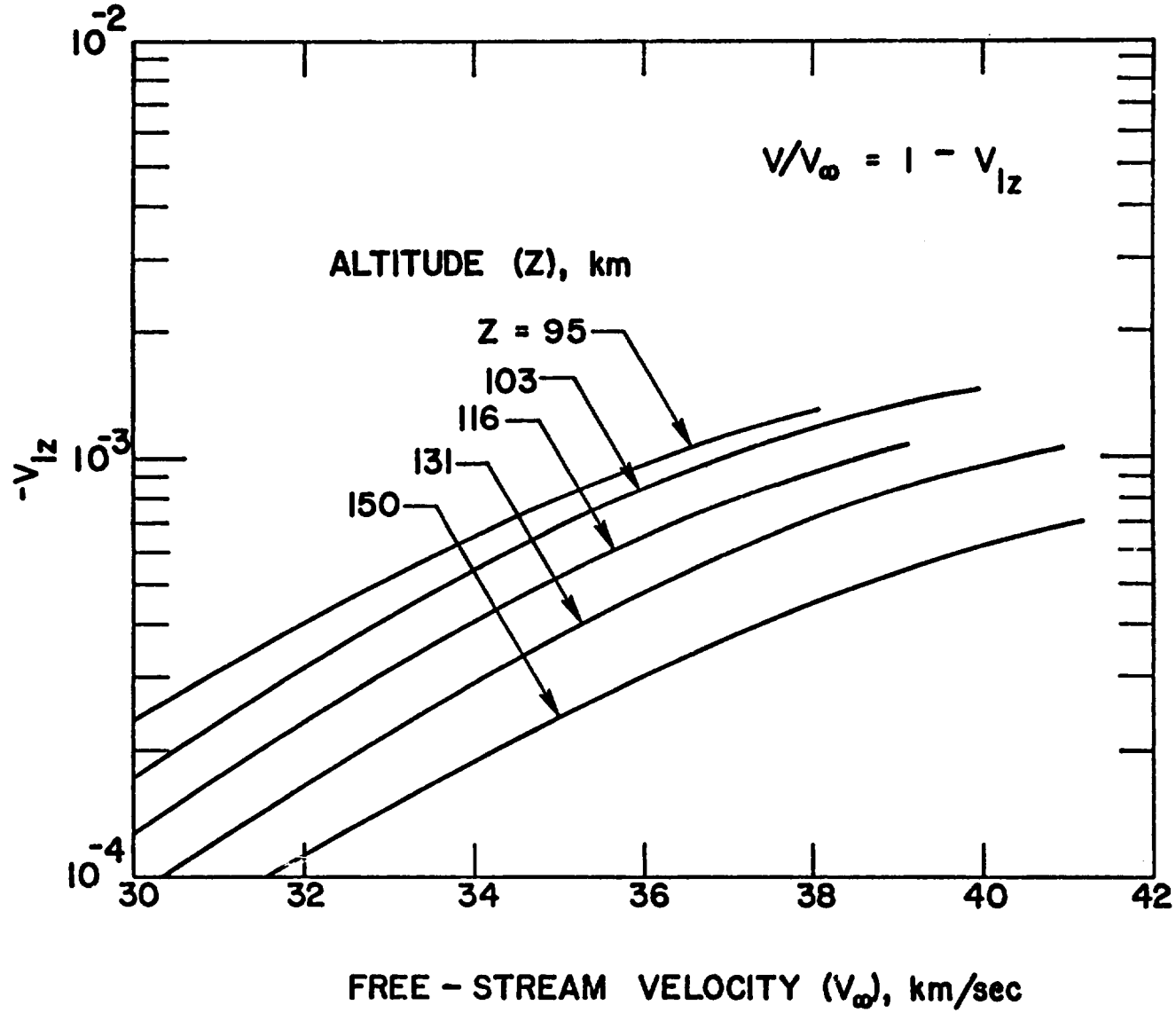

Figure 6.7. Velocity perturbation (just ahead of the shock) as a function of free-stream velocity for constant altitudes.

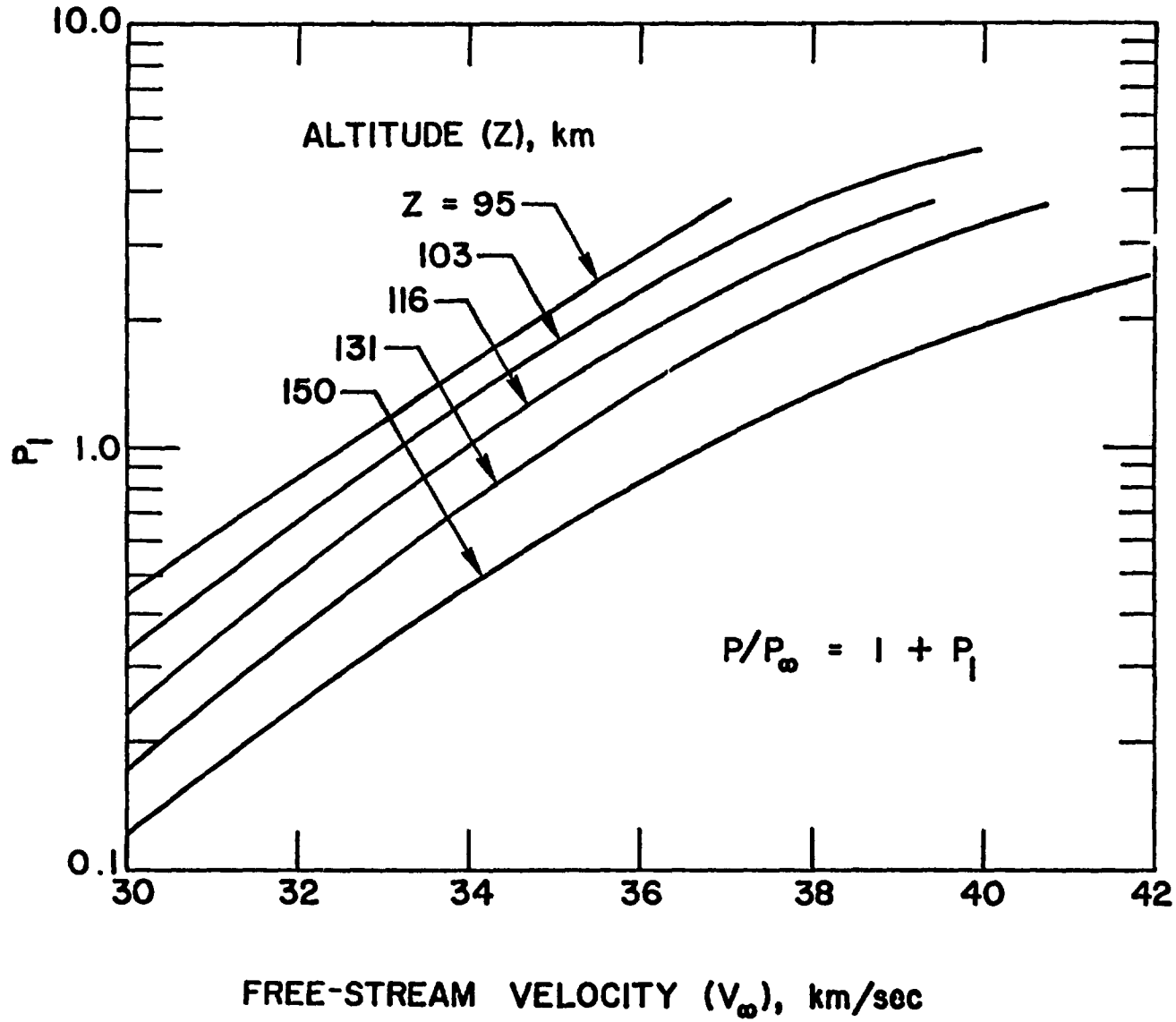

Figure 6.8. Pressure perturbation (just ahead of the shock) as a function of free-stream velocity for constant altitudes.

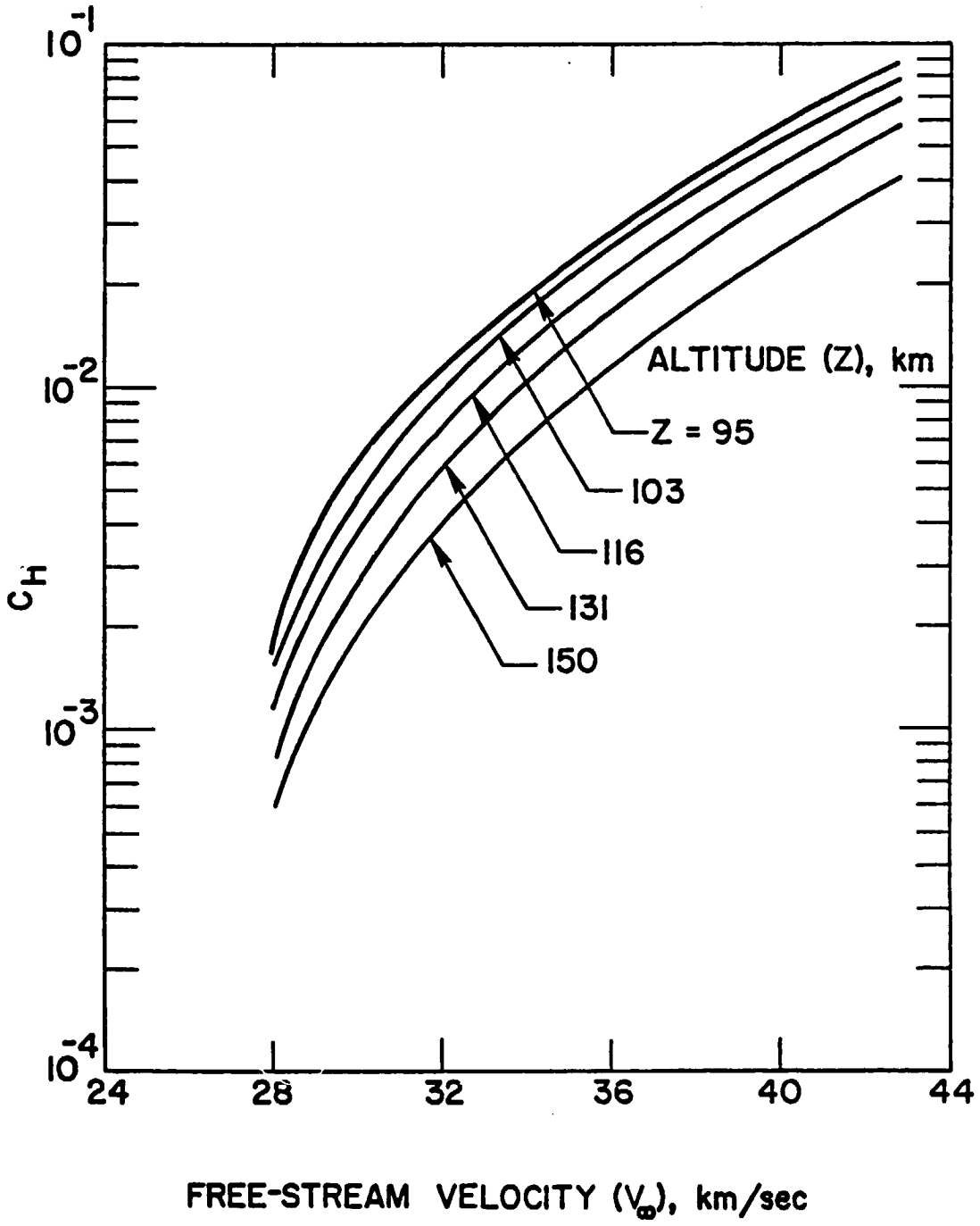

Figure 6.9. Mass fraction of H (just ahead of the shock) as a function of free-stream velocity for constant altitudes.

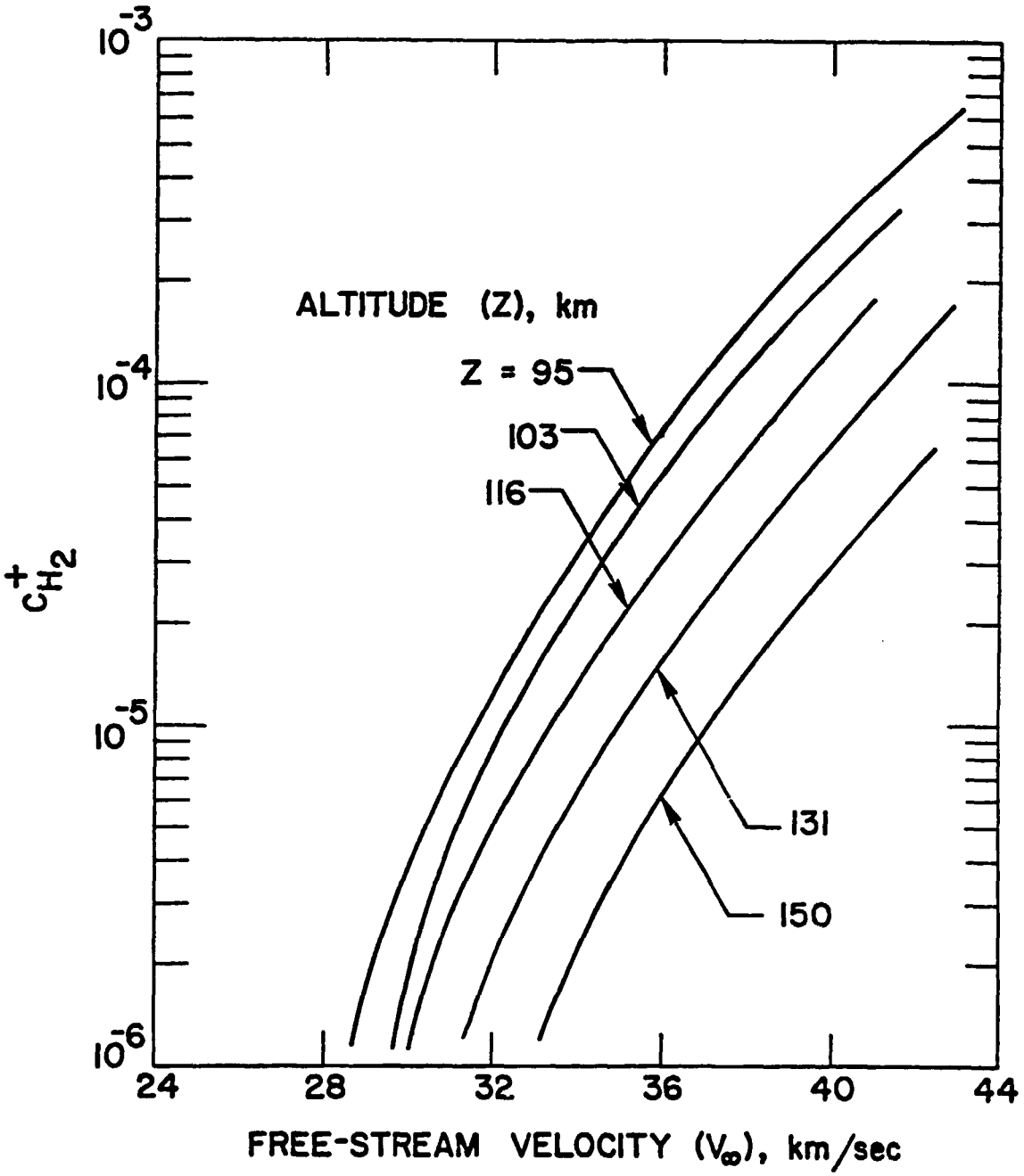

Figure 6.10. Mass fraction of H_2^+ (just ahead of the shock) as a function of free-stream velocity for constant altitudes.

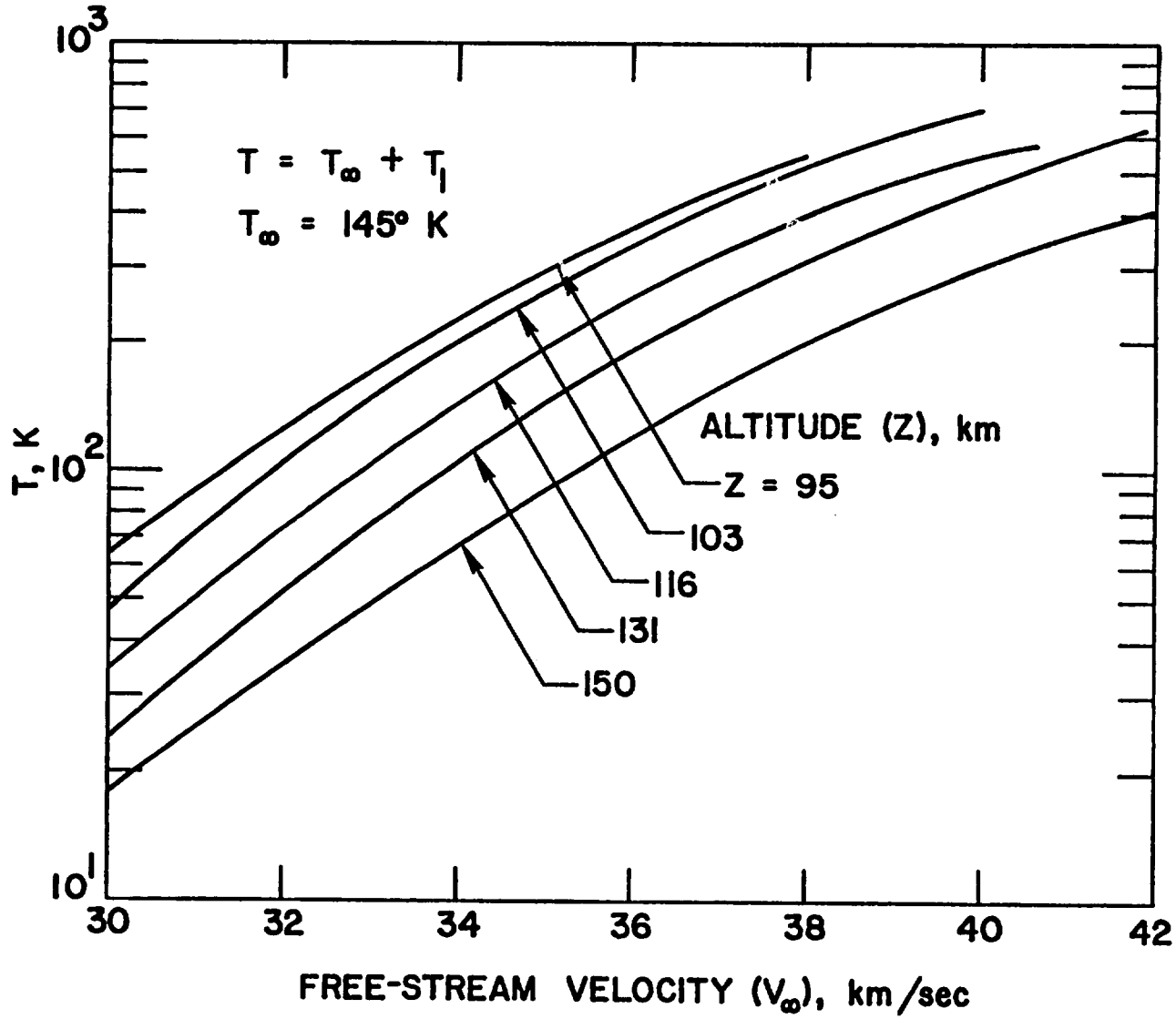

Figure 6.11. Temperature perturbation (just ahead of the shock) as a function of free-stream velocity for constant altitudes.

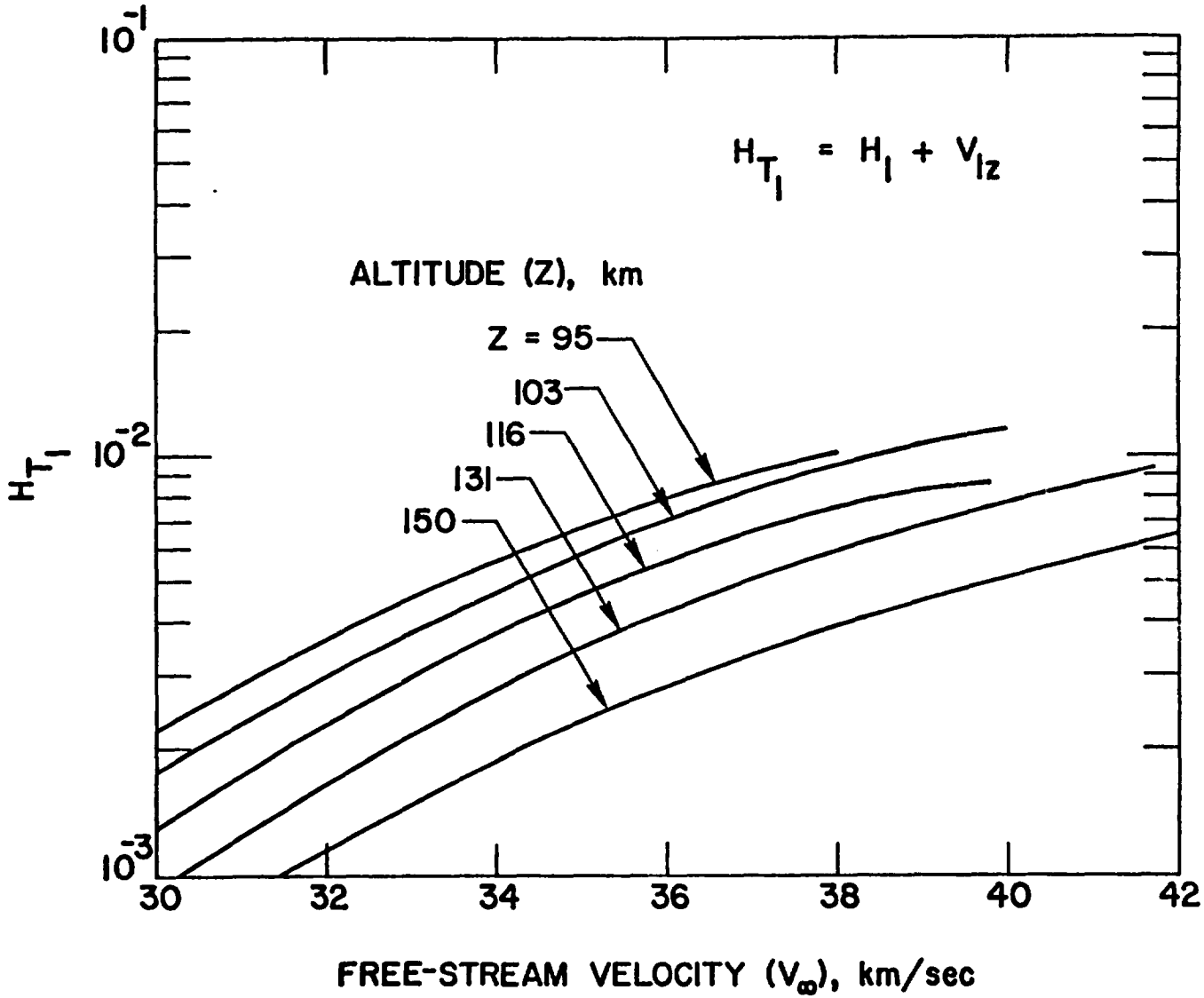

Figure 6.12. Specific total enthalpy perturbation (just ahead of the shock) as a function of free-stream velocity for constant altitudes.

The results of absolute enthalpy (as defined by Eqs. (5.5) and (5.7)) are plotted in Fig. 6.13 as a function of free-stream velocities. The trend of results of this figure are essentially the same as for specific total enthalpy perturbation results shown in Fig. 6.12. This again illustrates that the increase in enthalpy due to precursor absorption are greater for lower altitudes and higher entry velocities.

The per cent difference in total enthalpy of the gas (with and without precursor effects) entering the shock wave is illustrated in Fig. 6.14 for different altitudes. The results indicate that the maximum increase in total enthalpy is about 1.6% for $Z = 95$ km and entry speeds of 38 km/sec. For other entry conditions, the changes are seen to be smaller.

A few conclusions can be drawn from the results presented in this section. Within the limitations of the small perturbation technique used in this study, the results indicate that variations in velocity, density, species concentration, and enthalpy are small as compared to perturbations in pressure and temperature. Precursor effects, in general, are greater for lower altitudes and higher entry velocities. At higher altitudes, however, precursor effects are felt farther in the free-stream. At any particular altitude, the effects increase with increasing entry velocities. Specific results indicate that for Jovian entry velocities lower than 28 km/sec and altitudes of entry higher than 95 km, the precursor effects definitely can be neglected. For other entry conditions, the extent of flow perturbations and its influence on the entire flow field ahead of the entry body should be investigated.

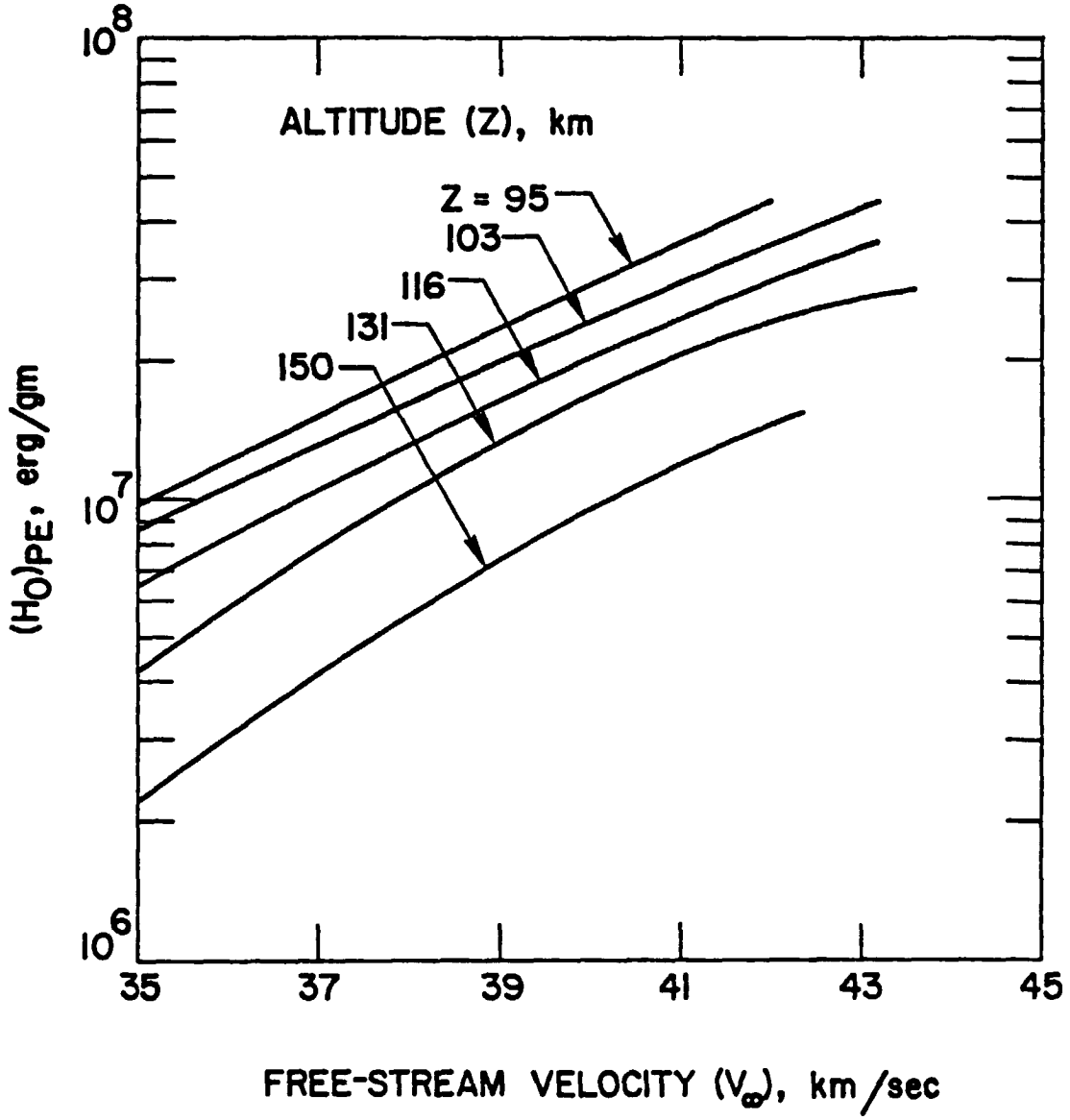

Figure 6.13. Absolute enthalpy (just ahead of the shock) as a function of free-stream velocity for constant altitudes.

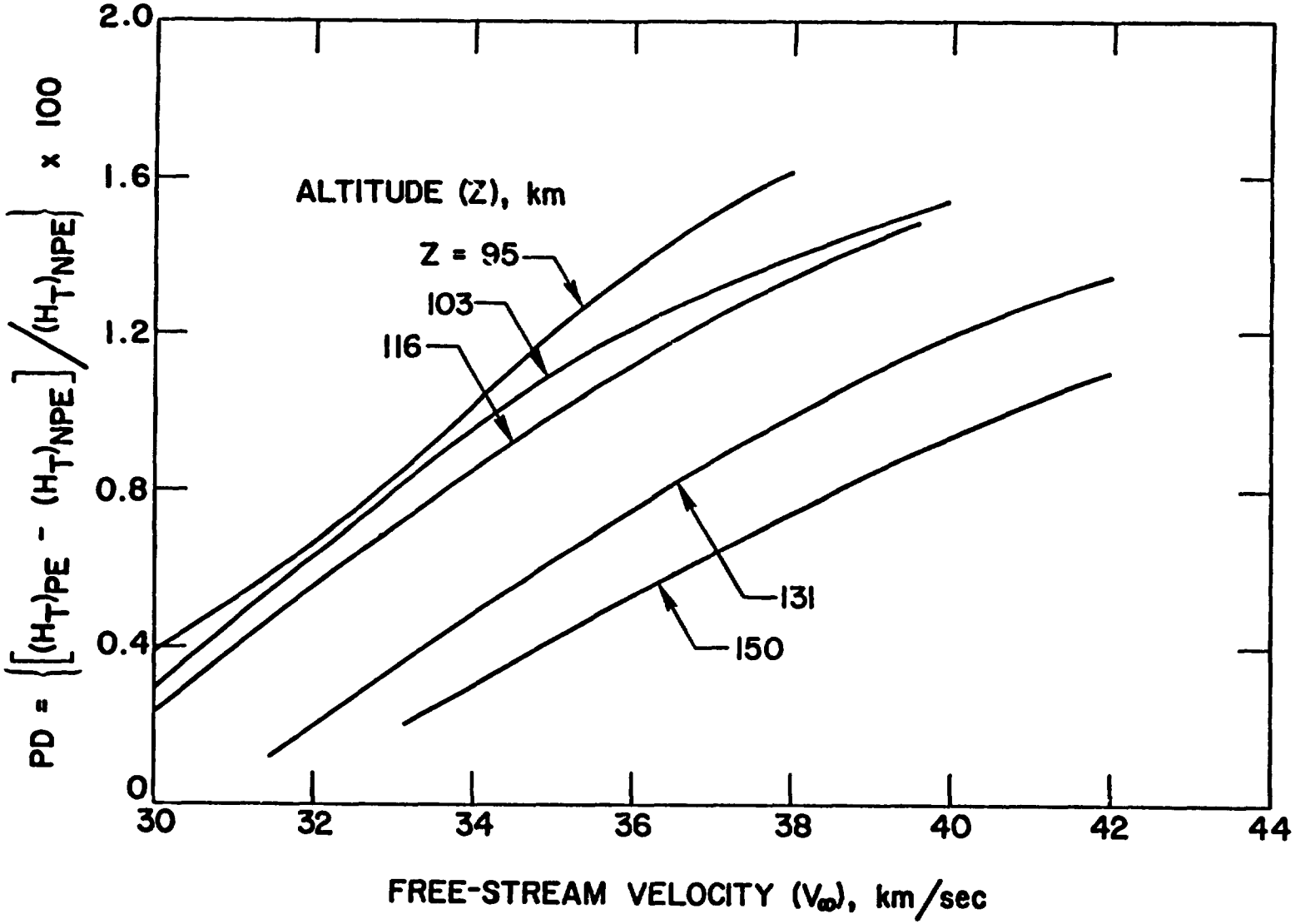

Figure 6.14. Increase in total enthalpy (just ahead of the shock) as a function of free-stream velocity for constant altitudes.

7. ALTERNATE APPROACH: THIN-LAYER APPROXIMATION

Another approach to investigate the precursor effects will be to apply the concept of thin shock layer theory (usually applied to hypersonic shock layer flows [36,37]) to the precursor region flow field. For this purpose, a curvilinear orthogonal coordinate system, shown in Fig. 7.1, is selected. In this figure s is the distance (measured from the stagnation point) along a reference surface (body or shock) and n the distance along the normal to this surface. For convenience, the reference surface is taken to be the outer edge of the shock layer.

The differential equations for a hypersonic plane or axisymmetric flow can be written in the present coordinate system as [36]

$$(\partial/\partial s)(\rho u r^j) + (\partial/\partial n)(\rho v X r^j) = 0 \tag{7.1a}$$

$$\rho[u(\partial u/\partial s) + Xv(\partial u/\partial n) - Kuv] + (\partial p/\partial s) = 0 \tag{7.1b}$$

$$\rho[u(\partial v/\partial s) + Xv(\partial v/\partial n) + Ku^2] + X(\partial p/\partial n) = 0 \tag{7.1c}$$

$$\rho[(u/X)(\partial H/\partial s) + v(\partial H/\partial n)] + (Xr^j)^{-1}\,[(\partial/\partial n)(Xr^j q_R)] = 0 \tag{7.1d}$$

$$\rho[(u/X)(\partial C_\alpha/\partial s) + v(\partial C_\alpha/\partial n) - K_\alpha = 0 \tag{7.1e}$$

where $K = K(s) = 1/R_s$, $X = 1 + Kn$, and $j = o$ for plane flows and 1 for axisymmetric flows.

If the precursor region is assumed thin, then one can make the approximations that $(n/R_s) << 1$, $\partial/\partial s << \partial/\partial n$, and r^j is not a function of n . In this case $X = 1$, and Eqs. (7.1) reduce to

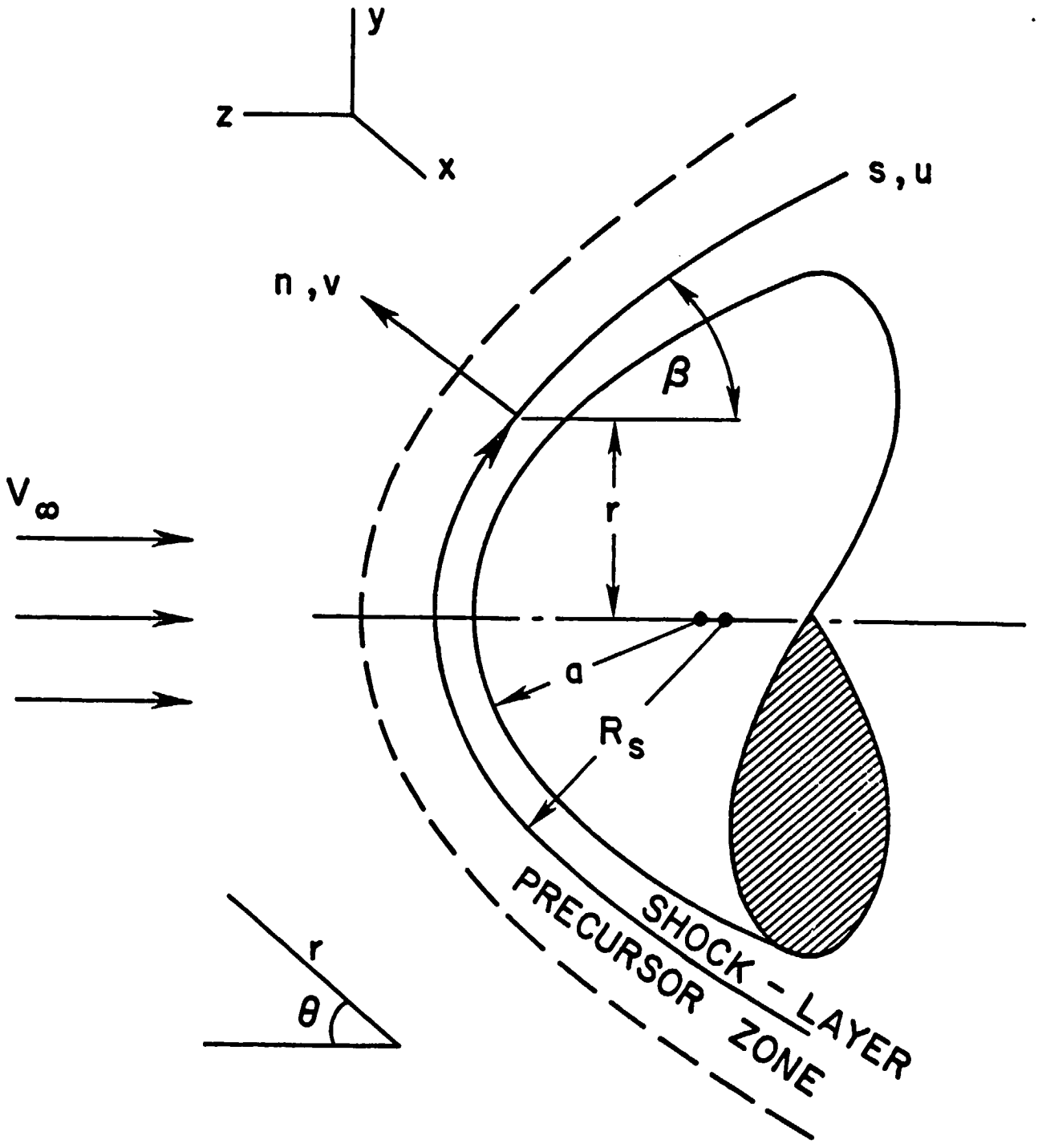

Figure 7.1. Curvilinear orthogonal coordinate systems for thin-layer approximation.

$$(\partial/\partial n)(\rho v) = 0 \tag{7.2a}$$

$$\rho v(\partial u/\partial n) = 0 \tag{7.2b}$$

$$\rho v(\partial v/\partial n) + (\partial p/\partial n) = 0 \tag{7.2c}$$

$$\rho v(\partial H/\partial n) + (\partial q_R/\partial n) = 0 \tag{7.2d}$$

$$\rho v(\partial C_\alpha/\partial n) - K_\alpha = 0 \tag{7.2e}$$

Direct integration of these results in

$$\rho v = \rho_\infty v_\infty \tag{7.3a}$$

$$\rho_\infty v_\infty (u - u_\infty) = 0 \tag{7.3b}$$

$$\rho_\infty v_\infty (v - v_\infty) + (p - p_\infty) = 0 \tag{7.3c}$$

$$\rho_\infty v_\infty (H - H_\infty) + q_R = 0 \tag{7.3d}$$

$$\rho_\infty v_\infty (\partial C_\alpha/\partial n) - K_\alpha = 0 \tag{7.3e}$$

where it has been assumed that $q_{R_\infty} = o$.

In present application to the hydrogen-helium atmosphere, Eq. (7.3e) will be written for atomic hydrogen and hydrogen ions. In Eq. (7.3d), H represents the total enthalpy and is given by the relation

$$H = H_T = h + (u^2 + v^2)/2 \tag{7.4}$$

where

$$h = 1.527\ RT + [(5/4)RT + I/2]C_{H_2} + [(3/4)RT + D]C_H \tag{7.5}$$

Note that Eq. (7.5) is slightly different than the relation for perturbation enthalpy given by Eq. (2.17).

For a diffuse nonreflecting shock front, the expression for one-dimensional spectral radiative flux and its spatial derivative is given by [24,38]

$$q_{R\nu}(\tau_\nu) = 2\,\varepsilon_\nu\, e_{b\nu}(T_s)\, E_3(\tau_\nu) + 2\int_o^{\tau_\nu} e_{b\nu}(t)\, E_2(\tau_\nu - t)dt \tag{7.6}$$

$$-dq_{R\nu}/d\tau_\nu = 2\,\varepsilon_\nu\, e_{b\nu}\,(T_s)\, E_2(\tau_\nu) - 2\, e_{b\nu}(T) + 2\int_o^{\tau_\nu} e_{b\nu}\,(t)\, E_1(\tau - t)dt \tag{7.7}$$

where

$$\tau_\nu = \int_o^n \kappa_\nu\, dn' \tag{7.8}$$

$$e_{b\nu}(T) = \pi\, B_\nu(T) = \pi(2h/c^2)\left\{\nu^3/[\exp(h\,/kT) - 1]\right\} \tag{7.9}$$

It should be noted that these equations do not account for any radiation from the free-stream. As before, if the number density of H_2 is assumed constant, then in the above equations κ_ν becomes independent of position.

The expression for total radiative flux is given by

$$q_R(n) = \int_o^\infty q_{R\nu}\,(\tau_\nu)d\nu \tag{7.10}$$

For a gray shock front, a combination of Eqs. (7.6) and (7.10) results in $q_R(o) = \varepsilon\sigma\, T_s^4$, which (as would be expected) is the same as $q(o)$ defined in Eq. (4.1).

If emission from the cold gas in front of the shock is neglected, then for a gray shock front, one can write

$$q_R(n) = 2\varepsilon\int_o^\infty e_{b\nu}(T_s)\, E_3(\tau_\nu)d\nu = 2\int_o^\infty q_\nu(0)\, E_3(\tau_\nu)d\nu \tag{7.11}$$

$$-dq_R/dn = 2\varepsilon\int_o^\infty \kappa_\nu\, e_{b\nu}(T_s)\, E_2(\tau_\nu)d\nu = 2\int_o^\infty \kappa_\nu\, q_\nu(0)\, E_2(\tau_\nu)d\nu \tag{7.12}$$

where $q_\nu(o)$ is defined by Eq. (4.2).

The general expression for the total radiative flux is obtained by combining Eqs. (7.6) and (7.10) as

$$q_R(n) = 2\int_o^\infty \left\{ q_\nu(0)\, E_3(\kappa_\nu n) + \pi\kappa_\nu \int_o^n B_\nu(T)\, E_2[\kappa_\nu(n - n')]dn' \right\} d\nu \tag{7.13}$$

where κ_ν is assumed to be independent of position. For the spectral model considered in section 4, Eq. (7.13) can be written as

$$q_R(n) = 2\pi \sum_{i=1}^{n} \left\{ (15/\pi^5)\, q(0)\, E_3(\kappa_i n) \int_{v_{1i}}^{v_{2i}} [v^3/(e^v - 1)]dv \right.$$

$$\left. + \kappa_i \int_o^n E_2[\kappa_i(n - n')] \int_{\nu_{1i}}^{\nu_{2i}} B_\nu(T)\, d\nu\, dn' \right\} \tag{7.14}$$

where $v = h\nu/k\, T_s$. The final form of the energy equation now can be obtained through a combination of Eqs. (7.3d, 7.4, 7.5, and 7.14).

Either by following the information given in Eqs. (2.18, 2.19, and 3.1) or from Ref. [19], the expression for concentration of the species α in Eq. (7.3e) can be written as

$$\rho_\infty\, v_\infty(\partial C_\alpha/\partial n) = -m_1 \int_o^\infty [(\partial q_{R\nu}/\partial n)/h\nu]d\nu \tag{7.15}$$

The appropriate expression for $(\partial q_{R_\nu}/\partial n)$, in this case, is given by Eq. (7.12). Thus, Eq. (7.15) can be expressed as

$$dC_\alpha/dn = (2m_1/h\rho_\infty\, v_\infty)\int_o^\infty [\kappa_\nu\, q_\nu(0)\, E_2(\kappa_\nu n)/\nu]d\nu \tag{7.16}$$

By noting that $\kappa_\nu = N_{H_2}\, \sigma(\nu)$ and following the procedure of section 4 ,

the relations for individual species are found to be

$$C_H = -2\,\beta_4 \sum_{i=1}^{n} Y_{D_i}\, E_3(\tau_i)(kT_s)^{-1}\, I(v_i^2) \tag{7.17}$$

$$C_{H_2^+} = -2\,\beta_4 \sum_{i=1}^{n} Y_{I_i}\, E_3(\tau_i)(kT_s)^{-1}\, I(v_i^2) \tag{7.18}$$

where β_4 , $I(v_i^2)$, and τ_i are defined by Eqs. (4.12d, 4.13, and 7.8) respectively. It should be noted that Eqs. (7.17) and (7.18) are exactly the same as Eqs. (4.25) and (4.26).

By employing the governing equations presented in this section and the spectral information of section 4, numerical results were obtained for velocity, pressure and temperature variations for different values of n at $s = o$. Specific results for an altitude of $Z = 116$ km are compared in Figs. 7.2-7.4 with corresponding results of the small perturbation theory. As indicated earlier, the equations for species concentration in this case are found to be exactly the same as for the small perturbation case. For the range of parameters considered, the results for velocity, pressure and temperature obtained by the two procedures are seen to be in excellent agreement. It is obvious from these results that either approach could be utilized in the investigation of the precursor region flow field. It was noted in section 5 that for the Jupiter's entry conditions, the general governing equations of the small perturbation theory reduced to the case of simple plane source. As such, use of this method to Jupiter's entry case is restricted to one-dimensional analyses. The advantage of thin layer approximation procedure is that it is physically more convincing and it can be extended easily to three-dimensional and axisymmetric cases. Furthermore, in more realistic situations, the thin layer approximation can be relaxed and the analysis can be extended easily to general cases.

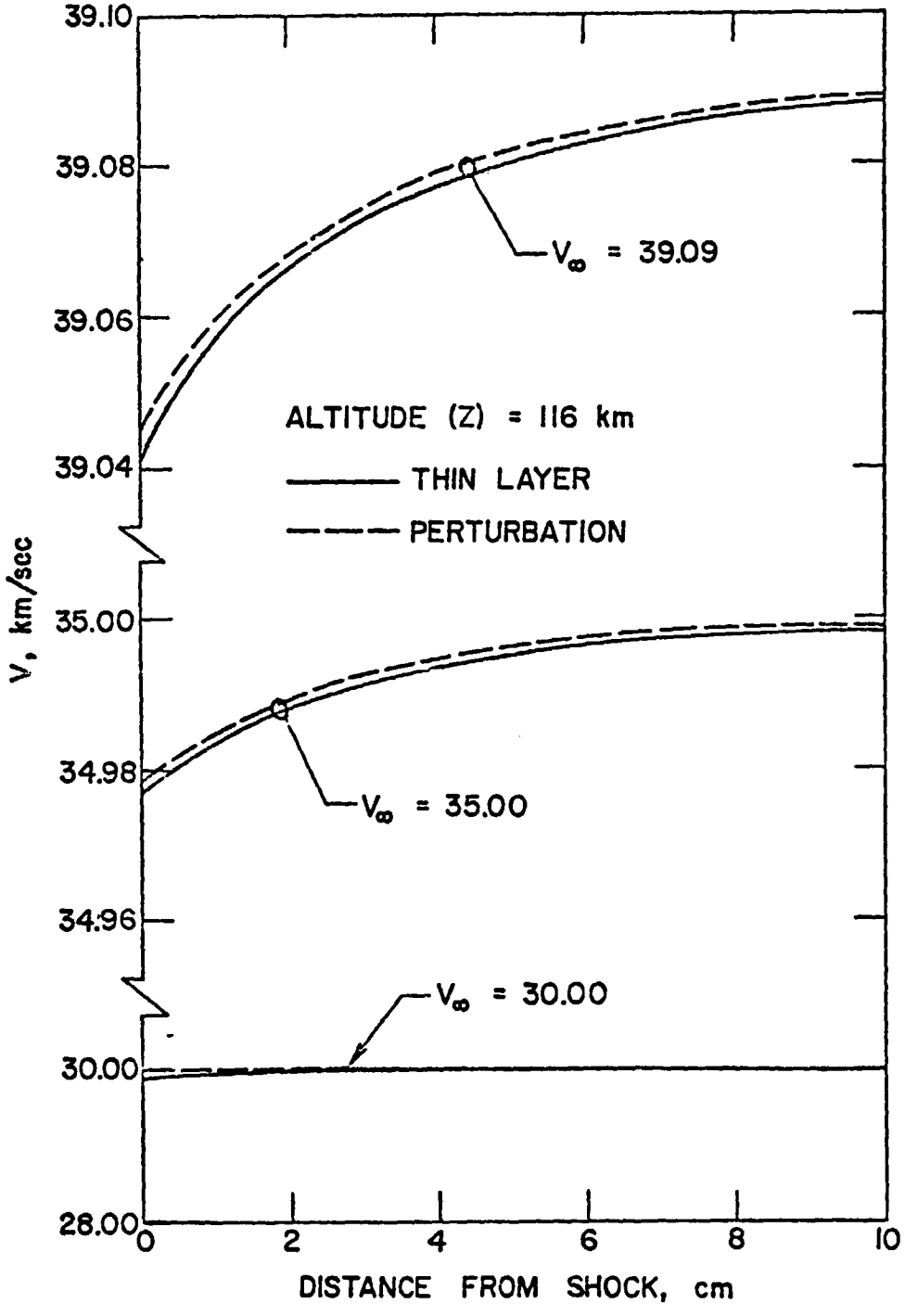

Figure 7.2. Comparison of results for velocity variation in the precursor zone.

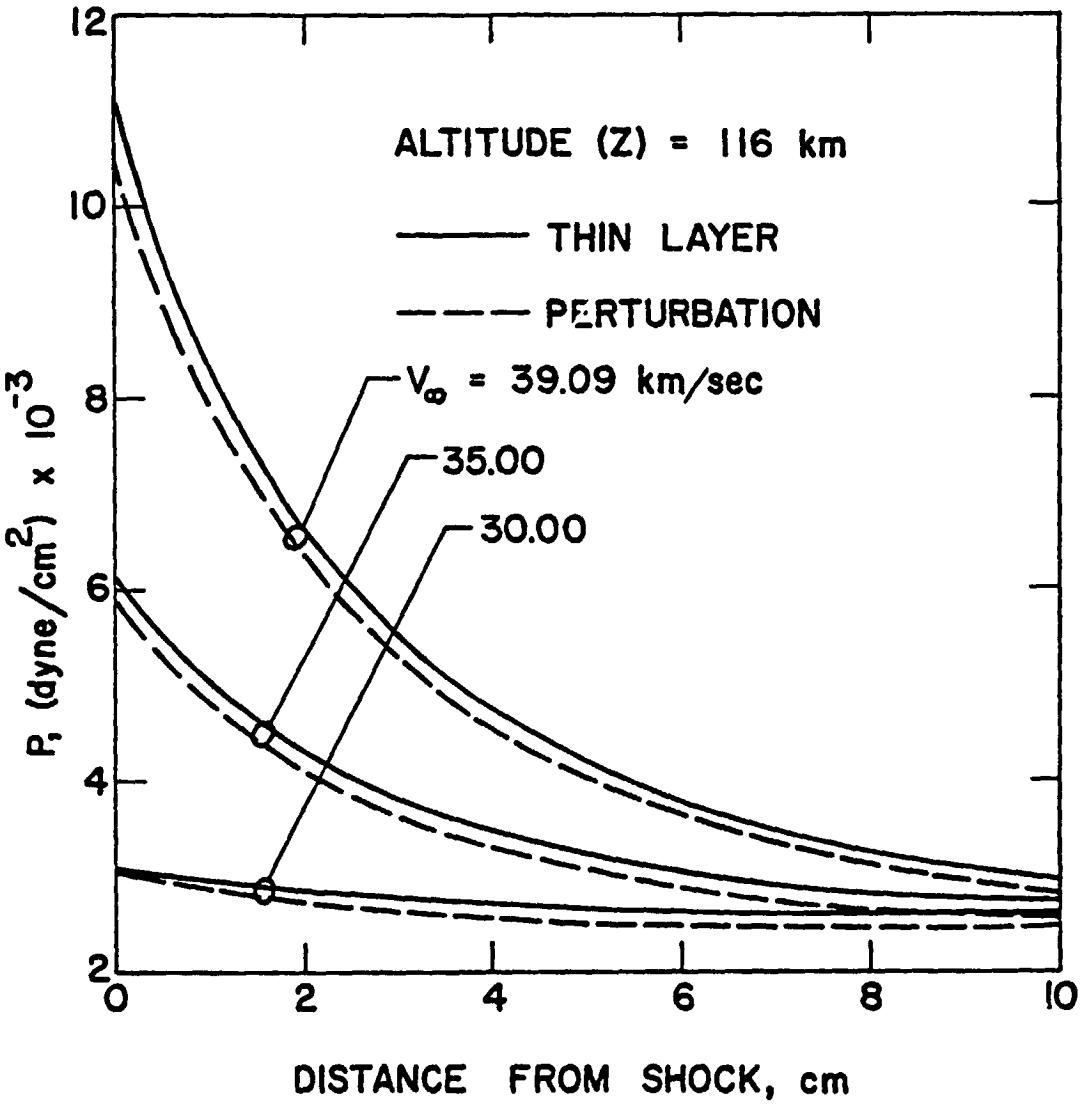

Figure 7.3. Comparison of results for pressure variation in the precursor zone.

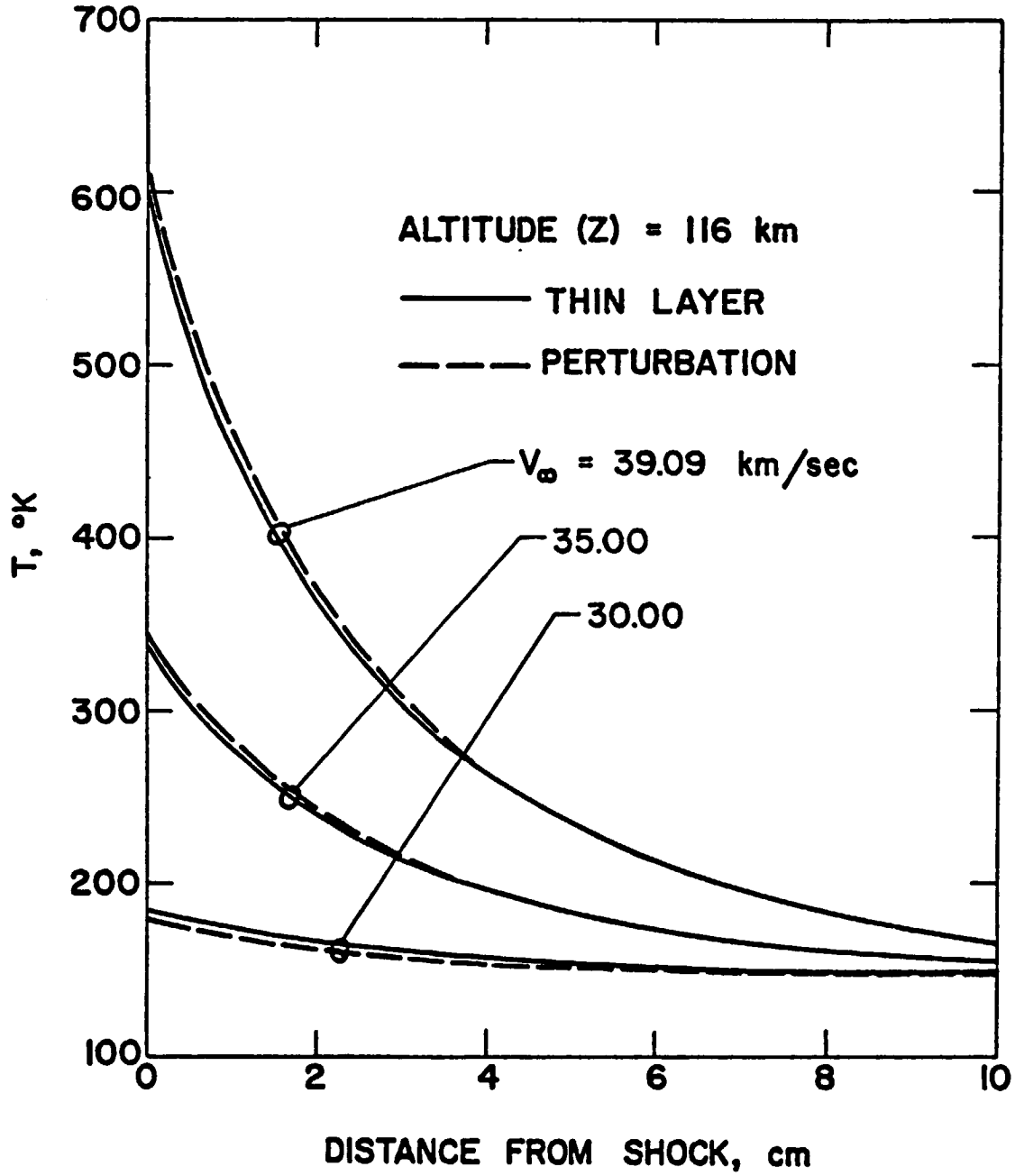

Figure 7.4. Comparison of results for temperature variation in the precursor zone.

8. CONCLUSIONS

Governing equations have been presented for investigating the precursor region flow by employing the small perturbation theory of classical aerodynamics and thin-layer approximations of hypersonic flows. In small perturbation method, the perturbation velocity potential is found to be governed by the wave equation with a driving term due to radiation absorption, ionization and dissociation. The thin layer approximation reduces the general hypersonic flow equations to simpler forms for which solutions are obtained by employing an iterative procedure.

By employing appropriate thermodynamic and spectral data for the hydrogen-helium atmosphere, variations in precursor region flow quantities were calculated by the two entirely different methods. For Jovian entry conditions, one-dimensional results obtained by the two methods were found to be in good agreement for the range of parameters considered. The results, in general, indicate that for certain combinations of entry speeds and altitudes of entry, the precursor effects cannot be ignored while analyzing flows around Jovian entry bodies. Specifically, it is seen that at an altitude of 95 km, the precursor effects are important for entry velocities greater than 35 km/sec.

The usefulness of the thin-layer approximation in analyzing the precursor region flow is demonstrated. The main advantage of this method is that it is physically more convincing and its use can be extended easily to axisymmetric and three-dimensional cases. It is suggested that precursor region flow phenomena be investigated in general without making assumption of the thin layer approximation. It might even be advisable to modify the radiation model for the precursor region absorption. The extent of precursor effects on the entire shock layer flow phenomena should be investigated thoroughly. It might even be essential to include two-dimensional

model for radiative flux and a detailed spectral model for radiation absorption and emission.

REFERENCES

1. Anderson, J. D., "An Engineering Survey of Radiating Shock Layers," AIAA Journal, Vol. 7, No. 9, Sept. 1969, pp. 1665-1675.

2. Olstad, W. B., "Nongray Radiating Flow about Smooth Symmetric Bodies," AIAA Journal, Vol. 9, No. 1, Jan. 1971, pp. 122-130.

3. Callis, L. B., "Coupled Nongray Radiating Flow about Long Blunt Bodies," AIAA Journal, Vol. 9, No. 4, April 1971, pp. 553-559.

4. Sutton, K., "Characteristic of Coupled Nongray Gas Flows with Ablation Product Effects About Blunt Bodies During Planetary Entries," Ph.D. Dissertation, North Carolina State University, 1973.

5. Sutton, K., "Coupled Nongray Radiating Flow about Ablating Planetary Entry Bodies," AIAA Journal, Vol. 12, No. 8, Aug. 1974, pp. 1099-1105.

6. Walberg, G. D. and Sullivan, E. M., "Ablative Heat Shields for Planetary Entries - A Technology Review." Presneted at the ASTM/IES/AIAA Space Simulation Conference, Gaithersburg, Maryland, 1970.

7. Rigdon, W. S., Dirling, R. B., Jr., and Thomas, M., "Stagnation Point Heat Transfer During Hypervelocity Atmospheric Entry," Report CR-1462, Feb. 1970, NASA.

8. Page, W. A., "Aerodynamic Heating for Probe Vehicles Entering the Outer Planets," AAS Paper No. AAS-71-144, 1971.

9. Moss, J. N., "Reacting Viscous-Shock-Layer Solutions with Multicomponent Diffusion and Mass Injection," TR R-411, June 1974, NASA.

10. Moss, J. N., "Radiative Viscous-Shock-Layer Solutions with Coupled Ablation Injection," AIAA Journal, Vol. 14, No. 9, Sept. 1976, pp. 1311-1316.

11. Smith, G. L., "Radiation-Induced Precursor Flow Field Ahead of a Reentering Body," Ph.D. Dissertation, Virginia Polytechnic Institute, March 1968.

12. Smith, G. L., "Radiation Induced Precursor Flow Field Ahead of a Reentering Body," AIAA Paper No. 68-667, June 1968.

13. Lasher, L. E. and Wilson, K. H., "Effect of Shock Precursor Absorption on Superorbital Entry Heating," AIAA Journal, Vol. 6, No. 12, Dec. 1968, pp. 2419-2420.

14. Lasher, L. E. and Wilson, K. H., "Effect of Shock Precursor Heating on Radiative Flux to Blunt Bodies," Report CR-1265, Feb. 1969, NASA.

15. Liu, J.T.C., "Synoptic: Influence of Upstream Absorption on the Stagnation Region Shock Layer Radiation," AIAA Journal, Vol. 8, No. 10. Oct. 1970, pp. 1729-1730.

16. Liu, J.T.C., "Influence of Upstream Absorption on the Stagnation Region Shock Layer Radiation," AIAA Journal, Vol. 8, No. 10, Oct. 1970, pp. 1730-1737.

17. Murty, S.S.R., "Effect of Line Radiation on Precursor Ionization," Journal of Quantitative Spectroscopy & Radiative Transfer, Vol. 8, No. 1, Jan. 1968, pp. 531-554.

18. Nelson, H. F. and Goulard, R., "Structure of Shock Waves with Non-equilibrium Radiation and Ionization," The Physics of Fluids, Vol. 12, No. 8, Aug. 1969, pp. 1605-1617.

19. Perri, A. N. and Clarke, J. H., "Radiative Ionization Patterns in Cold Precursor of Axisymmetric Detached Shock," AIAA Journal, Vol. 8, No. 9, Sept. 1970, pp. 1574-1581.

20. Leibowitz, L. P. and Kuo, T. J., "Ionizational Nonequilibrium Heating During Outer Planetary Entries," AIAA Journal, Vol. 14, No. 9, Sept. 1976, pp. 1324-1329.

21. Livingston F. R. and Poon, T. Y., "Relaxation Distance and Equilibrium Electron Density Measurement in Hydrogen-Helium Plasmas," AIAA Journal, Vol. 14, No. 9, Sept. 1976, pp. 1335-1337.

22. Shapiro, A. H., The Dynamics and Thermodynamics of Compressible Fluid Flow, Vol. I, The Ronald Press, New York, 1953.

23. Liepmann, H. W. and Roshko, A., Element of Gasdynamics, John Wiley and Sons, 1956.

24. Vincenti, W. G. and Kruger, C. H., Introduction to Physical Gas Dynamics, John Wiley and Sons, 1965.

25. Hudson, R. D., "Critical Review of Ultraviolet Photoabsorption Cross Section for Molecules of Astrophysical and Aeronomic Interest," Review of Geophysics and Space Physics, Vol. 9, No. 2, May 1971, pp. 305-406.

26. Lee, P. and Weissler, G. L., "Absolute Absorption of the H_2 Continuum,' Astrophysical Journal, Vol. 115, 1952, pp. 570-571.

27. Ditchburn, R. W., "Absorption of Ultra-Violet Radiation by the Atmospheric Gases," Proceedings of the Royal Society, Series A, Mathematical and Physical Sciences No. 1205, Vol. 236, Aug. 1956, pp. 216-226.

28. Cook, G. R. and Metzer, P. H., "Photoionization and Absorption Cross Section of H_2 and D_2 in the Vacuum Ultraviolet Region," Journal of the Optical Society of America, Vol. 54, No. 8, Aug. 1964, pp. 968-972.

29. Samson, J.A.R. and Cairns, R. B., "Total Absorption Cross Section of H_2, N_2, and O_2 in the Region 550-200 Å," Journal of the Optical Society of America, Vol. 55, No. 8, Aug. 1965, p. 1035.

30. McCarty, R. D., "Hydrogen Technology Survey: Thermophysical Properties," Report SP-3089, 1975, NASA.

31. Lee, L. C., Carson, R. W., and Judge, D. L., "The Absorption Cross Sections of H_2 and D_2 from 180 to 780°A," Journal of Quantitative Spectroscopy and Radiation Transfer, Vol. 16, No. 10, Oct. 1976, pp. 873-877.

32. Anon., The Planet Jupiter, Report SP-8069, Dec. 1971, NASA.

33. Babu, S. G., "Approximate Thermochemical Tables for some C-H and C-H-O Species," Report CR-2178, March 1973, NASA.

34. McBride, B. J., Heimel, S., Ehlers, J. G., and Gordon, S., "Thermodynamic Properties to 6000°K for 210 Substances Involving the First 18 Elements," Report SP-3001, 1963, NASA.

35. Hayes, W. D. and Probstein, R. F., Hypersonic Flow Theory: Vol. I, Inviscid Flows, Academic Press, 1966.

36. Cheng, H. K., "Viscous Hypersonic Blunt-Body Problems and the Newtonian Theory," Fundamental Phenomena in Hypersonic Flow (J. G. Hall, editor), Cornell University Press, 1966.

37. Sparrow, E. M. and Cess, R. D., Radiation Heat Transfer, Brooks/Cole Publishing Co., Belmont, California, 1966.

APPENDIX A1

EXPLANATION OF SYMBOLS USED IN THE COMPUTER PROGRAM "PERC"

A0, A1 A2, A3	Exponential integral constants
B0, B1 B2, B3	Exponential integral constants
CH	Mass fraction of H
CHE	Mass fraction of H_e
CHH	Mass fraction of H_2
CH2	Mass fraction of H_2+
DEN	Perturbation density
DEN2	Free-stream density, g/cm^3
ETH	Sum of sensible and chemical enthalpy of mixture gas, cal/g
ETHP1	Sum of sensible and chemical enthalpy of H_2, cal/g
ETHP2	Sum of sensible and chemical enthalpy of H_2+, cal/g
ETHP3	Sum of sensible and chemical enthalpy of H, cal/g
ETHP4	Sum of sensible and chemical enthalpy of H_e, cal/g
EX	Exponential integral
GARM	Specific heat ratio
GD	Dissociation energy, erg/mole
GI	Ionization energy, erg/mole
GMARC	Mach number
GNH2	Number density of H_2, $molecule/cm^3$
P	Boltzmann constant, erg/°K
PRE	Perturbation pressure

PRI	Free-stream pressure, dyne/cm^3
QO	Radiative heat flux at shock front, erg/cm^3-sec
RCAP	Shock radius, cm
ROE	Absorption cross section, cm^2
T	Absorption coefficient, cm^{-1}
TF1	Perturbation temperature, °K
TF111	Temperature, °K
TH	Planck's constant, erg-sec
TO	Free-stream temperature, °K
TS	Temperature at shock, °K
U	Universal gas constant, erg/mole-°K
V	Frequency, sec^{-1}
VINF	Free-stream velocity, cm/sec
VZ	Perturbation velocity component normal to the shock surface
W1	Molecular weight, g/molecule
Z	Distance from the shock

APPENDIX A2

EXPLANATION OF SYMBOLS USED IN THE COMPUTER PROGRAM "THIN"

A0, A1 A2, A3	Exponential integral constants
ARF	Absorption coefficient, cm^{-1}
B0, B1 B2, B3	Exponential integral constants
CH	Mass fraction of H
CHE	Mass fraction of H_e
CHH	Mass fraction of H_2
CH2	Mass fraction of H_2+
CK	Boltzmann constant, erg/°K
DEN	DENSITY, g/cm^3
DENI	Free-stream density, g/cm^3
DH	Planck's constant, erg-sec
E1, E2, E3	Exponential integrals of order 1, 2, and 3
ETH, ETHi ETH2, ETH3 ETH4	Defined in Appendix A1
GR	Euler's constant
MH	Mole fraction of H
MHE	Mole fraction of H_e
MHH	Mole fraction of H_2
MH2	Mole fraction of H_2+
NA	Number density of H_2, molecule/cm^3

NA1	Number density of H_2+, molecule/cm^3
P	Pressure, dyne/cm^2
PH	Sensible enthalpy, erg/g
PHT	Total sensible enthalpy, erg/g
PREI	Free-stream pressure
QO	Radiative heat flux at shock front, erg/cm^3-sec
QR	Radiative heat flux at any field point, erg/cm^2-sec
ROH	Absorption cross section, cm^2
S	Nondimensional coordinate measured along the shock surface
T	Temperature, °K
TS	Shock temperature, °K
U	Velocity component tangent to the shock surface, cm/sec
UI	Free-stream velocity component tangent to the shock surface, cm/sec
V	Velocity component normal to the shock surface, cm/sec
VELO	Free-stream velocity, cm/sec
VF	Frequency, sec^{-1}
VI	Free-stream velocity component normal to the shock surface, cm/sec
Y	Coordinate measured normal to the shock surface, cm
YD	Photodissociation yield
YI	Photoionization yield
Z	Altitude, km
ZETA	Shock angle

APPENDIX B1

PROGRAM "PERC" - TO COMPUTE PRECURSOR EFFECTS

USING PERTURBATION METHOD

```
      PROGRAM PERC (INPUT, OUTPUT,TAPE5=INPUT, TAPE6=OUTPUT)
      DIMENSION BATA(4), D(4), AA(4), AB(4), AC(4), AD(4), P2(4,2),P3(4,
     12), V(4,2), V1(4,2), PCI0(4), PCI1(4), G0(4), G1(4), T0(4), T1(4),
     2T(4),  E(80), YI(4), Y0(4), ROE(4), AI(4), BI(4), CI(4),C1(4), C2(
     14),D1(4),D2(4),D3(4),AE(4),AF(4),AG(4),AH(4),AK(4),AI0(4),EX(3,2),
     1SUM(6),IERR(8),D11(4),Z1(10)
      REAL MHH,MH2,MHE,MH
      EXTERNAL FX1, FX2
      Z1(1)=0.001
      Z1(2)=0.002
      Z1(3)=0.005
      Z1(4)=0.01
      Z1(5)=0.02
      Z1(6)=0.05
      Z1(7)=0.1
      Z1(8)=0.2
      Z1(9)=0.5
      Z1(10)=1.0
      U=8.3143E7
      TH=6.6256E-27
      GARM=1.433
      ROE(1)=4.1E-18
      ROE(2)=8.2E-18
      ROE(3)=2.1E-18
      DO 4 K=1,27
      READ (5,15) DEN2, VINF, TS, PRI, QQ
   15 FORMAT (5E11.3)
      GNH2=7.243112*PRI/145.*10.**16*0.89
      T(1)=ROE(1)*GNH2
      T(2)=ROE(2)*GNH2
      T(3)=ROE(3)*GNH2
      RCAP=25.
      A0=0.26777343
      A1=8.6347608925
      A2=18.059016973
      A3=8.5733287401
      B0=3.95846922
      B1=21.0996530
      B2=25.63295614
      B3=9.5733223454
      DO 88 M1=1,10
      Z=Z1(M1)*25.*(-1.)
   77 IF (ABS(Z).LE.1.0E-5) GO TO 555
      DO 11 N=1,3
```

```
      X=-Z*T(N)
      IF (X.LT.1.) GO TO 13
      E(1)=EXP(-X)*(A0+A1*X+A2*X**2+A3*X**3+X**4)/(X*(B0+B1*X+B2*X**2+B3
     1*X**3+X**4))
      EX(N,1)=E(1)
      GO TO 14
   13 E(1)=-0.577215664-ALOG(X)+X-X**2./4.+X**3./18.-X**4./96.+X**5./600
     1.-X**6./4320.+X**7./35280.-X**8./322560.+X**9./3265920.-X**10./362
     288000.
      EX(N,1)=E(1)
   14  DO 28 I=1,6
      E(I+1)=(EXP(-X)-X*E(I))/I
      EX(N,I+1)=E(I+1)
   28 CONTINUE
   11 CONTINUE
      GO TO 501
  555 EX(1,2)=1.
      EX(2,2)=1.
      EX(3,2)=1.
      EX(1,3)=0.5
      EX(2,3)=0.5
      EX(3,3)=0.5
  501 GMARC=VINF/(70.*(145.**0.5)*100.)
      P=1.385E-16
      V(1,1)=5.02E+15
      V(1,2)=8.70E+15
      V(2,1)=3.75E+15
      V(2,2)=5.02E+15
      V(3,1)=1.15E+15
      V(3,2)=3.75E+15
      V1(1,1)=V(1,1)*6.6256E-27/(1.3805E-16*TS)
      V1(1,2)=V(1,2)*6.6256E-27/(1.3805E-16*TS)
      V1(2,1)=V(2,1)*6.6256E-27/(1.3805E-16*TS)
      V1(2,2)=V(2,2)*6.6256E-27/(1.3805E-16*TS)
      V1(3,1)=V(3,1)*6.6256E-27/(1.3805E-16*TS)
      V1(3,2)=V(3,2)*6.6256E-27/(1.3805E-16*TS)
      X1=0.
      X2=0.
      X3=0.
      X4=0.
      X5=0
      X6=0
      X7=0
      X8=0
```

```
      X9=0
      X10=0
      DO 500 N=1,3
      EPS =0.001
      CALL ROMBS (V1(N,1),V1(N,2),FX1,EPS,SUM(N),IERR(N))
      CALL ROMBS (V1(N,1),V1(N,2),FX2,EPS,SUM(N+3),IERR(N+3))
      WRITE (6,32) SUM(N),SUM(N+3)
   32 FORMAT(3X,*P3=*,E10.3,3X,*P2=*, E10.3)
      T0=145.
      GH0=1.527*U*T0
      W1=3.280E-24
      GI=14.868E12
      GD=4.5E12/2.
      YI(1)=1.0
      YI(2)=0.875
      YI(3)=0.0
      YD(1)=0.
      YD(2)=0.125
      YD(3)=1.0
      AI(N)=GNH2*ROE(N)/(DEN2*VINF*GH0)
      BI(N)=-(GNH2*ROE(N)*W1)/(DEN2*VINF*GH0)*((GI-0.89*U*T0)*YI(N)+(2.*
     1GD-1.89*U*T0)*YD(N))/2.
      Q2=15/(3.14159**4)*Q0
      D(N)=EX(N,3)*(AI(N)*SUM(N)+BI(N)/(P*TS)*SUM(N+3))/T(N)
      D1(N)=EX(N,3)*SUM(N)
      D2(N)=YD(N)*EX(N,3)*SUM(N+3)/(P*TS)
      D3(N)=YI(N)*EX(N,3)*SUM(N+3)/(P*TS)
      D11(N)=Q2*D(N)
      X1=D(N)+X1
      X2=D1(N)+X2
      X3= X3+D2(N)
      X4=X4+D3(N)
  500 CONTINUE
      BAT=2./(0.727*GARM*GMARC**2-1.)
      VZ=-Q2*BAT*X1
      PRE=2.*GARM*Q2*X1
      DEN=-VZ
      GHT=2./(DEN2*VINF**3)*Q2*X2
      CH2=1.*W1*2.*Q2*X4/(VINF*DEN2)
      CH=2.*W1*Q2*X3/(VINF*DEN2)
      R=0.
      VR=0.
  810 TF1=145.*(PRE-DEN-(CH2+CH)*200./180.17)
      CHH=0.8019-CH2-CH
```

```
      CHE=0.1981
      TF1111=TF1+145.
      RT=TF1111*1.98726
      IF (TF1111.GT.1000.) GO TO 999
      IF (TF1111.GT.300.) GO TO 998
      ETHP2=CH2*((TF1111-100.)/200.*(1232.)+358305.)/2.
      ETHP1=CHH*((TF1111-100.)/200.*(1264.8)-1264.8)/2.
      ETHP3=CH*((TF1111-100.)/200.*(966.)+51134.)
      ETHP4=CHE*((TF1111-100.)/200.*(984.4)-984.4)/4.
      GO TO 1001
  998 ETHP1=CHH*RT*(2.846084E+4.1932116E-3*TF1111/2.-9.6119332E-6*TF1111
     1**2/3.-9.5152974E-9*TF1111**3/4.+3.3090492E-12*TF1111**4/5.-9.6725
     2372E2/TF1111)/2.
      ETHP2=CH2*RT*(2.817375+3.65761E-3*TF1111/2.-7.965548E-6*TF1111**2/
     13.+8.26140E-9*TF1111**3/4.-3.090228E-12*TF1111**4/5.+1.800273E5/TF
     21111)/2.
      GO TO 1000
  999 ETHP1=CHH*RT*(3.0436897+6.1187110E-4*TF1111/2.-7.3993551E-9*TF1111
     1**2/3.-2.0331907E-11*TF1111**3/4.+2.4593791E-15*TF1111**4/5.-8.549
     2190E2E2/TF1111)/2.
      ETHP2=CH2*RT*(3.328715+2.505067E-3*TF1111/2.+1.4224520E-7*TF1111**
     12/3.-4.459024E-11*TF1111**3/4.+3.733756E-15*TF1111**4/5.+1.7997470
     2E5/TF1111)/2.
 1000 ETHP3=CH*RT*(2.5+2.5470497E4/TF1111)
      ETHP4=CHE*RT*(2.5-7.45374E2/TF1111)/4.
 1001 ETH=ETHP1+ETHP2+ETHP3+ETHP4
      ETHK=ETH*4.184*1000.0
      WRITE (6,16)VINF, DEN2,TS
   16 FORMAT (//4X,*VINF=*,E11.3, 4X, *DEN=*,E11.3,3X,*TS=*,E11.4)
      WRITE(6,52)
   52 FORMAT(8X,*R*,10X,*Z*, 8X,*VZ*, 8X,*PRE*, 8X,*DEN*, 8X,*TF*, 8X,*C
     1H2+*, 7X,*CH*, 7X,*GHT*, 8X,*ETH*)
      WRITE (6,37)R,Z,VZ,PRE,DEN,TF1,CH2,CH,GHT,ETHK,Z1(M1)
   37 FORMAT (/2X,2F10.2,9E11.3)
      GO TO 88
      Z=Z+0.10
      IF (Z.GT.0.01) GO TO 4
      GO TO 77
   88 CONTINUE
    4 CONTINUE
   38 STOP
      END
      FUNCTION FX1(X)
      FX1=X**3/(EXP(X)-1)

      RETURN
      END
      FUNCTION FX2(X)
      FX2=X**2/(EXP(X)-1)
      RETURN
      END
```

APPENDIX B2

PROGRAM "THIN" - TO COMPUTE PRECURSOR EFFECTS

USING THIN-LAYER APPROXIMATION

```
      PROGRAM THIN  (INPUT,OUTPUT,TAPE5=INPUT,TAPE6=OUTPUT)
      COMMON ARF(3),SUM(12), II,T(50),TS,YI(3),YD(3), NA,ROH(3),IERR(12)
     1,VF(3,2), DH,CK,C,K,QQ,Y,S,E3(3),J,VELOI,DENI
      DIMENSION  V(50),U(50),P(50),PHT(50),PH(50),CH2(50),CH(50),DEN(50)
      REAL NA,NB,NA1,MH2,MHH,MH,MHE
      DO 21 N=1,20
      READ (5,1) Y,S,TS,PREI,ZTA,Z,QQ,VELOI,DENI
    1 FORMAT (4F8.2,2F5.3,E10.3,F8.0,E10.3)
      VELOI=-VELOI
      ZTA=ZTA*3.1415926535/(2.*90.)
      ROH(1)=4.1E-18
      ROH(2)=8.2E-18
      ROH(3)=2.1E-18
      DH=6.6256E-27
      CK=1.38054E-16
      C=3.0E10
      VF(1,1)=8.7E15
      VF(2,2)=3.75E15
      VF(3,1)=3.75E15
      VF(3,2)=1.15E15
      VF(1,2)=5.02E15
      VF(2,1)=5.02E15
      VI=VELOI*SIN(ZTA)
      UI=VELOI*COS(ZTA)
      V(1)=VI
      U(1)=UI
      P(1)=PREI
      DEN(1)=DENI
      CH2(1)=0.
      CH(1)=0.
      A=14.8E12
      D=4.5E12/2.
      YI(1)=1.0
      YI(2)=0.875
      YI(3)=0.
      YD(1)=0.0
      YD(2)=0.125
```

```
      YD(3)=1.
      R=8.3413E7
      PHT(1)=(VELOI**2)/2.+1.527*R*145.
      PH(1)=1.527*145.*R
      T(1)=145.
   20 DO 111 I=1,49
      II=I
      NA=(7.2431122E22*0.89)*P(1)/(T(1)*10.)
      NA1=NA*1.0E-6
      ARF(1)=ROH(1)*NA1
      ARF(2)=ROH(2)*NA1
      ARF(3)=ROH(3)*NA1
      DEN(I+1)=DENI*VI/V(I)
      V(I+1)=(DENI*(VI**2)-P(I)+P(1))/(DENI*VI)
      U(I+1)=UI
      CALL QRADIA(Y,S,QR)
      PHTI=1.527*R*145.+(VELOI**2)/2.
      PHT(I+1)=(DENI*VI*PHTI-QR)/(DENI*VI)
      PH(I+1)=PHT(I+1)-(V(I+1)**2+U(I+1)**2)/2.
      T(I+1)=(PH(I+1)-(5./4.*R*T(I)+A/2.)*CH2(I)-(3./4.*R*T(I)+D)*CH(I))
     1/(1.527*R)
      CALL PCH2(PCHI,PCHD)
      NB=1.
      CH(I+1)=NB*PCHD
      CH2(I+1)=NB*PCHI
      P(I+1)=DEN(I+1)*R*T(I+1)*(160.17/400.+0.5*(CH2(I+1)+CH(I+1)))
      IF (ABS((V(I+1)-V(I))/V(I)).GT.0.01) GO TO 59
      IF (ABS((T(I+1)-T(I))/T(I)).GT.0.01) GO TO 59
      IF (ABS((P(I+1)-P(I))/P(I)).GT.0.01) GO TO 59
      IF (ABS((PH(I+1)-PH(I))/PH(I)).GT.0.01) GO TO 59
      IF (ABS((PHT(I+1)-PHT(I))/PHT(I)).GT.0.01) GO TO 59
      IF (ABS((CH(I+1)-CH(I))/CH(I)).GT.0.01) GO TO 59
      IF (ABS((CH2(I+1)-CH2(I))/CH2(I)).GT.0.01) GO TO 59
      IF (ABS((DEN(I+1)-DEN(I))/DEN(I)).GT.0.01) GO TO 59
      GO TO 10
   59 GO TO 111
  111 CONTINUE
   10 WRITE (6,11) S,Y
   11 FORMAT (4X,*S=*,F10.3,X,*CM*,5X,*Y=*,F10.3,X,*CM*)
      WRITE (6,12) Z,VELOI,QQ
   12 FORMAT (4X,*ATTITUDE=*,F10.3,4X,*VELOCITY INF=*,E10.3,*CM/SC*,4X,*
     1Q(S)=*,E10.3,*ERG/CM3-SEC*,//)
      CHH=0.8019-CH2(I+1)-CH(I+1)
      CHE=0.1981
```

```
      ADD=CHH/2.+CH2(I+1)/2.+CH(I+1)+CHE/4.
      MHH=(CHH/2.)/ADD
      MH2=(CH2(I+1)/2.)/ADD
      MH=(CH(I+1))/ADD
      MHE=(CHE/4)/ADD
      RT=1.98726*T(I+1)
      IF (T(I+1).GT.1000.) GO TO 999
      IF (T(I+1).GT.300.) GO TO 998
      TF1111=T(I+1)
      ETHP2=MH2*((TF1111-100.)/200.*(1232.)+358395.)
      ETHP1=MHH*((TF1111-100.)/200.*(1264.8)-1264.8)
      ETHP3=MH*((TF1111-100.)/200.*(966.)+51134.)
      ETHP4=MHE*((TF1111-100.)/200.*(984.4)-984.4)
      GO TO 1001
  998 ETHP1=MHH*RT*(2.8460849+4.1932116E-3*T(I+1)/2.-9.6119332E-6*T(I+1)
     1**2/3.-9.5122974E-9*T(I+1)**3/4.+3.3090492E-12*T(I+1)**4/5.-9.6725
     2372E2/T(I+1))
      ETHP2=MH2*RT*(2.817375+3.65761E-3*T(I+1)/2.-7.965548E-6*T(I+1)**2/
     13.+8.26140E-9*T(I+1)**3/4.-3.090228E-12*T(I+1)**4/5.+1.800273E5/T(
     2I+1))
      GO TO 1000
  999 ETHP1=MHH*RT*(3.0436897+6.1187110E-4*T(I+1)/2.-7.3993551E-9*T(I+1)
     1**2/3.-2.0331907E-11*T(I+1)**3/4.+2.4593791E-15*T(I+1)**4/5.-8.549
     21002E2/T(I+1))
      ETHP2=MH2*RT*(3.328715+2.505067E-3*T(I+1)/2.+1.4224520E-7*T(I+1)**
     12/3.-4.459024E-11*T(I+1)**3/4.+3.733756E-15*T(I+1)**4/5.+1.7997470
     2E5/T(I+1))
 1000 ETHP3=MH*RT*(2.5+2.5470497E4/T(I+1))
      ETHP4=MHE*RT*(2.5-7.45374E2/T(I+1))
 1001 ETH=(ETHP1+ETHP2+ETHP3+ETHP4)*4.184*10000./2.314
      WRITE (6,28) ETH
   28 FORMAT (4X,*ENTHOPY (ABSOL)=*,E11.4,/)
      WRITE (6,13)
   13 FORMAT(3X,*V*,11X,*U*,12X,*T*,10X,*P*,10X,*DEN*,9X,*H*,10X,*HT*,11
     1X,*CH*,10X,*CH2*)
      WRITE (6,14) V(I+1),U(I+1),T(I+1),P(I+1),DEN(I+1),PH(I+1),PHT(I+1)
     1,CH(I+1),CH2(I+1),QR,I
   14 FORMAT (X,E10.4,2X,E9.3,2X,2X,E9.3,2X,E9.3,2X,E10.3,2X,E10.3,2X,E1
     10.3,2X,E10.3,2X,E10.3,3X,E11.3,3X,F3.1,///)
      IF (Y.GT.0.5) GO TO 15
      Y=Y+0.1
      GO TO 20
   15 Y=Y+0.4
      IF (Y.GT.2.) GO TO 21
```

```
      GO TO 20
   21 CONTINUE
      STOP
      END
      SUBROUTINE  QRADIA(Y,S,QR)
      COMMON ARF(3),SUM(12),I,T(50),TS,YI(3),YD(3),NA,ROH(3),IERR(12),VF
     1(3,2),DH,CK,C,K1,QQ,YY,SS,EJ(3)
      COMMON /FFF/ Z
      DIMENSION E2(3),ARY(3),E1(3),V1(3,2)
      EXTERNAL FX1,FX2,FX3
      F1=6.256E-27/(1.3805E-16*TS)
      V1(1,1)=VF(1,1)*F1
      V1(1,2)=VF(1,2)*F1
      V1(2,1)=VF(2,1)*F1
      V1(2,2)=VF(2,2)*F1
      V1(3,1)=VF(3,1)*F1
      V1(3,2)=VF(3,2)*F1
      EPS=0.002
      DO 50 K=1,3
      K1=K
      CALL ROMBS (VF(K,2),VF(K,1),FX1,EPS,SUM(K),IERR(K))
      IF (IERR(K).EQ.0) GO TO 30
      PRINT 31,K,IERR(K)
   30 CALL ROMBS (V1(K,2),V1(K,1),FX2,EPS,SUM(K+3),IERR(K+3))
      IF (IERR(K+3).EQ.0) GO TO 40
      K3=K+3
      PRINT 31, K3, IERR(K+3)
   40 A=0.0001
      Z=Y+0.0001
      B=Y
      IF (B.EQ.0.) GO TO 32
      CALL ROMBS (A,B,FX3,EPS,SUM(K+6),IERR(K+6))
      IF (IERR(K+6).EQ.0) GO TO 50
      K6=K+6
      PRINT 31,  K6,IERR(K+6)
   31 FORMAT (*K=*,I2,*IERR=*,I3)
      GO TO 50
   32 SUM(K+6)=0.
   50 CONTINUE
      QR1=0
      DO 100 K=1,3
      GR=0.5772
      ARY(K)=ARF(K)*Y
      IF (Y.LT.0.001) GO TO 33
```

```
      GO TO 20
   21 CONTINUE
      STOP
      END
      SUBROUTINE  QRADIA(Y,S,QR)
      COMMON ARF(3),SUM(12),I,T(50),TS,YI(3),YD(3),NA,ROH(3),IERR(12),VF
     1(3,2),DH,CK,C,K1,QQ,YY,SS,EJ(3)
      COMMON /FFF/ Z
      DIMENSION E2(3),ARY(3),E1(3),V1(3,2)
      EXTERNAL FX1,FX2,FX3
      F1=6.256E-27/(1.3805E-16*TS)
      V1(1,1)=VF(1,1)*F1
      V1(1,2)=VF(1,2)*F1
      V1(2,1)=VF(2,1)*F1
      V1(2,2)=VF(2,2)*F1
      V1(3,1)=VF(3,1)*F1
      V1(3,2)=VF(3,2)*F1
      EPS=0.002
      DO 50 K=1,3
      K1=K
      CALL ROMBS (VF(K,2),VF(K,1),FX1,EPS,SUM(K),IERR(K))
      IF (IERR(K).EQ.0) GO TO 30
      PRINT 31,K,IERR(K)
   30 CALL ROMBS (V1(K,2),V1(K,1),FX2,EPS,SUM(K+3),IERR(K+3))
      IF (IERR(K+3).EQ.0) GO TO 40
      K3=K+3
      PRINT 31, K3, IERR(K+3)
   40 A=0.0001
      Z=Y+0.0001
      B=Y
      IF (B.EQ.0.) GO TO 32
      CALL ROMBS (A,B,FX3,EPS,SUM(K+6),IERR(K+6))
      IF (IERR(K+6).EQ.0) GO TO 50
      K6=K+6
      PRINT 31,  K6,IERR(K+6)
   31 FORMAT (*K=*,I2,*IERR=*,I3)
      GO TO 50
   32 SUM(K+6)=0.
   50 CONTINUE
      QR1=0
      DO 100 K=1,3
      GR=0.5772
      ARY(K)=ARF(K)*Y
      IF (Y.LT.0.001) GO TO 33
```

```
      A0=0.26777343
      A1=8.6347608925
      A2=18.0590169730
      A3=8.573287401
      B0=3.958469228
      B1=21.09965308
      B2=25.63295614
      B3=9.5733223454
      IF (ARY(K).LT.1.) GO TO 200
      X=ARY(K)
      E1(K)=EXP(-X)*(A0+A1*X+A2*X**2+A3*X**3+X**4)/(X*(B0+B1*X+B2*X**2+B
     13*X**3+X**4))
      GO TO 220
  200 X=ARY(K)
      E1(K)=-0.57721566-ALOG(X)+X-X**2./4.+X**3./18.-X**4./96.+X**5./600
     1.-X**6./4320.+X**7./35280.-X**8./322560.+X**9./3265920.-X**10./362
     288000.
  220 E2(K)=(EXP(-X)-X*E1(K))
      E3(K)=(EXP(-X)-X*E2(K))/2.
      GO TO 35
   33 E2(K)=1.
      E3(K)=0.5
   35    QR2=2.* ARF(K)*DH/(C**2.)*SUM(K+6)
      QR4=E3(K)*SUM(K+3)*15.*QO/(3.14159**5)
      QR1=QR2+QR4+QR1
  100 CONTINUE
      QR=QR1*2.*3.14159
      RETURN
      END
      FUNCTION FX1(X)
      COMMON ARF(3),SUM(12),I,T(50),TS,YI(3),YD(3),NA,ROH(3),IERR(12),VF
     1(3,2),DH,CK,C,K,QO
      FX1=X**3*EXP(-(DH*X/(CK*T(I))))
      RETURN
      END
      FUNCTION FX2(X)
      COMMON ARF(3),SUM(12),I,T(50),TS,YI(3),YD(3),NA,ROH(3),IERR(12),VF
     1(3,2),DH,CK,C,K,QO
      DAT=5.6697E-5
      FX2=X**3/(EXP(X)-1.)
      RETURN
      END
      FUNCTION FX3(X)
      COMMON ARF(3),SUM(12),I,T(50),TS,YI(3),YD(3),NA,ROH(3),IERR(12),VF
```

```
     1(3,2),DH,CK,C,K,QQ
      COMMON /FFF/ Z
      FX3=(1.+(.577-1.+ALOG(ARF(K)*(Z-X)))*(ARF(K)*  (Z-X))-(ARF(K)*(Z-X
     1)) **2/2.+(ARF(K)*(Z-X))**3/12.)*SUM(K)
      RETURN
      END
      SUBROUTINE PCH2 (PCHI,PCHD)
      COMMON ARF(3),SUM(12),I,T(50),TS,YI(3),YD(3),NA,ROH(3),IERR(12),VF
     1(3,2),DH,CK,C,K,QQ,Y,S,E3(3),J1,VELOI,DENI
      DIMENSION V1(3,2),CH1(3),CH2(3)
      EXTERNAL FX4
      F1=6.256E-27/(1.3805E-16*TS)
      V1(1,1)=VF(1,1)*F1
      V1(1,2)=VF(1,2)*F1
      V1(2,1)=VF(2,1)*F1
      V1(2,2)=VF(2,2)*F1
      V1(3,1)=VF(3,1)*F1
      V1(3,2)=VF(3,2)*F1
      EPS=0.001
      DO 59 J=1,3
      J1=J
      CALL ROMBS (V1(J,2),V1(J,1), FX4, EPS, SUM(J+9),IERR(J+9))
      CH1(J)=YI(J)*E3(J)*SUM(J+9)/(1.3805E-16*TS)
      CH2(J)=YD(J)*E3(J)*SUM(J+9)/(1.3805E-16*TS)
   59 CONTINUE
      PDHI=CH1(1)+CH1(2)+CH1(3)
      PDHD=CH2(1)+CH2(2)+CH2(3)
      X1=GO*15.*2.*3.28E-24/(DENI*VELOI*3.14159**4)*(-1.)
      PCHI=PDHI*X1
      PCHD=PDHD*X1
      RETURN
      END
      FUNCTION FX4(X)
      COMMON ARF(3),SUM(12),I,T(50),TS,YI(3),YD(3),NA,ROH(3),IERR(12),VF
     1(3,2),DH,CK,C,K,QQ,Y,S,E3(3),J
      FX4=X**2/(EXP(X)-1)
      RETURN
      END
```